a0005

3.07 Optical Communications

Dan M. Marom, The Hebrew University of Jerusalem, Jerusalem, Israel

Glossary

g9000 **ATM** Asynchronous transfer mode
g9005 **BLSR** Bidirectional Line Switched Ring
g9010 **DBR** Distributed Bragg Reflector
g9015 **DFB** Distributed Feedback
g9020 **DMEMS** Diffractive MEMS
g9025 **DRIE** Deep Reactive Ion Etch
g9030 **DUV** Deep Ultraviolet
g9035 **DWDM** Dense Wavelength Division Multiplexing
g9040 **FSR** Free-Spectral Range
g9045 **GMPLS** Generalized Multi-Protocol Label Switching
g9050 **GR** Generic Requirement
g9055 **ILA** In-Line Amplifier
g9060 **LC** Liquid-crystal
g9065 **MARS** Mechanical Anti-Reflection Switch
g9070 **MEMS** Micro-Electro-Mechanical System
g9075 **MSPP** Multi-Service Provisioning Platform
g9080 **OADM** Optical Add-Drop Multiplexer
g9085 **OEO** Optical Electrical Optical
g9090 **OEOEO** Optical Electrical Optical Electrical Optical
g9095 **OOO** Optical Optical Optical
g9100 **OSNR** Optical Signal-to-Noise Ratio

g9105 **OTU** Optical Translator Unit
g9110 **OXC** Optical Cross-Connect
g9115 **PLC** Planar Lightwave Circuit
g9120 **RMS** Root Mean Square
g9125 **ROADM** Reconfigurable Optical Add-Drop Multiplexing
g9130 **SAN** Storage Area Network
g9135 **SOI** Silicon on Insulator
g9140 **SONET** Synchronous Optical NETworking
g9145 **TEC** Thermo Electric Cooling
g9150 **VCSEL** Vertical Cavity Surface Emitting Laser
g9155 **VOA** Variable Optical Attenuator
g9160 **WSS** Wavelength-Selective Switch
g9165 **WSXC** Wavelength-Selective Crossconnect

s0005 3.07.1 Introduction

p0005 Ubiquitous broadband communication has revolutionized all aspects of our lives in the early 21st century, affecting business and personal commerce, workplace mobility and globalization, military operations and security awareness, information distribution, learning, shopping, and entertainment, leading to unheralded empowerment of the individual. The infrastructure supporting and reliably delivering all this information within and between cities, countries, and continents is based on fiber-optic transport. The significant advantage of fiber-optic transport over alternative methods is its unique ability to carry high bit-rate information streams for substantial distances. This ability is the culmination of decades of research in the field of photonics, providing us with the elements of today's optical communication systems: diverse laser sources, high-speed optoelectronic devices for modulation and detection, low-loss optical fibers, optical amplifiers, dispersion management solutions, and means for multiplexing and demultiplexing many wavelength channels. But as optical communication systems flourished, and branched out further, and with improvements in transport distances and data rates, it became necessary and more economically viable to operate the transport infrastructure as optical networks, as opposed to static optical communication links. Optical networks are remotely managed, able to respond to changes in traffic demand and system conditions, and combine electronic and optical switches at the network nodes. The migration toward optical communication networks requires new components and subsystem elements that provide the functionality to enable the operation of these networks. These elements need to provide the adaptability, reconfigurability, and control to the network at relatively slow rates ranging from approximately a millisecond scale when service protection from failure is concerned to seconds and minutes for monitoring purposes. These requirements fit well with the capabilities of optical microsystems that rely on mechanical motion of micron-scale structures.

p0010 Optical microsystems and microelectromechanical system (MEMS) actuation are highly compatible, as the MEMS feature sizes are comparable in size to the optical wavelength. This compatibility enables interference-based devices to be constructed, and whose response will change significantly for wavelength-scale motion. MEMS brings many of the advantages of macroscopic elements, such as mirrors, shutters, translation stages, and lenses, but on a submillimeter scale. They maintain the performance of their macroscopic counterparts on account of the well-established microfabrication processes that have been developed by the electronics industry. MEMS is a batch fabrication method, driving down cost in mass production. MEMS devices can be highly complex, implementing the functional element that interacts with the optical field, its support structure, actuation mechanism, and alignment features, all with micron-scale resolution and registration. Because the integration complexity is assigned to the device fabrication process, completing the optical subsystem assembly is greatly simplified. The silicon material from which most MEMS devices are constructed can serve to guide the light, as it is transparent in the optical communication wavelength range, or reflect the light after metallization of mirror surfaces. Deployed communication equipment should be compact, lightweight, and robust, which are all attributes of well-designed optical microsystems.

p0015 This chapter provides an overview of the major applications where microsystems can impact optical communication networks. It starts with a review of optical networking that highlights the functional requirements of different network elements where microsystems may contribute. The optics of microsystems, which is based on free-space propagation of single-mode radiation, is examined afterwards.

Microsystem implementations that have been developed for five exemplary applications are subsequently reviewed. The future outlook for optical microsystems is addressed in the conclusion.

3.07.2 Emergence of Optical Networking

What is the difference between optical communications and optical networking? Optical communications has been researched and developed for many decades, and has brought the transport technology to a very mature level. Its fundamental goals are to increase the transmission capacity, the transmission range, and/or the transmission capacity-range product. This has been primarily achieved by utilizing many wavelength channels concurrently on the fiber (a technique known as DWDM or dense wavelength division multiplexing), optical amplification, dispersion compensation, and efficient modulation formats. Optical networking is what happens beyond optical communications, the effective utilization of the transport layer to deliver the connectivity, accessibility, reliability, and survivability at the network level. It is about protocols for access, routing, protection, and restoration, as well as the electronic, optical, and optoelectronic (or photonic) hardware required for implementing it. This new field even has a dedicated research journal inaugurated in 2002 (*Journal of Optical Networking*). Optical networks are customized and optimized for a specific operating environment; a continental-scale backbone network for connecting cities is very different from a neighborhood access network for individual households or from an optical data network within a supercomputing center. Backbone networks, which support the data and voice traffic infrastructure, are required to establish long-term light paths with high availability and fast restoration. Due to their geographical extent, they are the most expensive to deploy and maintain (Fishman *et al.* 2006). Access network are the most price conscientious, due to the economy of scales required for deployment. To reduce deployment and operational costs, access networks utilize passive optical networking strategies (Feldman *et al.* 1998). Computer data networks are designed for communication throughput between supercomputers as well as to mass storage, to maintain the processing cycles active. Such networks operate in accordance to changing resource allocations and demand variations, and can tolerate periodic changes to the topology (Taesombut *et al.* 2006).

Of the broad optical networking categories described above, backbone networks as well as the smaller scale metropolitan networks are most receptive to deployment of components offering adaptability and reconfigurability. There are several reasons for this acceptance. First, these networks are required to operate their communication services with defined restoration speeds stipulated under quality of service contractual obligations. An example for a stringent requirement for maintaining synchronization between two end points communication with SONET (Synchronous Optical NETworking) protocol is a 50 ms restoration of service in the case of interrupts (component failures, fiber cuts, etc.). This level of restoration requires that link and path protection schemes be employed, requiring basic switching elements with millisecond-scale response times. However, such protection schemes increase the network redundancy and cost while reducing the network capacity utilization. By using more advanced network protocols and more capable switching elements, shared path protection plans can be offered with high availability assurances, as the likelihood of multiple network interrupts occurring simultaneously is extremely low. Shared protection also increases the network's capacity utilization, achieving a better return on investment for the service provider (Ye *et al.* 2000). The second reason is related to path provisioning and reconfigurability. As bandwidth demand increases with the introduction of new electronic services, new light paths that traverse the network have to be established to support the increased load. This act of provisioning light paths may sometime include rerouting of existing light paths, to more evenly spread the load across the network links. Provisioning used to be a manual process, and required a technician's visit to every network node. The manual process was also prone to human error, and requires additional visits for verification, all leading to notoriously long provisioning times (measured in months from request to completion) and high operating expenses. By introducing advanced switching elements at the network nodes, remote provisioning from a centralized control center can be performed, reducing the provisioning time to potentially seconds. The third reason is related to the efficient utilization of the fiber transport capabilities. The advances made in transport technology have enabled deployed systems to achieve transmission distances beyond 2000 km. However, most light paths supported by the network have shorter path lengths. (Rent's rule for interconnection lengths applies; the distribution of network light path lengths is inversely proportional to the length. In other words, there

are more short light paths than there are long ones.) Hence, for efficiently using an optical network, light paths carried on specific wavelengths are required to be managed, i.e., extracted and reintroduced at different nodes of the network at the command of the centralized control center. This functionality is known as reconfigurable optical add-drop multiplexing (ROADM). More recently, the ROADM equipment has acquired the additional task of light path link switching at network nodes (Bonenfant and Jones 2003). Finally, a fourth reason for the greater acceptance of adaptable components in backbone networks is that they enable the optical network to operate more efficiently, from transport as well as maintenance points of view. The optical network topography is nonunifirm, having links of different lengths due to the locations of cities and possible mix of optical fiber types. Customized equipment can be placed on the different links to achieve a more uniform response, but inventorying many variants of a certain component is an inefficient solution. Adaptive components can be used instead of carrying many variants, with tunable dispersion compensators as an example. Stockpiling different laser transmitters for compatibility with any DWDM wavelength is another example where inventorying becomes prohibitively expensive. Tunable lasers spanning the entire communication window can be used instead. Balancing the signal levels within the network after changes such as the introduction or extraction of channels maintains the optical network performing at the correct power levels, and is important for maintaining the optical signal-to-noise ratio (OSNR). The price premium for the tunable and adaptable components over fixed components more than pays for itself in performance and operational savings.

p0030 To illustrate the form and functionality provided by optical networks, an exemplary backbone optical network as well as its interface to a metropolitan network is depicted in **Figure 1**. The backbone network is typically of national or continental scale, and serves to interconnect major sites where data needs to be introduced or extracted from the network, typically at major cities. Backbone networks are usually deployed with a mesh architecture, where each network node is attached to its nearby neighboring nodes (typically two to four links fan out per node). The links in a backbone network vary in length with the distribution of the network nodes or cities, and can vary from tens to hundreds of kilometers. In the latter case, optical amplification has to be periodically provided along the link, to maintain the signal strength. An optical in-line amplifier (ILA) is typically inserted for every 60–100 km of optical fiber; the actual distance between amplifiers is a network optimization parameter balancing performance versus cost (closely distributed amplifiers offer better optical signal-to-noise characteristic at the expense of higher amplifier count). The optical amplifier may include additional equipment to balance the optical signals as well as accompanying power taps and a monitor, for maintaining the proper signal strength and network performance. At an optical add-drop multiplexer (OADM) node, most of the DWDM channels typically continue unimpeded in the optical domain while a fraction is selected to be dropped and then added back after data are extracted and new data are introduced. The added and dropped signals are converted between the electrical and optical domains at optical translator units (OTU), which consist of optoelectronic components such as lasers, modulators, detectors, and electronic circuitry. The data in the electrical domain are handled by electronic equipment operating the protocols employed by the networks. This multiservice provisioning platform (MSPP) interoperates with the transport networks, performs grooming and tributary hand-off tasks (splitting, distributing, and combining the fractional data rate signals that make up the aggregate line signal), and enable services such as Ethernet, SAN (storage area networking), ATM (asynchronous transfer mode), GMPLS (generalized multiprotocol label switching), and private line circuits. The MSPP serves as a data gateway between different optical networks, in this case between the backbone mesh network and the metropolitan ring. The metropolitan DWDM ring distributes and collects data to and from its ring nodes, which separate the data streams to finer granularity and serve as gateways to local access networks (not shown in **Figure 1**). The basic OADM architecture is based on a power splitter, which generates two replicas of the signals, one for the drop and one for the channels that will continue through the nodes. A channel blocker prevents those channels that have been selected to be dropped from continuing to the OADM output. This architecture requires a fixed demultiplexer to separate the dropped channels, with deployed OTUs to receive the dropped channels. Such architecture is restrictive because a network reconfiguration is limited on the add and drop sides to specific channels that have OTUs on them, as there is a fixed assignment between the OTU and optical channel due to the fixed optical demultiplexer. An alternative OADM architecture is based on wavelength-selective switches (WSSs) for switching the dropped channels to individual ports.

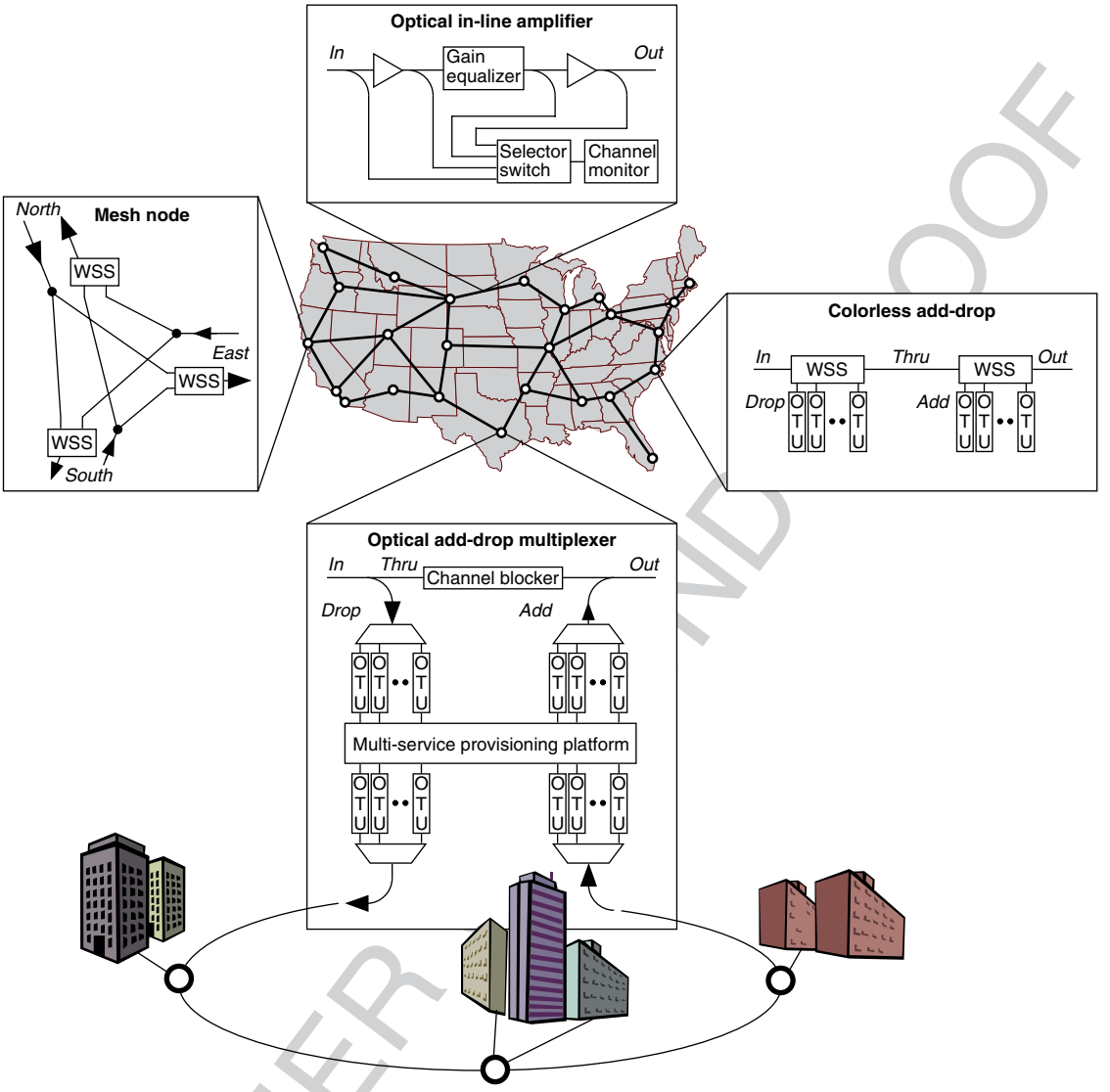

f0005 **Figure 1** A typical continental-scale backbone optical network layout, demonstrating the major functions at mesh switching nodes, add-drop nodes, and its interface to a local metropolitan-scale ring.

This colorless add-drop solution is completely reconfigurable; any wavelength channel can be selected to be dropped to any fiber port. Thus, the fixed association between OTU and DWDM channel is broken, enabling greater flexibility in the network operation and necessitating that OTU support all the DWDM channel on command (the major implication being for the laser transmitter to tune to any channel; detectors have negligible wavelength dependence). The WSS port count has to match the channel drop count, with eight ports typically sufficient for most add-drop sites. The DWDM channels in the backbone mesh network traverse intermediate nodes between their ingress and egress nodes. At these intermediate nodes, the channels are path switched to the proper link that will route the channel to its intended destination. This path switching task at mesh nodes is best accomplished with WSSs, which independently route each DWDM channel to an output port that is assigned to the desired output link. Each input link at the mesh node has a WSS for splitting and combining the channels according to the routing assignment. The WSS port count has to match the node fan-out, with four ports typically sufficient for most mesh nodes.

Many telecommunication components are based p0035 on optical microsystem principles. Some of these are

adaptive, by changing certain optical parameters using MEMS or liquid-crystal (LC) devices. Others are fixed, but still benefit from microsystem construction over other implementations. Some examples of fixed optical microsystems include optical isolators (used to prevent back reflections) and circulators (for separating light propagating in the forward and backward direction), free-space optical multiplexers and demultiplexers (achieve very good thermal stability for outdoor deployment), and spectral filters using thin-film interference (for implementing fixed OADM). Examples of active optical microsystems are fiber switches (small, medium, and large varieties for implementation of various network functions, according to size), variable optical attenuators (required to maintain acceptable power levels impinging on photodetectors), tunable filters (for channel selection in broadcast networks and for optical monitoring), WSSs (for realization of ROADMs), tunable dispersion compensators, and even beam steering mirrors for free-space optical links). The active optical microsystems listed above (and some described in depth in the bulk of the chapter) all exhibit operating speeds in the millisecond timescale. Even though this characteristic speed is much slower than the data bit rate of SONET or packet rate of IP (Internet protocol), it is more than suitable for tracking network changes due to ambient conditions (variations of the network infrastructure due mostly to temperature) and for supporting light path provisioning as well as protection and restoration functions. The component marketplace is flush with competing products and technologies from many companies (~1000 companies present at the largest technical conference and trade show, *Optical Fiber Communications*), all vying for a fraction of the global component sales.

s0015

3.07.3 The Optics of Telecommunication Microsystems

p0040 The optical communications field matured considerably since the days of the first deployment in 1978, in a sequence of several generations. First-generation systems were based on 780 nm GaAs laser transmitters using multimode fibers. The systems were limited to low bit rates due to modal dispersion. Second-generation systems addressed the bit-rate limitations by using single-mode fibers and shifting the operating wavelength to 1300 nm. Modal dispersion is nonexistent when using single-mode fibers, and at 1300 nm chromatic dispersion is minimized in glass (silica) waveguide. However, lacking optical amplifier technology at the time, the communication range became signal-level limited, due to propagation losses at 1300 nm (losses attributed to Rayleigh scattering, which decrease for longer wavelengths). Third-generation systems shifted the operating wavelength to 1550 nm, where the optical fiber exhibits its minimal losses of 0.2 dB km^{-1} (attenuation increases for longer wavelengths due to silica molecular vibration absorption). Many additional advancements have been introduced to create the fourth-generation systems, some of which must be mentioned for completeness: optical amplification allowing for compensation of the fiber's attenuation, DWDM enabling multiple channels to copropagate in the same fiber, dispersion management for reducing chromatic dispersion impairments, advanced optical modulation formats for achieving higher spectral efficiencies, and nonlinear propagation. However, fiber transport largely remains around 1500-nm wavelength over single-mode fiber, which will be the focus of this section (with the exception being in short-haul links and local area networks, where range is less of an issue).

p0045 Realizing optical networks requires integrating many additional components to the transport layer. These components must exhibit low losses, as losses must be compensated for with amplification, which reduces the OSNR. Hence, the design of optical components has to be extremely well engineered to minimize these losses. For components based on interaction with unguided light, or light propagating in free space, which is the case for most optical microsystems described in this chapter, this is especially challenging as the light must radiate out of the input fiber, be manipulated by the microsystem, and then be coupled back into the output fiber. Depending on functionality, the optical microsystem enables the interaction of the MEMS element with the delivered light, in the form of refraction, reflection, diffraction, or absorption. Loss sources can creep up quickly and they are usually cumulative; hence, the microsystem's optical design has to be optimized for high coupling efficiency as well as tolerant of natural component variations, misalignments, and deployment conditions.

3.07.3.1 Gaussian Beam Optics in Free Space

s0020

p0050 The light propagating within a step-index single-mode fiber is confined by the higher core refractive index. The light has a transverse profile given by

radial Bessel functions in the core and cladding regions. However, for optical microsystem design purposes, the precise transverse profile is approximated by a Gaussian one, with an excellent fit at a beam diameter of 10.4 μm at an operating wavelength of 1.55 μm. The advantage of using the Gaussian profile approximation is that it is a solution to the paraxial Helmholtz equation, which describes light propagation in a homogeneous region (Saleh and Teich 1991). Hence, a Gaussian profile shall remain Gaussian as long as it does not encounter nonhomogeneous regions, such as an aperture.

p0055 The Gaussian beam field, $U(x, y, z)$, is described in a Cartesian coordinate system with the propagation direction along the z-axis by

$$U(x,y,z) = U_0 \frac{w_0}{w(z)} \exp\left(-\frac{x^2+y^2}{w^2(z)} - \mathrm{j}\frac{2\pi n}{\lambda} \times \left(z + \frac{x^2+y^2}{2R(z)}\right) + \mathrm{j}\phi(z)\right)$$

where $R(z)$ is the field radius of curvature varying as

$$R(z) = z\left(1 + \left(\frac{z_0}{z}\right)^2\right)$$

$w(z)$ is the beam radius defined by

$$w(z) = w_0\sqrt{1 + \left(\frac{z}{z_0}\right)^2}$$

and $\phi(z) = \tan^{-1}(z/z_0)$ is a phase delay along the propagation direction giving rise to a Guoy phase shift associated with a π phase jump when propagating past the beam waist (**Figure 2**). The beam waist is defined at $z = 0$, and is the location where the beam is at its narrowest spot, a location associated with a minimal beam radius w_0 and an infinite radius of curvature (flat phase front as would appear on a plane wave; however, the field is apodized by a Gaussian envelope). The distance z_0 is known as the Rayleigh length, defined by

$$z_0 = \pi\frac{w_0^2 n}{\lambda}$$

where n is the refractive index of the medium. The Rayleigh length measures the distance from the waist to the location where the beam grows by a factor of $\sqrt{2}$. The Gaussian beam size is symmetric about the beam waist, with the radius of curvature defining whether the beam is converging toward the waist (negative radius of curvature) or diverging from the waist (positive curvature). The fiber mode is approximated by the Gaussian beam with the waist located at the fiber tip. Hence, light radiating out of the fiber diverges, with a Rayleigh length of 55 μm (for air with $n = 1$), and the same parameters have to be satisfied for efficient coupling into a fiber.

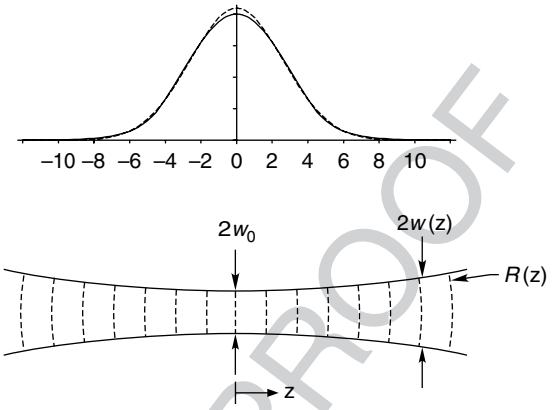

Figure 2 *Top*: The mode shape of the standard single-mode optical fiber (solid line), and its Gaussian approximation of width $2w_0 = 10.4\,\mu\mathrm{m}$ at an operating wavelength of 1.55 μm (dashed line). *Bottom*: A Gaussian beam propagating in free-space, dashed lines show phase fronts. The beam has a minimal waist at location $z = 0$. A Gaussian beam converges toward the waist and diverges afterward. The light radiating out of a cleaved optical fiber is well approximated by a Gaussian beam. f0010

p0060 The Gaussian beam can be manipulated in free space by mirrors, lenses, and prisms. Flat mirrors do not affect the Gaussian beam profile evolution, but do change the propagation direction. Curved mirrors have a lensing effect, with the effective focal length equal to half the mirror radius. Lenses, when treated as thin lenses, change the Gaussian beam radius of curvature by a factor of $F/(F–R)$, where F is the lens focal length and R is the Gaussian beam radius of curvature impinging on the lens. Simple beam relationships can be established with the aid of Gaussian beam propagation formulas and the lens radius transformations for cases of interest such as the maximum throw distance of a lens (i.e., for a given input Gaussian beam and lens focal length, how far and large can a Gaussian beam waist be projected from the lens). Prisms refract light in accordance to Snell's law, and can be used to expand or contract the beam in one direction, converting the circular Gaussian beam to an elliptical profile. Note that the beam propagation calculations can be in the forward or backward directions, and are valid as long as the beam does not encounter an aperture.

3.07.3.2 Misalignment Losses s0025

p0065 A Gaussian beam can be propagated within an aperture less optical microsystem in a lossless fashion, as the

beam propagation does not take into account Fresnel reflections at dielectric interfaces (which can be minimized to ~0.1 dB per interface with antireflection coating), and finite metallic reflectivity (~0.25 dB per reflection). The forward propagation eventually leads to the output fiber end face, where the beam has to couple back into a single-mode fiber. The coupling can be evaluated with the complex ovelap integral between the incident beam wavefront $\varphi(x,y)$ and the fiber mode profile $\phi(x,y)$, which is approximated by the Gaussian distribution, and given by

$$\eta = \frac{\int_{-\infty}^{\infty} \varphi(x,y)\phi^*(x,y)\mathrm{d}x\mathrm{d}y}{\sqrt{\int_{-\infty}^{\infty} \varphi(x,y)\varphi^*(x,y)\mathrm{d}x\mathrm{d}y}\sqrt{\int_{-\infty}^{\infty} \phi(x,y)\phi^*(x,y)\mathrm{d}x\mathrm{d}y}}$$

p0070 The calculated coupling η can yield complex results, leading to spectral phase variations or chromatic distortions. The power coupling, $|\eta|^2$, is typically the quantity of interest and is often expressed in decibel scale $\left(10\cdot\log_{10}\left[|\eta|^2\right]\right)$. When using normalized field distributions, the denominator of the coupling integral is unity. An incident wavefront that exactly matches the fiber mode profile will achieve a power coupling efficiency of one. The coupling integral can be evaluated numerically for any field distribution, and analytically for the Gaussian beam case. It is instructive to inspect the effects of lateral misalignment, angular misalignment, mode mismatch, defocus, and combinations thereof (**Figure 3**). The power coupling in the presence of lateral and angular misalignments is

$$|\eta|^2 = \exp\left(-\frac{x_0^2+y_0^2}{w_0^2} - \frac{w_0^2\pi^2\left(\theta_x^2+\theta_y^2\right)}{\lambda^2}\right)$$

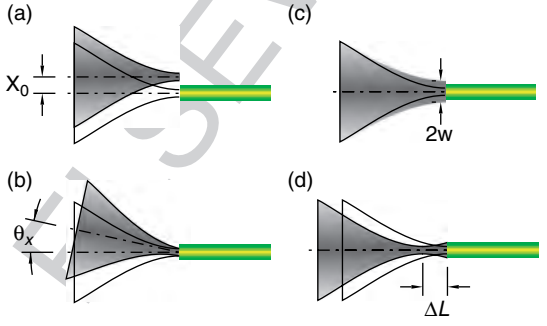

f0015 **Figure 3** Mechanisms for coupling losses into single-mode fiber. (a) Lateral misalignment between incident Gaussian beam and fiber endface. (b) Angular misalignment. (c) Mode-size mismatch. (d) Waist location shift or defocus.

and has Guassian distributions in the lateral misalignment, x_0 and y_0, and angular misalignments, θ_x and θ_y. For single-mode fiber, a total lateral misalignment of 4.4 μm or a total angular misalignment of 4.5° will give rise to a 3-dB penalty (half the power is lost). Because the lateral and angular misalignment dependencies are Gaussian, or quadratic in decibel scale, a factor of $1/x$ improvement in power coupling requires a factor of $1/\sqrt{x}$ tightening in the misalignment. For example, reducing fiber misalignment losses from 3-dB to 1-dB penalty (factor 1/3 improvement) shall require a 2.5 μm lateral misalignment (factor of $1/\sqrt{3}$ tightening). Mode mismatch (different waist size incident on fiber) and defocus (longitudinal displacement of waist location) do not follow a Guassian relationship. The mode mismatch coupling loss, given by

$$|\eta|^2 = \frac{4w_0^2w_1^2}{\left(w_0^2+w_1^2\right)^2}$$

is small for waist variations as large as 20%. The defocus coupling loss is given by

$$|\eta|^2 = \frac{1}{1+\left(\frac{\Delta L}{2z_0}\right)^2}$$

where ΔL is the defocus distance and will provide 80% efficiency (or a loss of about 1 dB) at the Rayleigh distance (55 μm for single-mode fiber).

The coupling integral was evaluated above at the p0075
output fiber end face. However, as the Gaussian beam can be propagated forward as well as backward, the overlap integral can be evaluated anywhere within the optical microsystem. This propagation to a different location within the microsystem is instructive for cases involving a single aperture in the beam path.

3.07.3.3 Beam Clipping Losses s0030

After a Gaussian beam is clipped by an aperture, the p0080
field distribution is no longer Gaussian and the beam propagation formulas provided above are no longer valid. Because all real elements in the beam path have finite extent, we shall define a criterion for a tolerable aperture size for a given Gaussian beam size later in this section. For the instructive case of a single clipping element in the beam path, we can use the forward and backward Gaussian beam propagation technique to meet at the aperture. Consider the configuration shown in **Figure 4**, where the input fiber waist is projected by a collimator lens of infinite

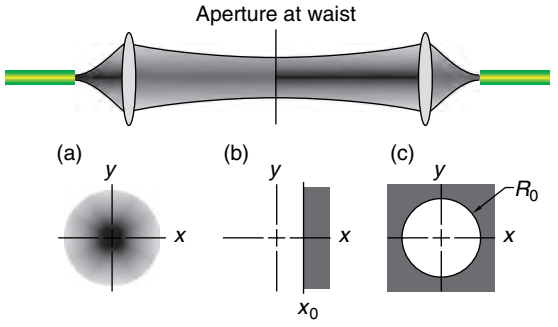

f0020 **Figure 4** *Top*: Imaging arrangement between two fiber endfaces, having a wide collimated beam region in between where optical devices may be inserted. Effect of single aperture in the beam path can be analyzed: (a) circular Gaussian beam profile at aperture location; (b) shutter aperture blocking parts of beam; and (c) circular aperture.

extent to create a secondary waist of size w_1, and a similar collection lens couples the light into the output fiber. The configuration can be properly designed with ideal lenses to deliver a perfect mode to the output fiber with no coupling losses. If an edge shutter is inserted into the beam path at the Gaussian beam waist location, the beam will be clipped by the edge of shutter. The coupling integral can easily be evaluated at the location of the shutter using the ideal Gaussian waist of w_1; the impact of the shutter is introduced by adjusting the integration area. If the edge of the shutter is at position x_0, then beam regions for $x > x_0$ are clipped and the power coupling is given by

$$|\eta|^2 = \frac{1}{4}\left(1 + \mathrm{erf}\left(\frac{\sqrt{2}x_0}{w_1}\right)\right)^2$$

p0085 The power coupling approaches 1 for $x_0 \gg w_1$ (shutter far from interacting with the beam), and approaches zero for $x_0 \ll -w_1$ (shutter blocks most of the beam). It is interesting to note that when the shutter is blocking half the beam (edge is at $x_0 = 0$) the power coupling is 1/4 (or -6 dB). This somewhat surprising results occur because half the beam is clipped (1/2 power lost) and the modal overlap contributes another factor of 1/2. Clipping effects from sharp edges often occur in variable optical attenuators, blockers, and WSSs (see Sections 3.07.4.3 and 3.07.4.5).

p0090 Lenses and other optical elements are oftentimes circular, and will clip the extent of the circularly Gaussian mode. The analysis of a single beam clipped by a circular aperture can be performed in the same fashion as for the shutter edge. Adopting the configuration of **Figure 4**, a circular aperture of radius R_0 is placed at the location of the Gaussian waist of radius w_1. The aperture and beam centers are aligned, and beam regions for $r > R_0$ are clipped, defining a power coupling efficiency of

$$|\eta|^2 = \left(1 - \exp\left(\frac{2R_0^2}{w_1^2}\right)\right)^2$$

The power coupling approaches 1 for $R_0 \gg w_1$ p0095 (aperture far from interacting with the beam), and approaches zero $R_0 \to 0$ (aperture blocks most of the beam). When $R_0 = 1.5w_0$, the fiber coupling loss is nearly lossless at -0.1 dB.

When multiple apertures are present in the beam p0100 path, the analysis becomes much more complex. The Gaussian beam from the input fiber can be propagated until the first aperture. Likewise, the Gaussian mode from the output fiber can be back propagated to the last apertures. Gaussian beam propagation cannot be used for the region between the first and large apertures, and Fresnel propagation must be used instead. Because Fresnel propagation in the presence of apertures is difficult to compute, a design rule has been established stating that if the aperture is 50% larger than the Gausian beam, then clipping effects can be ignored and Gaussian beam propagation can be still be used. When the condition is satisfied $(R_0 > 1.5w)$ the light throughput of the aperture is 99%. Note that the stated condition does not consider any beam to aperture misalignment tolerance, so a slightly more stringent condition might be adopted in practice to avoid clipping effects.

The characterization of optical components p0105 intended for integration into optical communication systems is not complete without procedural tests to ascertain the compliance to generic requirements (GR) put forth by Telcordia, the advising body to the regional service providers in the United States (www.telcordia.com). The two most often cited documents are GR-1209, GR for passive optical elements, which specifies the operating conditions that components must achieve, and GR-1221 that specifies the reliability testing procedures. The listed tests include temperature cycling and temperature and humidity cycling, high-temperature storage, high-temperature and humidity storage, cold temperature storage, vibrational tests, and shock tests. Some of the tests are performed while the device is in operation, others mimic extreme conditions the component may experience in storage conditions. The components have to pass the tests to gain Telcordia compliance certification.

s0035 3.07.4 Exemplary Optical Networking Microsystems

p0110 Of the many possible networking applications for which optical microsystems have been demonstrated, at both the research or development levels, five concerted efforts are reviewed here. For each highlighted application, several microsystem implementations are reviewed, demonstrating the diversity of creativity in the face of a challenging task.

s0040 3.07.4.1 MEMS Tunable Lasers

p0115 Optical communications have been utilizing semiconductor lasers almost exclusively, from early systems lasing at 850 nm and based on GaAs, to modern systems based on InGaAsP and operating at either the 1300- or 1550-nm communication bands. The main advantages of semiconductors lasers for communications are their compactness, high power conversion efficiency, wafer-scale processing, and the capability of direct modulation of the electrical pump current, even though the latter has been abandoned as the communication bit rate has reached $10\,\mathrm{Gb\,s^{-1}}$ due to chirp effects (leading to bandwidth broadening). The basic structure of a laser consists of an optical cavity with a gain section introduced into it. The semiconductor section provides a relatively broad and continuous gain spectrum, whereas the cavity provides finite, equally spaced modes defined by the phase continuity of the cavity round trip travel for specific wavelengths. The basic Fabry–Perot cavity laser, formed from a cleaved section of a semiconductor chip with a waveguiding structure defining the transverse confinement, lases at the multiple longitudinal cavity modes under the gain spectrum. However, lasers for high bit-rate optical communications are required to lase on a single cavity mode only, to minimize chromatic dispersion-induced distortions upon propagation. To limit the laser cavity modes, a filtering component is introduced into the cavity that selects a particular cavity mode while attenuating all others. The cavity filter can be incorporated into the fabrication of the semiconductor chip, by slightly etching or longitudinally modulating the waveguide structure at the cavity ends. This periodic modulation forms a reflective filter for a wavelength component satisfying the Bragg criterion, limiting the lasing to a single frequency in each distributed feedback (DFB) laser.

p0120 DWDM transmission necessitates discrete individual lasers to match the channel numbers in operation by the optical communication system. With DWDM channel counts of few tens to one hundred or more, having unique single-frequency lasers poses a manufacturing, inventory, and management cost to the component manufacturers, system vendors, and network operators. Tunable semiconductor lasers can eliminate the inventory cost and manufacturing variations by having a single laser serve any wavelength used in the communications band on command. The overall cost savings that can be afforded by using tunable lasers should more than offset the price premium for such lasers over their single-frequency counterparts. Optical networking introduces additional functional motivations for deploying full band tunable lasers. New light paths in the network can be established by provisioning an available wavelength channel through intermediary network nodes. Networks can respond to changes in demand patterns due to daily, weekly, or seasonal variations, releasing resources (wavelengths) from one end and reassigning them to others. These scenarios require that the laser transmitter be capable of tuning to any prescribed DWDM channel (Coldren *et al.* 2004).[b0120]

p0125 The earliest tunable lasers utilized thermal tuning of the DFB laser. The DFB laser already incorporates a thermal feedback loop for stabilizing its center wavelength, so providing tunablility by tuning the temperature setting came practically free. However, the possible thermal tuning range of DFB lasers is a few nanometers only, far short of the full communication bandwidth. Full band tunable lasers require greater complexity, and the research community has demonstrated several innovative solutions. The principle behind all the tuning techniques is based on an intracavity filter that can effectively span the entire communication band and select a single cavity mode for lasing. A differentiator among the tuning technique is the tuning speed; physical property variations such as thermal or mechanical requires a few milliseconds or longer, whereas electronic techniques can switch faster than microsecond speed. For the foreseeable future, the relatively slow tuning speed should suffice for applications in optical networking. The faster switching speeds are reserved for optical packet switching applications, which are currently under the exploratory research realm. Slow tunable lasers pose fertile ground for MEMS ingenuity, as exemplified in the following.

s0045 3.07.4.1.1 DFB array selector

p0130 One of the main advantages of single-frequency DFB lasers is that the entire laser is completely integrated on a semiconductor chip, guaranteeing that the laser

cavity is very stable and robust. The laser package is completed after fiber attachment, typically via collimation optics that converts the elliptical laser output mode to the circular fiber mode for efficient coupling and also incorporates an optical isolator to prevent back reflections into the laser. One possible tuning approach is to capitalize on this mature laser technology, and to provide wide-band tuning by fabricating an array of DFB lasers in close proximity, each with an offset center wavelength that can be thermally tuned over a few nanometers. A MEMS switching mirror is placed within the free-space collimation optics and serves to select which waveguide of the waveguide array is coupled to the output fiber (**Figure 5**). Any wavelength can be set by electrically activating the single laser waveguide that can tune to the desired waveguide and thermally tuning the entire chip to the predetermined temperature (Pezeshki *et al.* 2002, Ton *et al.* 2004, Zou *et al.* 2004). The lasing characteristics are similar to those of conventional DFB lasers.

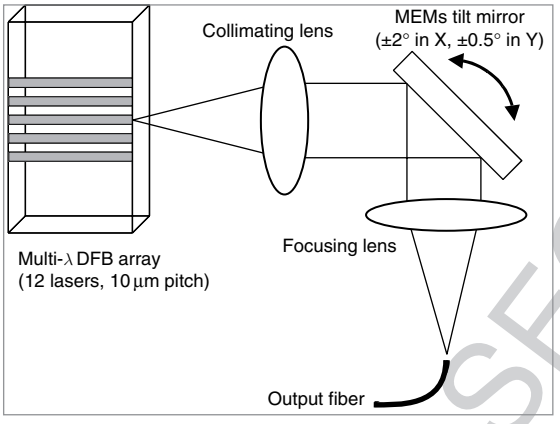

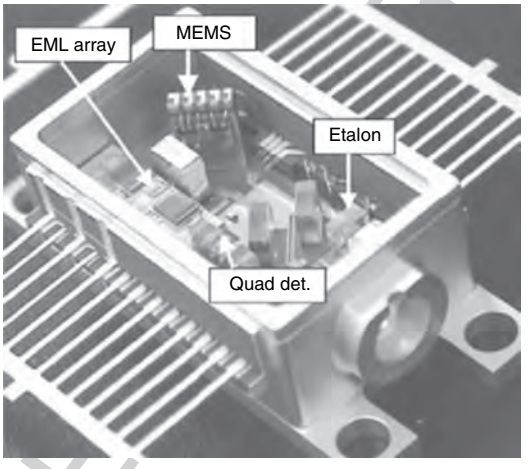

f0025 **Figure 5** Tunable laser using an array of thermally tunable distributed feedback (DFB) lasers and a microelectromechanical systems (MEMS) selector switch. *Top*: Schematic of laser structure. *Bottom*: Packaged laser in standard butterfly package. (Source: Pezeshki B *et al.* 2002 20-mW Widely tunable laser module using DFB array and MEMS selection. *IEEE Photon. Technol. Lett.* **14**, 1457–9, © [2002] IEEE.)

The MEMS micromirror angle is tilted to the p0135
angle that couples the selected output laser from the DFB array to the fiber output and associated optics and isolator. The laser array consists of 12 lasers on a 10-μm pitch, each with a center wavelength shift of 2.8 nm by varying the longitudinal grating pitch. The chip size is similar to that of a fixed wavelength DFB laser, and contains no additional processing steps. To prevent erroneous wavelengths from being emitted from the laser to the optical communication system during the tuning process and thermal settling time, the MEMS mirror is intentionally misaligned from the output fiber during the tuning operation. When tuning is complete, the mirror is adjusted to optimally couple the laser output to the fiber. A 1.5 mm diameter mirror consisting of a gimbaled structure with torsional springs, is fabricated using bulk silicon micromachining, and reaches its maximum deflection angle at 120 V. The MEMS steering mirror can tilt ±2° in the waveguide selection direction, and ±5° in the orthogonal axis. The large mirror tilt range in two axes allows for loose placement of the optical components within the laser package, and using the MEMS mirror for correcting for the placement errors. A feedback loop based on 1% power dither at 50 Hz applied to the mirror maintains the optical alignment and compensates for any possible mechanical drift or creep. Shock and vibration do not influence the wavelength stability of the laser, as the cavity is self-contained within the chip, and only results in coupled output power variations.

The laser chip, MEMS mirror, and all other col- p0140
limation optics and control electronics are packaged in a standard butterfly package, as well as a wavelength locker to provide a feedback signal for the chip heater. The laser module provides 20 mW fiber coupled power, tunable over the entire C-band (greater than 30 nm tuning). A typical ~1 s laser tuning speed is limited by the thermoelectric cooler (TEC) cooling capacity.

3.07.4.1.2 External cavity with grating filter s0050

The DFB laser's small refractive index change limits p0145
their useful thermal tuning range to a few

nanometers. Different filtering techniques must be introduced into the laser cavity to extend the tuning range to cover the entire communication band. When the wide-tuning filtering mechanism cannot be implemented directly on the semiconductor gain chip due to an imcompatibility with the lithographically predefined and rigid cavity structure, external cavity laser architecture can be utilized. In an external cavity laser, the cavity consists of a semiconductor gain waveguide, typically with a cleaved facet mirror on one end and an antireflection coating on the second end, followed by a free-space propagation section with collimation optics to an end mirror defining the cavity. Within the free-space section of the external cavity laser, other tunable filtering elements can be introduced. A tunable external cavity laser can be based on a Littman–Metcalf geometry (b0320 Littman and Metcalf 1978, b0325 Liu and Littman 1981), consisting of a diffraction grating illuminated at near-grazing incidence for angularly dispersing light and a mirror on a rotation block for retroreflecting finite spectral components (**Figure 6**). Continuous tunability is achieved by rotating the mirror and selecting the wavelength that satisfies retroreflection. However, as the cavity supports equally spaced discrete modes, the cavity length typically needs to be minutely perturbed to shift the cavity mode to coincide with the desired lasing wavelength. Moreover, the filter passband has to provide sufficient loss to the adjacent cavity modes to suppress their lasing. Because the cavity mode spacing is inversely proportional to the cavity length and the external cavity

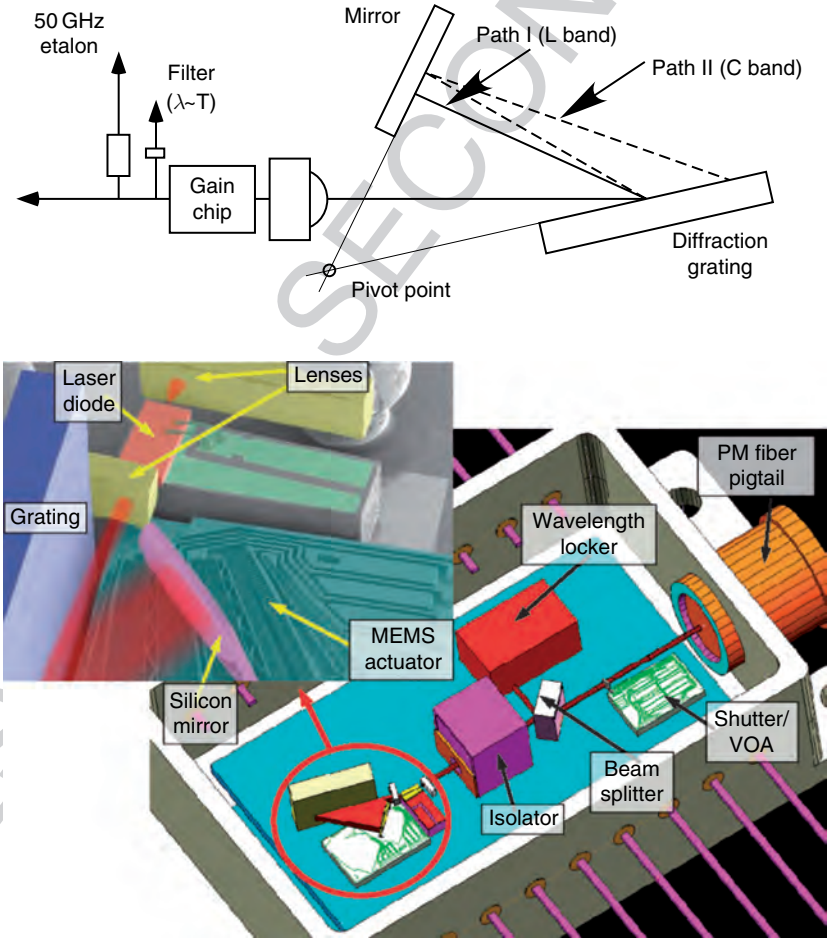

f0030 **Figure 6** Tunable laser with an intracavity grating spectral filter. *Top*: Schematic of laser cavity with rotating end mirror for wavelength selection. *Bottom*: Schematic of packaged laser. *Inset*: Cavity and mirror mounted on microelectromechanical systems (MEMS) actuator. (Source: Anthon D, Berger J D Tselikov A 2004a C+L band MEMS tunable external cavity semiconductor laser. *Optical Fiber Conference (OFC)*, Los Angeles, CA, USA, paper WL2, © [2004] IEEE.)

laser has significant length due to the space necessary for collimation optics and the tunable components, the filter must have narrowband characteristics.

p0150 The retroreflection mirror can be placed on a MEMS rotation block fabricated from 85-μm-thick single-crystalline silicon using deep reactive ion etching (DRIE) (Anthon *et al.* 2004a, b, Berger *et al.* 2001). Multiple comb drives electrostatically rotate the actuator about a virtual pivot point that is at the intersection of the grating and mirror planes. The pivot point placement is critical for mode-hop free tuning per the Littman–Metcalf design, where the mirror rotation is accompanied by displacement for maintaining the overlap of the cavity mode and the filter center wavelength. In practice, and especially for full communication band tuning range, additional controls need to be added for controlling the cavity mode locations. Cavity length control is provided by a piezoelectric actuator that translates the diffraction grating. To reduce the mirror's angular rotation range requirement, which is directly related to the filter's tuning range, a double reflection–diffraction arrangement is used (the light diffracts from the grating toward the mirror, reflects back to the grating, diffracts a second time from the grating and then in incident on the mirror at retroreflection for the center wavelength). The double reflection–diffraction arrangement also increases the cavity length, which decreases the cavity mode spacing, but the double diffraction generates a narrower filter passband that more than compensates for the tighter mode spacing. The MEMS actuator rotates the mirror $\pm 2.8^\circ$ for 140 V driving voltages, providing at ± 2.5 THz laser tuning range, easily covering the communication band. Because both the cavity and the tuning element are defined by the large rotating end mirror, vibrational sensitivity of the cavity is a major concern with this design.

p0155 The laser can be tuned continuously and mode-hop free with simultaneous control of the mirror rotation angle and grating position. However, in an optical networking environments the laser cannot emit light during tuning to prevent interference with other signals. This can be addressed by adding a MEMS optical shutter between the laser cavity and the optical fiber to blank the signal during tuning. Additionally, a wavelength locker is used to provide a feedback signal necessary for wavelength tuning the laser with the MEMS and piezoelectric actuators. Laser tuning is complete in less than 15 ms, and the laser's wavelength locker ensures stable long-term operation.

3.07.4.1.3 Vernier thermal etalons s0055

A different approach to tuning an external cavity laser p0160 is demonstrated by utilizing dual silicon etalons within the cavity (Finot *et al.* 2004, McDonald *et al.* 2006). The standard external cavity layout is formed with a semiconductor gain chip (one facet used for the cavity end mirror and the other antireflection coated) and a second mirror in the free-space region. The cavity mode selection is accomplished by the cascaded filtering response of the two etalons that are inserted within the free-space region (**Figure 7**). Each etalon, fabricated from a polished silicon wafer of unique thickness, has a transmission function consisting of a frequency comb. The comb spacing is determined by the etalon thickness, and as the silicon etalon is much shorter than the laser cavity length, its modes are spaced much wider apart. The etalon comb mode widths and position are determined by the etalon reflectivity, or finesse (see Section 3.07.4.2 for definition), and etalon phase – the desired reflectivity achieved by proper coating of the silicon and the etalon phase controlled by thermally tuning the silicon's refractive index. Because the two etalons are slightly different in width, their cavity mode spacing is also slightly different. The etalons are engineered such that their spacing difference and finesse ensure that only a single etalon mode overlaps over the laser gain spectrum. This Vernier effect tuning determines the desired lasing wavelength, and allows the dual etalons to cover a wide bandwidth with only a small cavity mode shift. Finally, for the laser to operate at this overlap peak, it must also coincide with one of the laser cavity's modes. The laser cavity's modes are tuned by varying the cavity phase with a lithium niobate crystal.

The silicon etalons are fabricated using wafer-level p0165 MEMS processing, even though the etalons have no moving parts. A polished silicon-on-insulator (SOI) wafer is used to define the silicon disks that form the etalons. The silicon handle on the backside is removed and the disk is suspended with a SiN membrane in tension. The etalon is thus thermally isolated from the handle, reducing the heating load required to stabilize its temperature. The fundamental resonance frequency of the silicon and membrane is above 10 kHz. The etalons have integrated heaters and temperature sensors formed by two Ti/Pt conductors tracing the etalon's optical aperture circumference. Heating is achieved by the power dissipation from the heating conductor, and the temperature is sensed by circuitry that registers the resistance of the second conductor, which depends on the etalon temperature. A 30°C temperature rise is achieved with 15 mW power

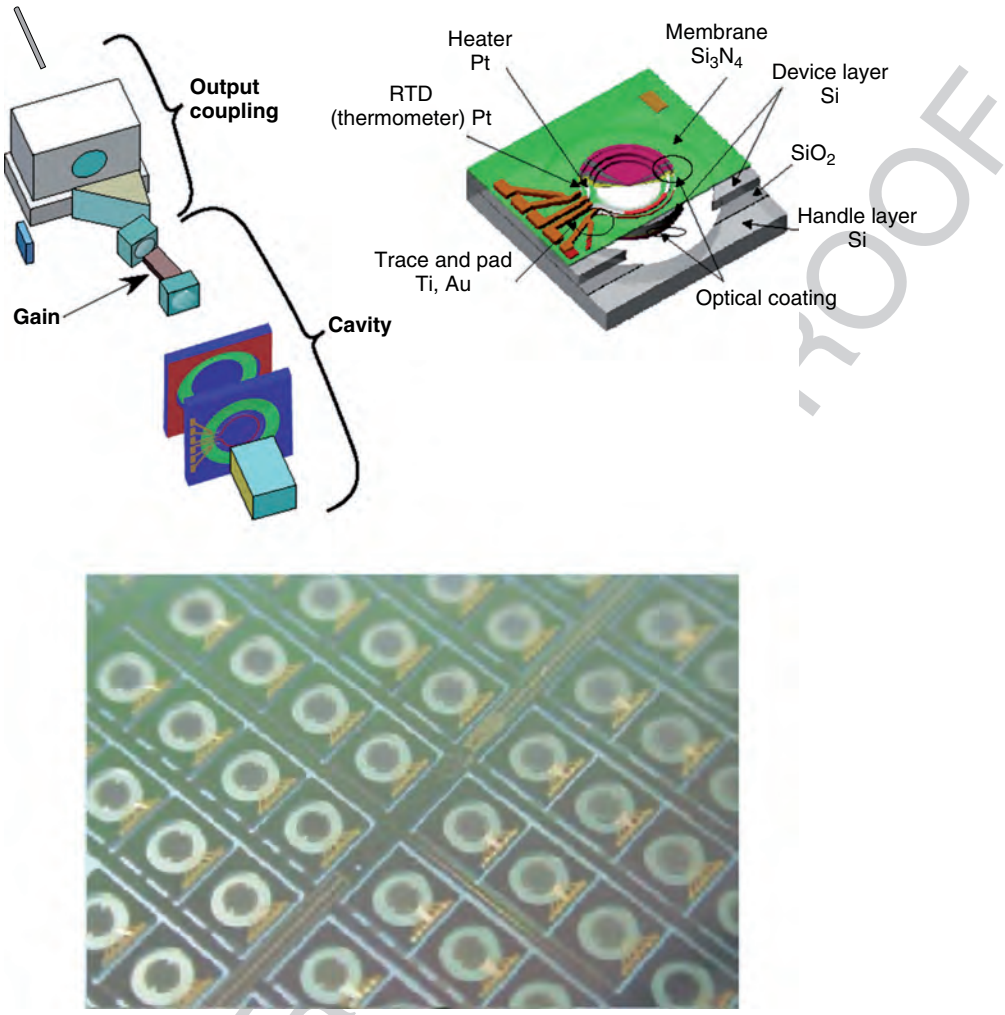

f0035 **Figure 7** Tunable laser with intracavity thermally tuned etalon filters. *Top-left*: Schematic of laser cavity with two filters. *Top-right*: Details of thermally tuned silicon microfabricated etalon filter. *Bottom*: Wafer-level batch fabrication of filters. (Source: Finot M *et al.* 2004 Automated optical packaging technology for 10 Gb/s transceivers and its application to a low-cost full C-band tunable transmitter. *Intel Technol. J.* **8**; McDonald M *et al.* 2006 Wavelength filter with integrated thermal control used as an intracavity DWDM laser tuning element. *IEEE Optical MEMS Conference*, Piscataway, NJ, USA, © [2006] IEEE.)

dissipation. The thermal time constant, determined by the resistance and thermal mass of the etalon, is under 1 s. The etalon's finesse is achieved with a four-layer reflection coating.

p0170 The stability and repeatability of the etalon's response allows the etalon to serve as the wavelength reference for the laser. Laser tuning is performed by heating the two etalons to the prestored values and then adjusting the cavity phase to maximize the lasing power. The cavity phase is determined by a peak-locating algorithm with electro-optical dithering of the lithium niobate modulator. Because the inter cavity etalons serve as the wavelength reference, no wavelength locker is necessary after the laser. Moreover, the etalon wavelength tuning can be performed without lasing, so the laser cavity can be tuned in the dark state and turned on with the pump current when the temperature has settled, eliminating the need for an additional shutter.

3.07.4.1.4 Tunable cavity VCSEL

s0060 p0175 If placing a filter in an external cavity is challenging, why not do away with it entirely? VCSEL (vertical cavity surface emitting laser), in contrast to the aforementioned edge emitting lasers, have a vertical optical cavity that enables different laser designs,

fabrication sequences, and beam characteristics. VCSELs are fabricated in a single epitaxial growth sequence, starting from a bottom distributed Bragg reflector (DBR), a semiconductor gain section, followed by a top DBR mirror, resulting in a short pillar laser geometry. The DBR consists of many alternating layers of lattice-matched materials; the large number of layers is required to achieve high reflectivity from materials with similar refractive indices. The high reflectivity is crucial for reducing the cavity losses, as the small gain available from the short gain section must be larger than the losses to support lasing. The short cavity length implies that the cavity modes are spaced widely apart, and typically only a single cavity mode exists within the gain bandwidth. Hence, no mode-selection filter is required in a VCSEL. Other advantages VCSEL offer are wafer-level inspection, as the laser emits out of plane, circular beam modes compatible with optical fiber mode, and 2D array geometries important for some applications. Conversely, their output powers are much lower than those of the DFB laser, and heat removal is challenging due to their pillar structure leading to high thermal resistance.

Tunable VCSEL can be realized by thermally changing the refractive index or by changing the cavity length. Thermal tuning is compounded by the laser's inherent thermal resistance, and cavity length changes are incompatible with the monolithic pillar structure. By introducing an air gap into the cavity and integrating a MEMS actuator with the top mirror, the cavity length and lasing wavelength can be directly tuned (**Figure 8**). Many variations on this theme have been reported in the scientific literature: using a flat mirror

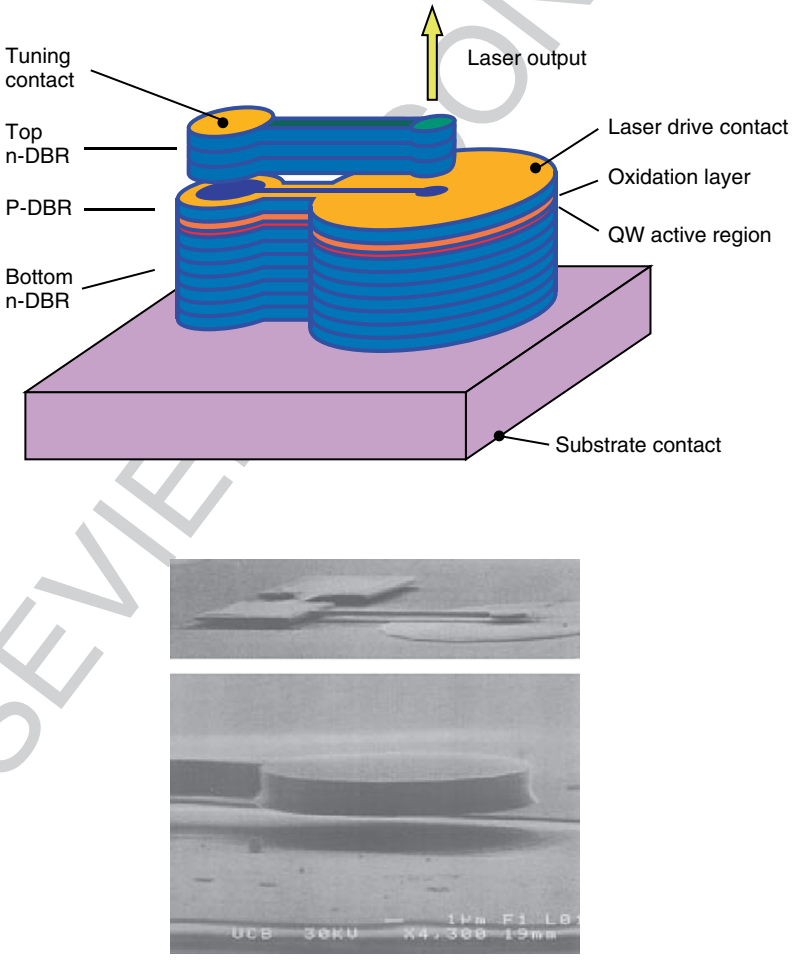

Figure 8 Tunable vertical cavity surface-emitting laser (VCSEL) with cavity length modulation. *Top*: Schematic of piston-motion VCSEL. *Bottom*: Top mirror mounted on piston motion actuator. (Source: Chang-Hasnain C J 2000 Tunable VCSEL. *IEEE J. Select. Top. Quant. Electron.* **6**, 978–87, © [2000] IEEE.)

versus a curved mirror, suspending the movable mirror with a continuous membrane versus a symmetric beam support structure or a cantilevered beam, electrostatic versus thermal actuation, one- and two-chip laser assemblies, and electrical or optical pumping of the laser. Each variation has its unique traits, but all share the principle that the cavity tunes by adjusting the air gap regions (Chang-Hasnain 2000, Kner *et al.* 2003, Li *et al.* 1998, Sugihwo *et al.* 1998, Tarraf *et al.* 2004, Tayebati *et al.* 1998).

p0185 As an exemplary VCSEL design, an electrically pumped, single-chip laser depicted in **Figure 8** is described. The entire laser is grown in one epitaxy run. The DBR mirrors are fabricated from a GaAs–AlGaAs heterostructure, and an InGaAs active region. An oxidation layer serves as a current guide, for effective electrical pumping of the gain region. The top mirror is suspended with a cantilever beam from a large, parallel plate electrostatic actuator. Because the actuator is physically decoupled from the laser section, its design can be optimized for operation at low voltages (<30 V), with a reported switching time of 1–10 ms. The mirror can displace up to a 1/3 of the initial gap size, with the lasing wavelength shifted toward shorter wavelengths as the gap size decreases upon actuation. The laser utilizes a wavelength locker for stabilizing the mirror position and emission onto the DWDM grid. The VCSEL can be directly modulated via the injection current at 2.5 Gb s^{-1} and the signal carried with a small impairment for 100 km on single-mode fiber, making it suitable for metropolitan-scale networks. However, the laser had a reported limited tuning range of ~10 nm in the 1.55 μm communication window and DC power levels approaching 1 mW. It should be noted that optically pumped VCSEL can exhibit a tuning range spanning the entire communication window and higher output powers, as less heat is generated at the active region (heat removal associated with electrical pumping remains an issue with VCSELs).

s0065 ## 3.07.4.2 MEMS Tunable Filters

p0190 Fourth-generation DWDM optical communication systems achieve increased capacity through efficient utilization of the optical fiber bandwidth by multiplexing many wavelength channels. Optical networking uses the foundation of DWDM optical transport to interconnect geographically dispersed end users. The role of the optical network is to provide communication conduits at high or guaranteed availability between any two end points wanting to exchange information. An early optical network prototype based on DWDM used a broadcast-and-select topology (Dono *et al.* 1990). Each network user is distinguished by a unique laser wavelength, and all users transmit their signals simultaneously into a common fiber distribution network. An end user can select a communication partner by tuning his receiver to the wavelength corresponding to the desired transmitter. The receiver tuning is accomplished by placing a tunable filter in front of the optical detector. The filter permits the desired wavelength channel to go through, while blocking all the other DWDM channels. This early broadcast-and-select network topology could not support many users or reuse wavelength, and did not offer any security measures. More advanced network prototypes ensued (Kaminow *et al.* 1996), providing routing and wavelength management features present in modern networks, while continuing to advocate for tunable receivers. In today's deployed optical networks, both at the core and metro levels, tunable channel selection filters are not used for establishing connections (that task is performed by reconfigurable add-drop filters with WSSs). However, as fiber network venture deeper into access network and eventually to individual homes, tunable filters may once again be considered as they are the least expensive wavelength-tunable element. Other uses for tunable filters in today's networks are primarily for system monitoring. It is imperative to maintain the operational parameters of optical networks, and track any deviations from them. This is typically accomplished by tapping a fraction of the optical signal, and scanning the optical bandwidth with the filter to monitor the presence and power level of all channels in the fiber.

p0195 MEMS technology is very attractive for implementing tunable filters, as most tuning mechanisms are based on motion. Other competitive technologies do exist; however, the wide tuning requirement for spanning the entire communication window is typically more challenging for these alternative technologies. The tunable filter structures most commonly implemented using MEMS can be categorized by function: tunable resonant devices, deformable gratings, and spatial filters of spectrally dispersed light.

s0070 ### 3.07.4.2.1 Tunable resonant devices

p0200 One of the simplest and well-known spectral filters is the Fabry–Perot interferometer or etalon, comprised of two partially reflective and mutually parallel surfaces separated by a finite gap. The transfer function of

the Fabry–Perot etalon consists of narrow spectral peaks with unity transmission; the complementary reflectance consists of the entire spectrum except for narrow spectral notches. The transmission/reflection is periodic in frequency, with the frequency period denoted by the free spectral range, $\mathrm{FSR} = c/(2d)$, where d is the etalon gap and c is the speed of light in vacuum, under the assumption that the gap region refractive index is unity (air) and under normal incidence. A transmission peak occurs whenever the round trip path length is equal to an integer multiple of an optical wavelength; hence, it is said to be resonant when the condition is satisfied. The half-width, Δf, of the Fabry–Perot etalon spectral peak is determined by the mirror reflectivity, R, and is defined by

$$\Delta f = \frac{c(1-R)}{2\pi d\sqrt{R}}$$

p0205 Narrow peak widths, which are necessary for channels isolation in DWDM, are achieved when the reflectivity approaches unity. The dimensionless ratio of the FSR to the half-width Δf is denoted by the finesse, $\mathcal{F}$, of the etalon and is given by

$$\mathcal{F} \equiv \frac{\mathrm{FSR}}{\Delta f} = \frac{\pi\sqrt{R}}{1-R}$$

p0210 The finesse measures the resolving power of the etalon, and is strictly determined by the mirror reflectivity. Locations of the transfer peaks are shifted by adjusting the gap separation. The FSR periodicity is inherent to resonant structures and is an undesirable feature when one wants to select a signal channel from the communication bandwidth. To overcome this effect, a telecom Fabry–Perot filter is constructed with a very narrow gap, which has a correspondingly large FSR. The requirements that need to be satisfied are that the FSR be larger than the communication bandwidth – to eliminate the periodicity within the bandwidth – and that the resolving power is sufficient to perform channel selection, implying that the gap region be on the order of a few wavelengths and that the mirrors have high reflectivity. The gap size as well as the mirror displacement requirement suggests that MEMS devices are well suited for construction of the etalons. MEMS Fabry–Perot etalons have been demonstrated in both in-plane and surface-normal arrangements (**Figure 9**). The latter is more common, as it is easier to fabricate using surface micromachining processes, and high mirror reflectivity is achieved by metallization and/or multilayer coatings. The actuation of one of the etalon's end mirrors is typically achieved with electrostatic forces or thermal bimorph displacement. The high finesse values that can be achieved with high-quality mirrors in the surface micromachining processes results in narrow transmission peaks. The MEMS surface micromachining diversity of material systems is demonstrated in the reported Fabry–Perot implementations in silicon (Niemi *et al.* 2001[b0085], GaAs (Amano *et al.* 2000[b0020], Kim *et al.* 2003a[b0265]), InP (Daleiden *et al.* 2002[b0125]), and elastomers (Blake 2003[b0080]). In-plane Fabry–Perot implementations are based on DRIE in a thick SOI wafer (Yun *et al.* 2003[b0620]). The two etalon mirrors are formed by etching vertical sidewalls in the silicon, one of which electrostatically actuates toward the other for tuning, and achieving relatively low finesse due to the low Fresnel reflectivity between silicon and air. Because it is difficult to metalize the vertical mirrors, the reflectivity can be enhanced by etching multiple vertical mirrors satisfying the Bragg criterion (Lipson and Yeatman 2005[b0315], Saadany *et al.* 2006[b0450]). To achieve a significant reflection enhancement from the multiple reflectors, the surface quality of the vertical mirrors has to be improved after the deep etch process. The tuning speeds for electrostatic mirror actuation are typically submilliseconds, with a few volts required for submicron motion necessary for tuning across the communication band. Thermal bimorph actuation requires longer settling times, and consumes power in maintaining a filtering wavelength. Narrowband thermal tuning can also be used for modulating the refractive index of the gap region of a solid Fabry–Perot filter, as demonstrated with a silicon ridge waveguide with etched Bragg end mirrors (Angulo Barrios *et al.* 2004[b0025], Yun 2003[b0615]). However, with extreme temperature tuning (up to 450°C), 41.7 nm was achieved for a silicon Fabry–Perot membrane with dielectric Bragg mirrors (Hohfeld and Zappe 2005[b0235]).

p0215 A second category of resonant filters is implemented with microrings or microdisks disposed between two optical waveguides. Both the microdisks and microrings support propagation modes; in the microring case these modes are those of the curved waveguide structure, whereas in the microdisk case the propagation modes are azimuthal and are commonly termed whispering gallery modes (**Figure 10**). Each of the waveguides can couple energy into the microdisk/ring evanescently. The microdisk/ring form a recirculating cavity for the propagating light, and a resonance condition occurs when propagation around the disk/ring is an integer multiple for a certain wavelength of light. If the light coupled into the microdisk/ring from the input waveguide does not

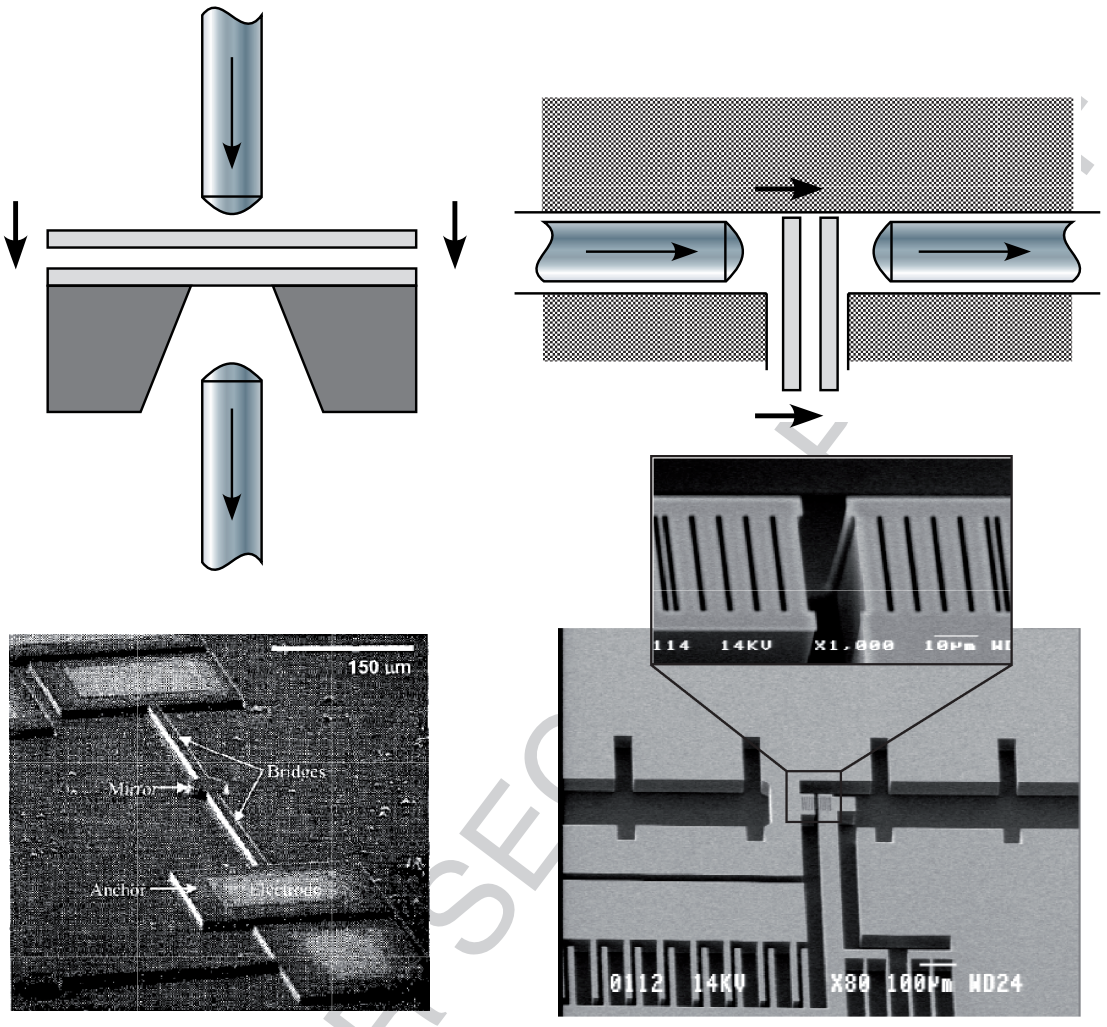

f0045 **Figure 9** Fabry–Perot tunable filters. *Left*: Surface-normal arrangement and implementation. (Source: Kim C-K *et al.* 2003a 47 nm Tuning of thermally actuated Fabry–Perot tunable filter with very low power consumption. *IEEE Optical MEMS Conference*, Hawaii, HI, USA, © [2003] IEEE.) *Right*: In-plane arrangement and implementation. (Source: Saadany B *et al.* 2006 Electrostatically-tuned optical filter based on silicon Bragg reflectors. *IEEE Optical MEMS Conference*, Piscataway, NJ, USA, © [2006] IEEE.)

satisfy the resonance condition, the light will also couple out to the same waveguide and continue to propagate on the same input waveguide unimpeded. However, if the light does satisfy the resonance condition, the light will couple into the microdisk/ring from the input waveguide, and likewise will couple out of the disk/ring onto the second, drop waveguide. As in the Fabry–Perot case, the microdisk/ring bandwidth will be determined by the coupling coefficient into the cavity (similar to the partial reflectivity of the etalon), and the path length around the disk/ring. Moreover, the resonance condition is satisfied periodically in frequency, giving rise once again to a free spectral range. Their ratio is the characteristic quality factor, or Q, of the resonator. Because it is desirable to have only one resonance peak within the communication bandwidth, the microdisk/ring diameter is reduced to the order of a few microns. The described microdisk/ring resonators are fixed structures, and have been extensively explored for passive filtering applications. The operation of the microdisk/ring can be modulated by controlling the coupling into the resonator, as has been demonstrated by moving freely suspended waveguides closer to the microdisk (Lee *et al.* 2005), or by reducing the resonator's quality factor, as demonstrated by a metallic plate approaching the cavity and increasing the cavity's propagation losses (Nielson *et al.* 2005). A thermally wavelength-tunable and MEMS bandwidth-tunable microdisk cavity has been demonstrated on a silicon substrate.

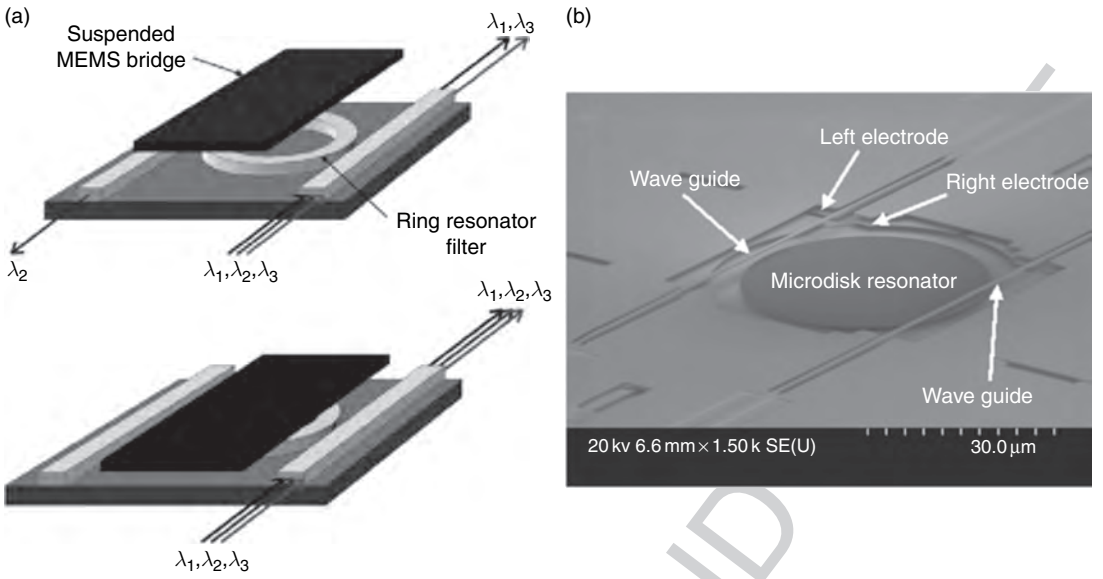

f0050 **Figure 10** Microring and microdisk resonant filters. (a) Fixed-wavelength microring with modulation provided by inducing resonator losses by a metallic plate interacting with the light upon proximity. (Source: Nielson G N *et al.* 2005 Integrated wavelength-selective optical MEMS switching using ring resonator filters. *IEEE Photon. Technol. Lett.* **17**, 1190–2, © [2005] IEEE.) (b) Micrograph of microdisk with moving waveguides to control coupling coefficient. (Source: Yao J *et al.* 2005 Wavelength- and bandwidth-tunable filters based on MEMS-actuated microdisk resonators. *Optical Fiber Conference (OFC)*, Anaheim, CA, USA, paper OTuM1, © [2005] IEEE.)

Heaters placed near the microdisk increase its refractive index and coupling to the resonator with electrostatic attraction provides a tunable passband between 12 and 41 GHz (Yao *et al.* 2005).

p0220 A final class of a tunable resonant devices is based on a thin waveguiding slab with a grating pattern formed on top (Rosenblatt *et al.* 1997). When such a structure is illuminated with an incident light beam, part of the beam is directly transmitted through the structure and part is diffracted by the grating and is trapped in the waveguide layer. Some of the trapped light in the waveguide layer is then diffracted out so that it interfaces destructively with the transmitted part of the light beam. At a specific wavelength and angular orientation of the incident beam, the structure resonates; namely, complete interference occurs and no light is transmitted. For wavelength tuning purpose, the resonant filter is attached to a MEMS tiltable platform (Niederer *et al.* 2004). The reflected wavelength is tuned by changing the angle of incidence of the resonant grating filter. The grating is patterned by holographic recording and dry etching. The demonstrated filter worked over a wavelength range of 1520–1580 nm with a 0.5 nm half-width for a single polarization. The MEMS platform is DRIE processed, and electrostatically actuated over ±4° with a driving voltage of about 60 V. Alternatively, a modulated resonant grating structure has been demonstrated, in which a thin suspended silicon layer is etched with the grating structure (Kanomori *et al.* 2006). The gap separation between the patterned silicon layer and the underlying silicon can be controlled with bimorph actuators, resulting in a disruption of the resonant guiding. The silicon layer was patterned in two dimensions, resulting in polarization-independent operation.

3.07.4.2.2 Deformable gratings

s0075 p0225 A grating-based spectral filtering arrangement utilizes the dispersive property of diffraction to collect a finite bandwidth of light by an aperture, such as an optical fiber. The bandwidth captured by the fiber is a design parameter, influenced by the grating frequency and spatial dispersion. One method for wavelength tuning the filter is to change the grating frequency. The change in grating frequency changes the spatial dispersion, resulting in a different center wavelength impinging on the collecting fiber. Changing the grating frequency is typically impractical, as bulk gratings have fixed ruling. A tunable grating frequency can be achieved by implementing the diffractive element as a movable sequence of grating lines with a constant periodicity that can be continuously changed. The constant periodicity property is important for a

uniform diffraction response resulting in high resolving power; without this uniformity, the filtering response would broaden. Therefore, MEMS tunable grating frequency designs implement identical support structures for the grating elements, such that the displacement is uniformly distributed (**Figure 11**). The displacement can be achieved by thermal expansion of the inter elements' support structure (Zhang and Liu 2000), strain distribution by spring structures upon electrostatic actuation applied to the end point (Torman *et al.* 2006), and distributed expansion by a piezoelectric effect of the support structure (Wong *et al.* 2004). Both the electrostatic and piezoelectric actuation mechanisms achieve submillisecond actuation speeds. An alternative tunable grating frequency implementation uses independent analog control of the position of each of the grating elements (Li *et al.* 2006). The moving elements are blazed at an angle to achieve high diffraction efficiencies, using a process that combines KOH etching and DRIE to realize mirror surfaces with a root mean square (RMS) roughness of 26 nm and stiff structures that resist out-of-plane bending. An optical experiment using the tunable blazed grating with a small number of elements demonstrated their basic filtering functionality. The challenge in using this approach is associated with the scaling to a large number of grating elements, required for high-resolution filtering.

A different technique for controlling the diffraction response of a grating utilizes a 1D micromirror array, where each micromirror can piston out of plane for phase encoding. The independently controllable phase modulators can be set to coherently direct light of a certain frequency to a diffraction direction (Belikov and Solgaard 2003, SasBerg *et al.* 2003). Various synthesis techniques can be employed for designing different filter response functions as a rectangular frequency response. Such filters use very large mirror arrays with simple piston-motion functionality for achieving high-resolution filtering. The 1D phase modulator can also be placed within a cavity to form a segmented Gires–Tournois interferometer (Yu and Solgard 2004). The back reflection plane of the traditional interferometer is replaced with the 1D micromirror array for phase modulation, resulting in both amplitude and phase control for

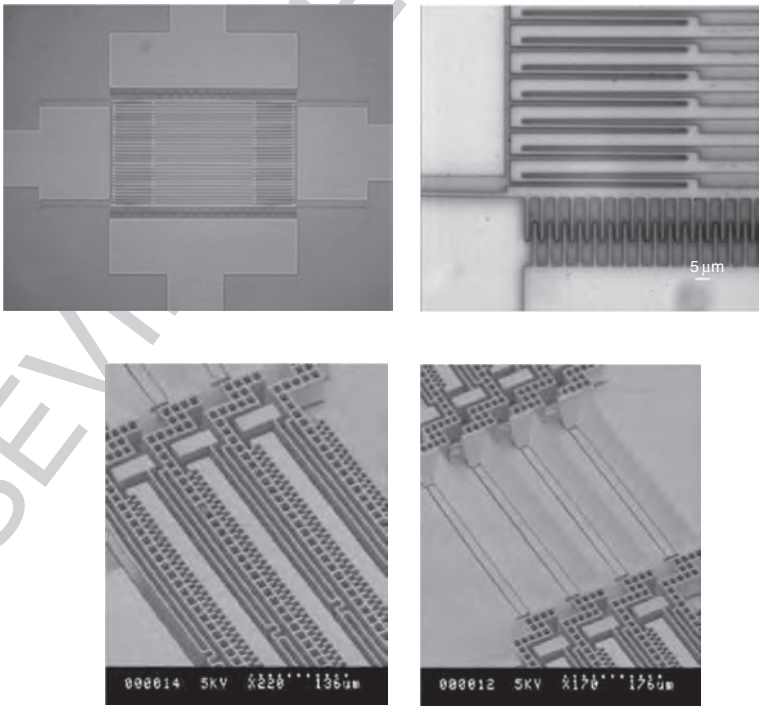

Figure 11 Deformable gratings. *Top*: Micrographs of electrostatic tunable grating frequencies with spring details on right. (Source: Torman M *et al.* 2006 Deformable MEMS grating for wide tenability and high operating speed. *J. Opt. A Pure Appl. Opt.* **8**, S337–40, © IOP.) *Bottom*: Tunable grating with independent motion of each grating element. (Source: Li *et al.* 2006 Tunable blazed gratings. *IEEE J. Microelectromech. Sys.* **15**, 597–604, © [2006] IEEE.)

each micromirror reflection. Collecting all the mirror reflections and performing an optical spatial Fourier transform results in a transfer function for the device that has the same form as a transversal filter in digital signal processing. Thus, conventional filter synthesis techniques can be used for tailoring the filter's bandpass as well as chromatic dispersion.

s0080 ### 3.07.4.2.3 Spatial filter of spectrally dispersed light

p0235 The most common technique for wavelength tuning a grating and lens-based filter is by changing the tilt angle of the grating, resulting in a shift of the spatial dispersion and a selection of a different center wavelength impinging on the collecting fiber. However, as high-quality gratings utilize thick and thereby heavy substrates for stability, they are not compatible with MEMS actuation. However, a shift of the spatial dispersion can be similarly accomplished by a tilting micromirror inserted in the beam path (Berger *et al.* 2003). The resultant passband shape when coupling spatially dispersed light into a single-mode fiber is Gaussian, and the reported implementation achieved a 32 GHz–3 dB bandwidth, tunable over 40 nm. Similar implementations have achieved wider tuning with correspondingly wider passbands as well, demonstrating the interplay between resolving power and tuning range (Kimura *et al.* 2004). The collecting fiber can also be replaced with an apertured photodetector, for implementing a complete tunable receiver (Berger *et al.* 2004). While angle tuning of a bulk grating is difficult to implement in MEMS technology, thin-film filters are much more compatible. A thin-film filter with a 200 GHz bandpass response was mounted on a thermally actuated MEMS rotation stage (Unamuno and Uttamchandani 2005). The measured mass of the filter was 6 g, and the MEMS rotation stage achieved 1.5° rotation for a 700 mW power draw. However, thin-film filters have weak angular tuning range, in the reported case of 100 GHz only.

p0240 The Gaussian passband shape associated with the direct coupling of dispersed light to a single-mode fiber is often undesirable. An alternative approach often utilized by WSSs and blockers (see Sections 3.07.4.5 and 3.07.4.5.1) is that of dispersing the light with a grating and filtering by a finite mirror, followed by the reverse process of combining the spectral components with the same grating and coupling to the fiber. The double passing of the grating (first to disperse and second to recombine) removes any frequency dependence for spectral component beams striking the mirror far away from the mirror edges. A filter with tunable passband width and center frequency has been demonstrated using this approach together with a MEMS tilt mirror (Wilson 2006). The MEMS mirror shifts the spatially dispersed light that is incident on the spectral mirror (**Figure 12**). The reflective spectral mirror in this case is triangular, chosen to select the passband width. The center frequency of the tunable filter is selected by shifting the dispersed light along the axis of the dispersion. The passband width of the tunable filter is chosen by translating the dispersed light in the orthogonal direction, such that the dispersed light encounters a broader or narrower segment of the triangular mirror. This filter can also operate in hitless mode, which is a unique distinguishing feature compared to all the above filters. Hitless operation is important for channel add-drop, where the act of channel tuning cannot cause a disruption to the intermediate channels. The MEMS micromirror has to tilt a broad beam in the filter implementation due to resolution requirements, and the experiment used a magnetically actuated mirror with an aperture of 4.5 mm × 6 mm, with an angular range of ±1.5° for a ±2.3 V drive. The filter demonstrated wavelength tuning over 36 nm, and passband width settings from 28 to 210 GHz, with a 4.6 dB insertion loss. Transmission experiments with 10 Gb s^{-1} data rate signal showed negligible power penalty due to the grating double passing arrangement.

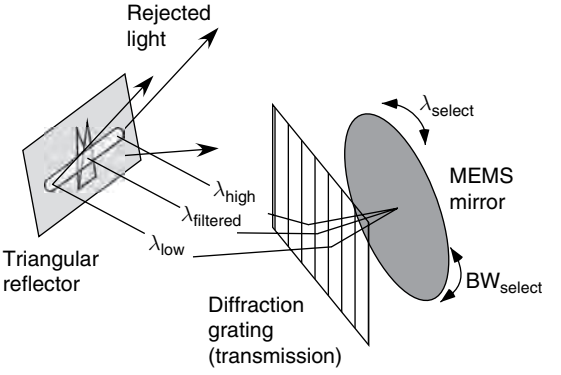

f0060 **Figure 12** Wavelength and bandwidth tunable filter. Spatially dispersed signals can be scanned with microelectromechanical systems (MEMS) mirror in left–right direction to select wavelength and up–down to prescribe bandwidth. (Source: Wilson G 2006 Spectral passband filter with independently variable center wavelength, bandwidth. *IEEE Photon. Technol. Lett.* **18**, 1660–2, © [2006] IEEE.)

s0085 ### 3.07.4.3 MEMS Variable Optical Attenuators

p0245 Terrestrial optical communications systems are required to operate over large dynamic ranges, as topography dictates irregular distribution of nodes (or cities) and amplifying stations. The path length diversity of optically amplified systems implies that the optical powers can vary by up to 20 dB, but as these are known system attributes, they can be addressed by placing fixed attenuation elements in the system. Other factors lead to changing conditions, such as the number of wavelength division multiplexing (WDM) channels, which typically increases as the network is required to handle more users and capacity, and less gain per channel is available. Furthermore, the system is designed with extra margin to allow for component aging, resulting in lower transmitter powers and amplifier gain over the lifetime of the system. This leads to a large variation in the incident power that the optical receiver might experience. On the other hand, the optical receiver, comprised of an optoelectronic detector and electrical amplifiers, typically operates over a limited dynamic range. To limit the receiver's impinging optical power to the acceptable dynamic range, a variable optical attenuator (VOA) is normally introduced as part of the receiver. The VOA is a simple device with a single input fiber and a single output fiber, where the experienced optical loss between the input and output fibers can be continuously set. VOA can also be used as replacement for simple 1×2 switches, in an arrangement consisting of a power splitter and a VOA placed on each branch, enabling broadcast and select topology at the cost of higher losses. Other uses, requiring faster VOA in optical networks, are for transient suppression of amplifier dynamics that can wreak havoc on the stability of the network, and for possible low-frequency modulation of the transmission bit stream to encode system signaling information that can be received by a low-frequency response photodetector (a technique known as pilot tones) (Darcie[b0130] *et al.* 2005).

p0250 Because the VOA is integrated into each channel receiver and has additional network uses, it is a high-volume optical component, implying it must be inexpensive, compact, and preferably consume very little power. These attributes make VOA functionality well suited for a MEMS implementation.

s0090 #### 3.07.4.3.1 Shutter VOA

p0255 Optical loss can be introduced by blocking the light radiating out from the input fiber en route to the output fiber. A movable shutter placed in the beam path can selectively block the light in proportion to the shutter's displacement. The optical arrangement can be very simple by setting a minimal gap between the input and output fibers, where the gap region is intended for the shutter placement (**Figure 13**). Such an arrangement does not require any imaging optics, greatly simplifying the packaging requirements, and has a planar form factor. The intrinsic optical loss of this arrangement is due to light diffraction between the input and output fibers, as well as a possible contribution from lateral fiber misalignment in the packaging process. To minimize the intrinsic optical losses, it is necessary to minimize the gap size; hence, the shutter width should be very small, a requirement compatible with MEMS technology. Counter to the requirement that the shutter width should be small, its lateral dimension should be comparable to the optical fiber diameter, or $\sim$125 μm. The shutter range of motion should preferably be greater than the fiber radius so that the unactuated shutter should be further from the optical fibers during the assembly process. The shutter normal should also be tilted with respect to the fiber axis, so that back reflections will not couple back into the input fiber.

p0260 The large lateral dimension and travel range requirements for the MEMS shutter and its orientation normal to the fiber plane impose design limitations. A surface micromachined optical shutter VOA has been demonstrated with the shutter element rotated 90°, normal to the substrate (Barber[b0045] *et al.* 1998, Giles[b0200] *et al.* 1999). The shutter element was attached via a lever arm to a parallel plate capacitor actuator. Upon actuation, the shutter elevated further from the substrate via a pivot and hinge structure. A voltage range of 0–28 V applied to the capacitor plate resulted in full attenuation, with a switching speed faster than 100 μs. The fiber-to-fiber gap size of 20 μm yielded a minimal loss of 0.8 dB. An alternative bulk micromachining process optical shutter VOA utilizes DRIE in a thick silicon layer on an insulator wafer (Marxer[b0375] *et al.* 1999). The VOA uses a comb-drive actuated shutter and fiber placement grooves for simple alignment. To minimize the risk of damage during fiber placement, the large gap size of 60 μm was maintained. To reduce the effect of beam diffraction and subsequent optical losses upon coupling to the output fiber, the entire package including the gap region was filled with index matching oil. The optical losses were reduced from 2.5 to 1.5 dB, with an additional damping benefit provided by the oil, eliminating mirror ringing effects. A voltage

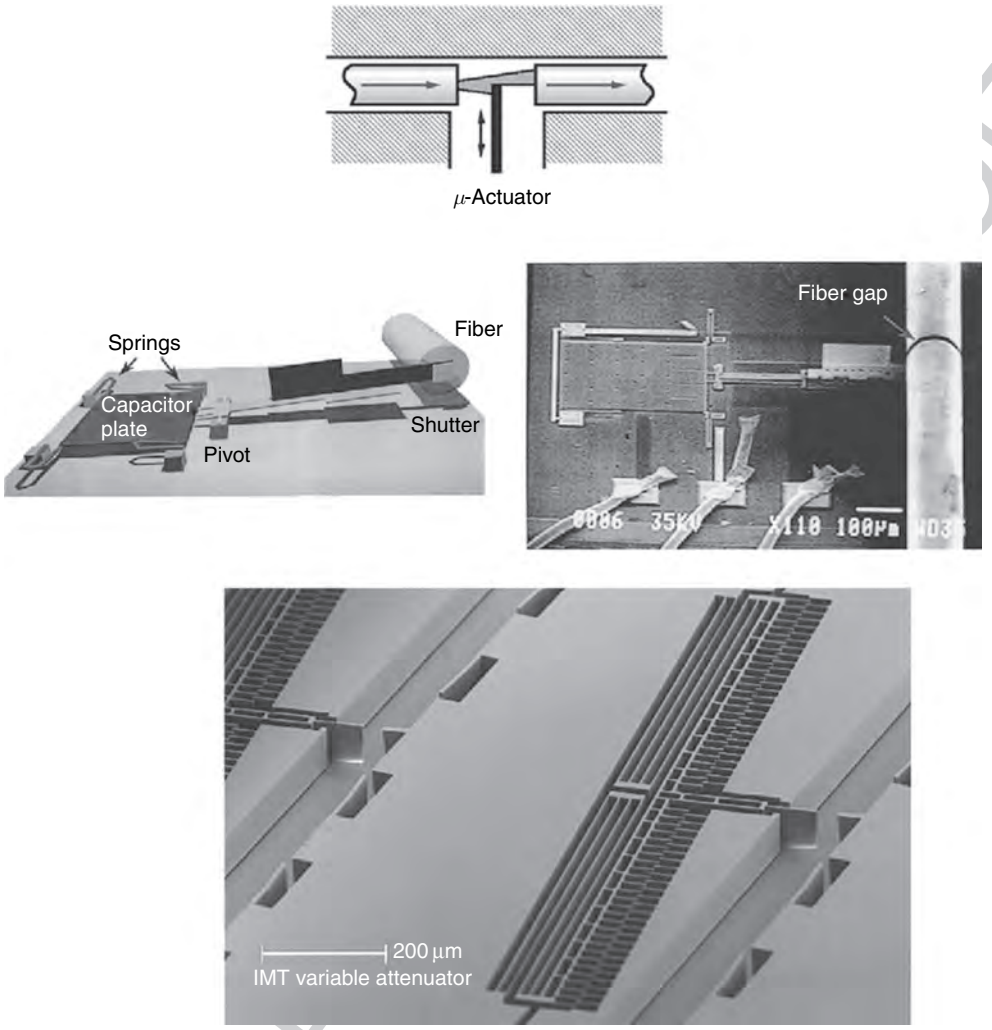

f0065 **Figure 13** Shutter-type variable optical attenuator. *Top*: Schematic representation. *Middle*: Surface micromachining implementation. (Source: Barber B *et al.* 1998 A fiber connectorized MEMS variable optical attenuator. *IEEE Photon. Technol. Lett.* **10**, 1262–4, © [1998] IEEE.) *Bottom*: Bulk micromachining shutter (Source: Marxer C, Griss P, de Rooij N F 1999 A variable optical attenuator based on silicon micromechanics. *IEEE Photon. Technol. Lett.* **11**, 233–5, © [1999] IEEE.)

range of 0–30 V applied to the comb-drive actuator resulted in full attenuation, with switching speed of 4.5 ms (due to the oil damping effect).

p0265 The VOA implementations described above require a steady voltage to maintain the attenuation settings, sometimes coupled with a feedback loop for added stability. A desired alternative is a latching switch, which requires active actuation in order to reach an attenuation state, but can then hold the state indefinitely with no power draw. A Vernier latching technique can be used to hold the shutter in the desirable attenuation state (b0485 Syms *et al.* 2004b, b0570 Unamuno and Uttamchandani 2006). The Vernier latch attenuation level progresses in discrete steps in one direction, and has a release actuator to return the VOA to the unactuated state. This operation mode is not amenable to active power level control feedback, often necessary for stable operation of optical networks. Moreover, the latch release operation and re-engagement can cause deleterious transient effects in networks.

p0270 Some concerns with polarization dependence exist when using the shutter-type actuator, due to vectorial diffraction effect from the shutter's edge. A MEMS iris alternative to the shutter has been demonstrated, with has greater symmetry about the optical fiber mode. The iris consists of four simultaneously moving blades, continuously adjusting the size of a central opening in the beam path (b0480 Syms *et al.* 2004a).

p0275 A self-powered VOA offers an interesting feature for surge suppression in optical networks (Aksyuk *et al.* 1999, Hirat *et al.*, 2005). The VOA includes a photogenerator, which provides sufficient voltage to drive the VOA in feedback mode. A power tap after the shutter drives the photogenerator in a self-governing mode; as the incident power on the detector increases, so does the photogenerator voltage, engaging the VOA shutter and regulating the output through increased attenuation.

s0095 ### 3.07.4.3.2 Beam displacement VOA

p0280 An alternative loss-generating scheme to the optical shutter consists of an optical arrangement that displaces the beam emerging from the input fiber, thus controlling the coupling efficiency into the output fiber. The scheme suggests that a more complicated optical system is required compared to the simple fiber gap arrangement of the shutter solution. However, the optical losses associated with a well-designated optical system between the input and output optical fibers can result in lower losses compared to propagation over a finite fiber gap. MEMS micromirrors are well suited for implementing the beam displacement mechanism of the optical system.

p0285 One method for imparting beam translation utilizes a tilting micromirror in the beam path. A 3D configuration often used places the input and output fibers side by side with their polished endfaces at the front focal plane of a common lens (**Figure 14**). The MEMS tilting mirror is placed at the back focal plane of the lens. When the mirror is in the unactuated state, light from the input fiber is collimated by the lens onto the mirror, is reflected back, and subsequently focused by the common lens into the output fiber. The intrinsic coupling efficiency of this configuration is limited only by the quality of the lens (antireflection losses and aberrations) and the mirror reflectivity, and can routinely achieve better efficiency than −1 dB. Polarization effects are also minimized because the beam is almost normally incident onto the mirror. When the mirror is tilted, the focused beam is shifted from the output fiber and coupling losses increase according to fiber misalignment calculations. The relationship between the mirror tilt $\Delta\theta$ and beam shift Δx is $\Delta x = 2f\,\Delta\theta$, where f is the focal length of the lens (obtained by geometric optics using small angle approximations). Thus, larger focal lengths require smaller tilt angles for imparting the same loss values. However, the collimated optical mode size at the mirror also increases with the focal length, requiring a larger mirror with greater sensitivity to mirror curvature. The lens focal length is typically kept small (order of 1 mm), resulting in a smaller system size. The collimated beam diameter is $D = 2f\lambda/(\pi w_0)$

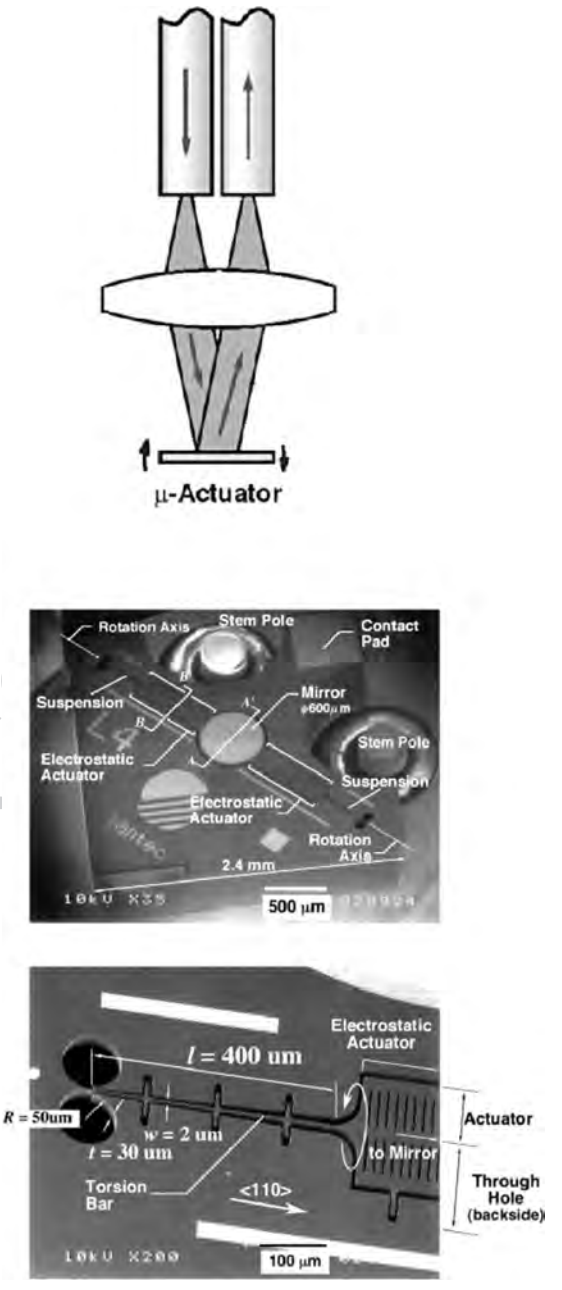

Figure 14 Beam scanning-type variable optical attenuator in a 3D layout. *Top*: Schematic representation. *Bottom*: Micromirror and support details fabricated using silicon bulk micromachining. (Source: Isamoto K *et al.* 2004 A 5-V operated MEMS variable optical attenuator by SOI bulk micromachining. *IEEE J. Selec. Top. Quant. Electron.* **10**, 570–8, © [2004] IEEE.) f0070

($D = 200\,\mu m$ using a 1-mm lens), requiring a mirror size of $1.5D$ (or 300 μm for a 1-mm lens) for minimal insertion losses, a size that is compatible with MEMS technology. A commercial, bulk micromachining, electrostatic MEMS tilting mirror (30-μm-thick, 600 μm diameter silicon mirror) demonstrated 5 V full actuation and a 3 ms underdamped response time (b0240 Isamoto *et al.* 2004). The entire VOA package is 5.6 mm in diameter and 23 mm long. Alternative actuation techniques for the tilting micromirror can be employed (b0140 Diemeer and Dekker 2002).

p0290 A planner beam translation method places one or more micromirrors in the beam path between the input and output fibers (**Figure 15**). Both fibers have a lens attached to their end facets, creating a collimated beam with an extended propagation distance between the two lensed fibers (typically hundreds of microns). A 90° folded geometry with a single MEMS translation or rotation mirror (b0050 Bashir *et al.* 2004, b0605 Yeh *et al.* 2006), or a 180° folded goemetry with two MEMS translation mirrors have been demonstrated (b0100 Cheng *et al.* 2004). In all cases, DRIE must be employed due to the fiber diameter and the planar configuration. The different MEMS designs utilize comb-drive actuators with low driving voltage (up to 30 V) and fast response times (millisecond range). The optical arrangements have low intrinsic losses (<1 dB), but the long beam path is sensitive to fiber placement errors, sometimes requiring active alignment within the alignment grooves. Because the reflective mirror surface is the etched silicon sidewall, surface roughness contribute to the intrinsic device loss and can limit the attenuation range due to scattering.

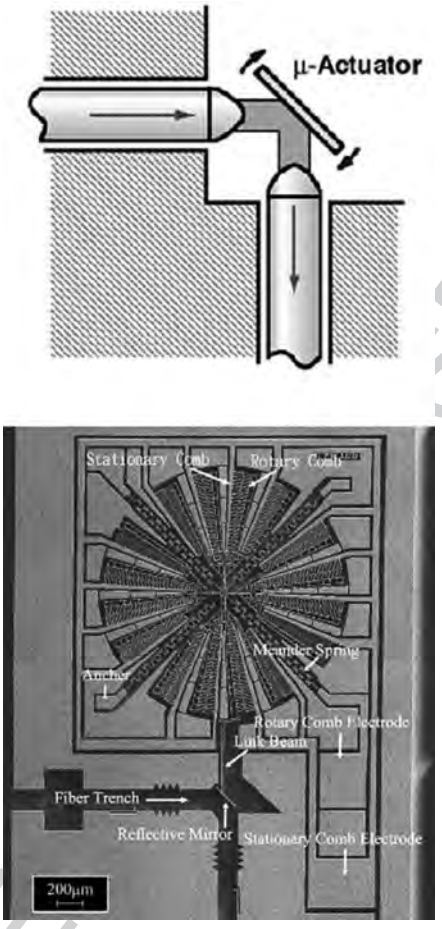

f0075 **Figure 15** Planar beam scanning-type variable optical attenuator (VOA). *Top*: Schematic representation. *Bottom*: VOA with micromirror attached to a rotation stage, fabricated using bulk micromachining. (Source: Yeh J A, Jiang S-S, Lee C 2006 MOEMS variable optical attenuators using rotary comb drive actuators. *IEEE Photon. Technol. Lett.* **18**, 1170–2, © [2006] IEEE.)

p0295 An alternative beam displacement technique to a mirror in the beam path is a displacement of the input fiber with respect to the output fiber with the aid of MEMS actuators (b0255 Kanamori *et al.* 2003). One implementation utilized moving silicon waveguides suspended in air instead of optical fibers (b0510 Tilleman *et al.* 2005), with the silicon waveguides operating in the multimode regime (having a cross section of $14\,\mu m \times 14\,\mu m$). The moving waveguide is attached to a comb-drive actuator. Due to the multimode structure, the attenuation versus displacement is highly dependent on mode number and polarization. However, the fundamental mode is very well behaved. The small air gap in the waveguide introduces diffraction losses and can also introduce Fabry–Perot effects, in the form of wavelength-dependent attenuation, due to the high reflectivity in the silicon-to-air interface.

3.07.4.3.3 Variable reflectivity mirror s0100

p0300 The previous solutions, whether based on a shutter inserted into the optical beam or beam displacement with tilting or moving mirrors, require MEMS devices with a relativity large motion range. An alternative arrangement based on mirrors whose reflectivity is adjustable can be utilized. The simple and low-loss optical arrangement with the common imaging lens is often used, with the variable reflectivity mirror replacing the tilting mirror. The variable mirrors can be based on interferometric and diffractive MEMS (DMEMS) solutions, both requiring a motion range smaller than the optical wavelength.

p0305 An interferometric mirror based on the interference between two membranes with a controllable gap size between them achieved tunable reflectivity (b0190 Ford *et al.* 1998). The mirror, termed mechanical antireflection switch (MARS), functions effectively as a dielectric coating on a silicon substrate. The active element is a silicon nitride layer one-quarter wave optical thickness, just as for a single layer dielectric antireflection coating (**Figure 16**). This silicon nitride layer is separated from the silicon substrate by $(3/4)\lambda$. At the $(3/4)\lambda$ separation, the antirefection coating becomes a single layer dielectric mirror with up to 72% reflectivity. However, the membrane is deformable. Voltage applied to electrodes on top of the membrane creates an electrostatic force, which pulls the membrane closer to the substrate. When the membrane gap is reduced to $\lambda/2$, the layer becomes an antireflection coating with close to zero reflectivity. Due to the small range of motion and the high silicon nitride film stress, the device can operate at 3 μs response times. A 28 dB attenuation dynamic range was observed for a 0–35 V operating voltage range. The device is nearly polarization independent on account of the normal incidence. However, due to the wavelength dependence in the interference effect, there is a strong wavelength-dependent attenuation. The wavelength dependence is especially pronounced about the peak attenuation value, where perfect destructive interference can only be achieved for a single wavelength.

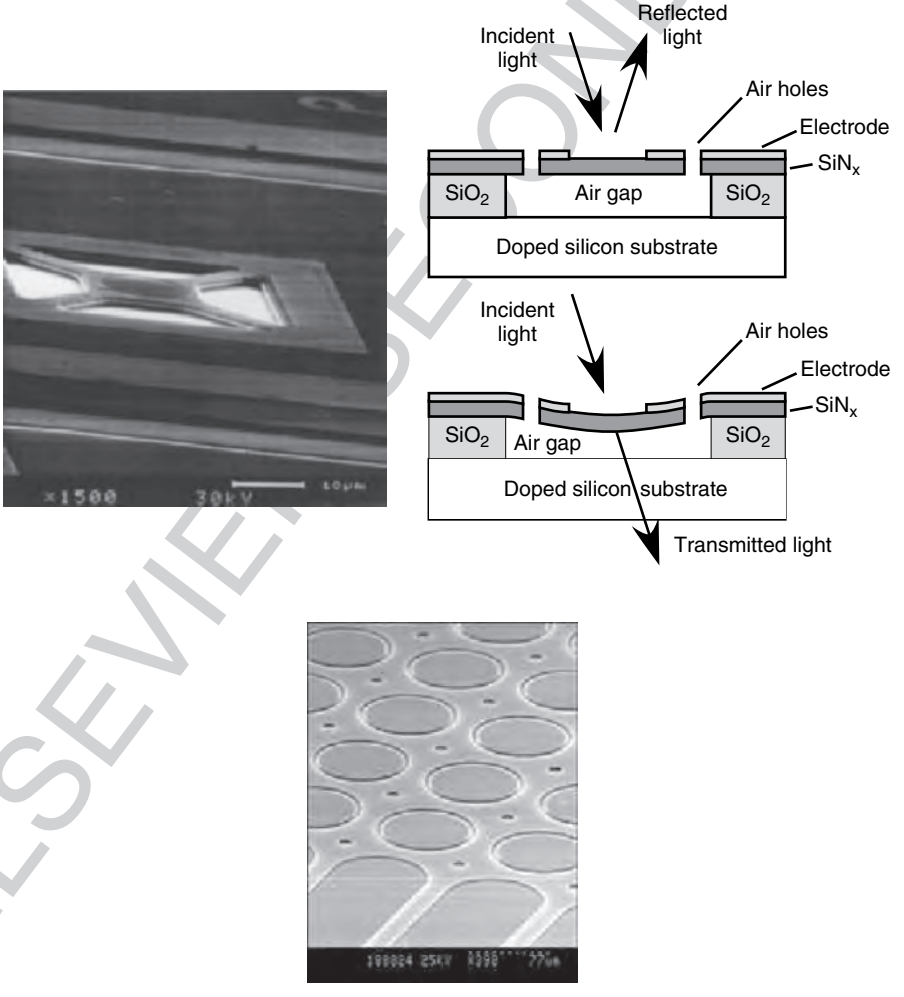

f0080 **Figure 16** Variable reflectivity mirrors. *Top*: Controlled interference between moving thin membrane and substrate layer. (Source: Ford J E *et al.* 1998 Micromechanical fiber-optic attenuator with 3 μs response. *IEEE J. Lightwave Technol.* **16**, 1663–70, © [1998] IEEE.) *Bottom*: Controlled interference between moving plate and static pillars. (Source: Godil A 2002 Diffractive MEMS technology offers a new platform for optical networks. *Laser Focus World*, May.)

p0310 DMEMS mirrors can also be used in a VOA application, by utilizing the zeroth diffraction order for coupling back into the output fiber (Godil 2002). However, the traditional DMEMS, consisting of periodic ribbons where half can be actuated, does not offer the necessary performance for optical communication application. Ignoring the gap region in the DMEMS, the power in the zeroth diffraction order is proportional to $(1/2)\,(1+\cos(\Delta\phi))$, where $\Delta\phi$ is the phase difference between the reflected signal from the actuated versus unactuated ribbons. The attenuation can be set to zero when the phase difference, $\Delta\phi$, is π ($\lambda/4$ translation), but the condition is satisfied for a single wavelength only due to the wavelength dependence in the phase delay. To circumvent the wavelength dependence, the DMEMS device can be optimized taking three parameters into account; the phase and period fractions of the movable ribbons, the stationary ribbons, and the exposed substrate in the gap regions. The extra gap factor allowed for a design that is nearly achromatic in the attenuation state. The ribbon structure gives rise to polarization dependence, due to the inherent orientation asymmetry. By creating a grating structure that is perfectly symmetrical in the two directions, polarization-independent operation is achieved, and the achromatic response criterion is also included in the design. The reflective surface is comprised of fixed round disks, a movable membrane around the disks, and a gap region between the membrane and the disks. Incident light is reflected on all three surfaces, and the geometrical layout ensures low polarization and wavelength dependence. The packaged VOA is 5.4 mm in diameter, and 18 mm long, and operates at a 0–5 V voltage range. According to a commercial press release, as of March 2005, 40 000 VOAs have been shipped to customers, demonstrating the large market demand for VOA modules.

s0105 3.07.4.4 MEMS Optical Fiber Switches

p0315 Optical fiber switches route the entire guided optical signal from one fiber to another, and scale in size from fundamental 1×2 and 2×2 switches to $N \times N$ switches, where N can be as large as one thousand. When possible, it is more desirable to switch signals in the optical domain due to the cost and power savings over optoelectronic equipment. Their uses in optical communication systems and networks are as diverse as the scale range they encompass. The basic 1×2 switch is often used for protection against equipment failure. For example, metropolitan-scale fiber rings often utilize fiber redundancy using a BLSR (bidirectional line switched ring) topology. The 1×2 switch is used to switch from the main fiber to the backup fiber when a loss-of-signal occurs (e.g., fiber cut). A fundamental 2×2 switching element can be used as a stand-alone switch or within a multistage interconnection network architecture (such as a Benes network) for constructing larger switch fabrics. The 2×2 switch can be used for implementing optical add-drop architecture on a per-channel basis. A $1 \times N$ switch, which routes from one fiber to one of any N fibers, can be used for efficient equipment sharing, such as optical monitoring at an amplification site. Finally, large $N \times N$ switches, often referred to as optical cross-connects (OXCs), are used to establish a desired connectivity pattern across many fibers. An OXC is therefore sometimes referred to as an automated patch panel, whose connectivity can be changed without the need for a technician's visit to the switch site. The OXC can be used to route individual WDM channels at a network node using opaque or transparent operating modes. A transparent switch, also termed OOO, is one where an input *optical* signal is switched in the *optical* domain and exits the switch in the *optical* domain. The photons flow through the switch unimpeded. OOO terminology contrasts the transparent switch to OEO switches, where an input *optical* signal is switched in an *electronic* switch fabric and exits in the *optical* domain again. An opaque switch uses the same switching fabric as the transparent switch, but isolates the optical switch from the optical input and output signals with electronic conversion. Hence, the opaque switch with OEOEO functionality regenerates the optical signal and does not suffer from wavelength contention issues.

p0320 While the smaller 1×2 and 2×2 optical fiber switches can be constructed using many competitive technologies, the larger switches are implemented exclusively using MEMS technology. The most common switching method uses micromirrors, yet other MEMS alternatives exist as well. Companies offering MEMS optical fiber switches have received much attention, as well as investment, during the telecom boom years. Very few of these companies survived, as the demand and deployment of large OXC switches never materialized. An opaque OXC architecture, while offering complete freedom of WDM channel routing restriction due to the signal regeneration, was too expensive to deploy. Transparent OXC functionality could be more effectively implemented using WSSs.

s0110 ***3.07.4.4.1 Small lensless MEMS switches***

p0325 Small switches require simple optical arrangements, and the simplest optical arrangements have no imaging optics between the input and output fibers. The distance between the input and output fiber end faces in such nonimaging solutions has to be very small, so that the coupling losses due to beam diffraction will be minimal. The gap region between the fibers can be minimized if no intervening elements need to be placed in it. Hence, the basis for a simple 1×2 switch is a movable input fiber, which can be laterally actuated to a position in front of either output fibers (**Figure 17**). The positional accuracy or placement in front of the fiber is very important for minimizing the coupling loss. Therefore, moving fiber switches rely on bistable designs with mechanical stops that define the parking positions (b0165 Field *et al.* 1995, b0220 Herding *et al.* 2003, b0230 Hoffmann *et al.* 1999). The optical fibers are placed in alignment grooves, with the single fiber typically placed onto a moving thermal actuator owing to the required large fiber bending forces. While the power consumption of the thermal actuator is high (~1 W), it is only required in actuation, due to the bistable design. Reported switching time is 400 ms, which is too slow for a protection application. An electrostatic switch using a metalized fiber offers an alternative actuation method. The electrostatic actuation at 75 V achieved a 10 ms switching time. One disadvantage associated with the moving fiber switch is that the three fibers are manually inserted into their alignment grooves, and offer no axial alignment mechanism. Hence, the gap region is intentionally larger than the minimal clearance (typical values of 25 μm) and the gap will be different for the two output fibers, resulting in uneven losses. The moving fiber concept can also be implemented with moving waveguides, in which case the gap region can be photolithographically defined (b0040 Bakke *et al.* 2002, b0410 Ollier 2002, b0470 Stuart *et al.* 2003). The moving waveguide approach using electrostatic actuation has been demonstrated in buried glass waveguides with metallization around the cladding region, in polymer waveguides deposited on top of a conducting SOI actuator, in GaAs waveguides, and in silicon ridge waveguides. The moving waveguide approach typically achieves submillisecond switching times and actuation voltages of a few tens of volts. Due to Fresnel reflections at the waveguide–air interface, the gap region forms a Fabry–Perot cavity. The gap region has to be precisely etched to ensure that its width will coincide with the cavity transmission peak.

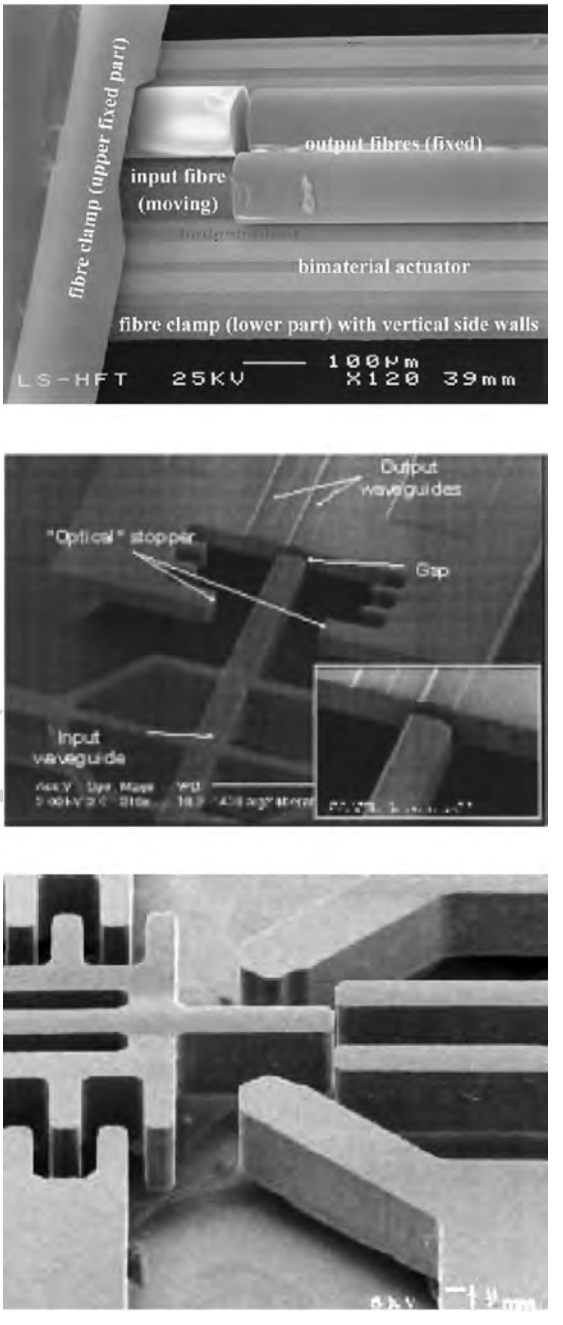

Figure 17 Lensless 1×2 switch with moving fibers/waveguides. *Top*: Fiber moving switch in a silicon actuator. (Source: Hoffmann M, Kopka P, Voges E 1999 All-silicon bistable micromachincal fiber switch based on advanced bulk micromachining. *IEEE J. Select. Top. Quant. Electron.* **5**, 46–51, © [1999] IEEE.) *Middle*: Silica-on-silicon moving waveguide. (Source: Ollier E 2002 Optical MEMS devices based on moving waveguides. *IEEE J. Select. Top. Quant. Electron.* **8**, 155–62, © [2002] IEEE.) *Bottom*: GaAs moving waveguide. (Source: Bakke T *et al.* 2002 Planar microoptomechanical waveguide switches. *IEEE J. Select. Top. Quant. Electron.* **8**, 64–72, © [2002] IEEE.) f0085

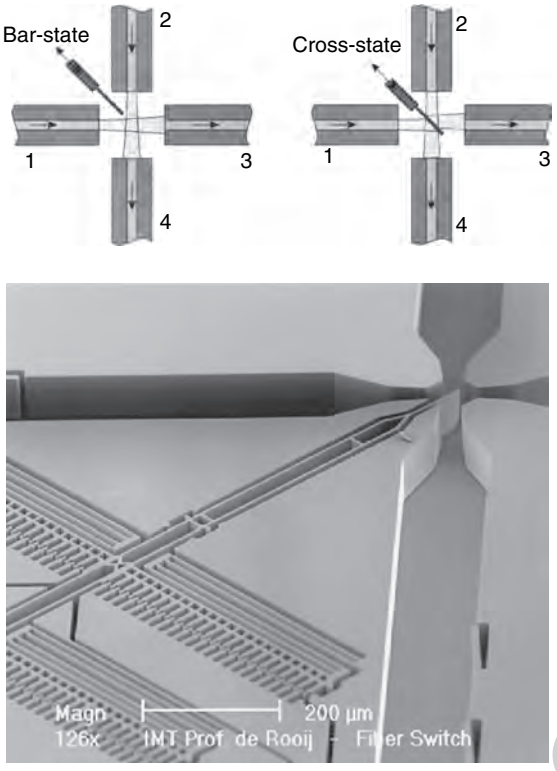

f0090 **Figure 18** Lensless 2 × 2 fiber crossbar switch with inserted mirror. *Top*: Schematic representation of switch. *Bottom*: Image of microelectromechanical systems (MEMS) switch fabricated in silicon using bulk micromachining. (Source: Marxer C, de Rooij N F 1999 Micro-opto-mechanical 2 × 2 switch for single-mode fibers based on plasma-etched silicon mirror, electrostatic actuation. *IEEE J. Lightwave Technol.* **17**, 2–6, © [1999] IEEE.)

p0330 A more complicated arrangement is required for lensless 2 × 2 optical fiber switches, which is counter to the minimal gap requirement. The lensless approach brings the four fibers together in a cross configuration (**Figure 18**). Light from the two input fibers, labeled 1 and 2, can free-space propagate across the junction region and couple to two output fibers, labeled 3 and 4. When a mirror is placed across the junction region, the light is reflected from the mirror and the switch is placed in the cross state. The mirror is inserted into the beam path in a similar fashion to the optical shutter in bulk micromachined VOA. A DRIE in a thick silicon layer on insulator wafer forms the shutter, the comb-drive actuator, and fiber placement grooves (b0370 Marxer and de Rooij 1999). The etched silicon layer is 75 µm thick, sufficient to cover the entire core region when standard single-mode fiber is used. The fiber gap size is required to be at least as large as the fiber's outer diameter, due to geometric constraints associated with placing four fibers at 90°. However, the insertion losses due to diffraction after propagation over such large gaps are large. The gap size can be reduced by using fibers with reduced cladding, resulting in a smaller outer diameter. Losses can be further reduced by placing index matching oil in the gap region, reducing the diffraction angles. The index matching oil also serves to dampen the mirror response, eliminating mirror ringing. The mirror's actuation voltage was 60 V, and the response time was about 0.5 ms. Insertion losses at the bar state (no mirror inserted) was below 1.2 dB (best achieved value of 0.55 dB). In the cross state (with mirror reflection) losses increased to a typical value of 1.8 dB (best achieved value of 1.55 dB). The added loss originates from the mirror quality, as a vertically etched mirror will exhibit roughness impacting the reflectively.

3.07.4.4.2 Sharing 1 × N fiber switches

s0115 p0335 As the number of fiber ports in a switch increases, imaging optics have to be introduced in order to collect the light radiating out of the input fiber and efficiently couple the light to the output fiber. $1 \times N$ optical switches, which switch light from an input port to one of N output ports, have an optical system that accommodates $N+1$ optical fibers. Typical values for the number of fibers N is 4 or 8. Such switches are typically used in reverse, as $N \times 1$ switches, for sharing a common resource among the N fibers. Beam displacement with one tilting micromirror in the beam path is an effective switching technique for $1 \times N$ switches. The arrangement is similar to the dual fiber collimator employed by beam displacement VOA, with the $N+1$ fibers in the lens's front focal plane and a tilting micromirror in the back focal plane (**Figure 19**). Each of the N fibers can be addressed by a unique mirror angle. Because the beam size and the micromirror size scale with the lens' focal length, it is desirable to use a short focal length lens. However, as opposed to the two fibers required for VOA, $N+1$ fibers occupy a larger lens field of view that will result in aberrations playing a significant factor in the coupling to fibers that are farther off-axis. One way to reduce this effect is to use a longer focal length, compound lens, which is better corrected for aberrations. This approach has been used in the demonstration of a 1×160 fiber switch (b0180 Ford and DiGiovanni 1998). However, as the beam size increases with the focal length, the resulting mirror size is beyond the size of MEMS devices, and enters the realm of precision mechanical mechanisms. A

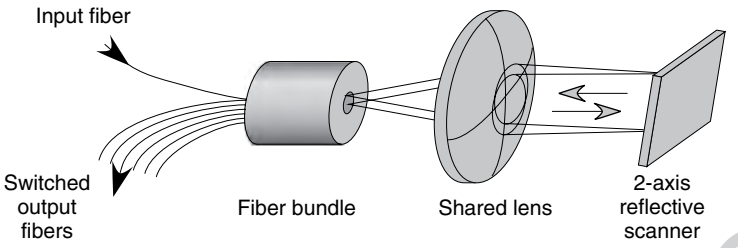

f0095 **Figure 19** Sharing $1 \times N$ fiber switch. Schematic representation of beam scanning for selecting output fiber. (Source: Ford J E, DiGiovanni D J 1998 $1 \times N$ fiber bundle scanning switch. *IEEE Photon. Technol. Lett.* **10**, 967–9, © [1998] IEEE.)

large switch implementation used galvanometer rotation actuators with prisms in a reflective arrangement to accomplish the beam scanning, with a 20 ms switching time and a worst-case insertion loss of 3.5 dB. A second way to reduce the effects of the off-axis aberrations is to place a deformable mirror instead of the micromirror (Peter *et al.* 2002). The mirror shape can be optimized to reduce the coupling losses for each fiber. The reported demonstration packed 32 fibers in a linear array, placing the input fiber at the array end and on the lens axis for studying the aberration limitations. Thus, the results are equivalent to a 62-fiber switch with 1D packing, or 3019 fibers using 2D fiber packing. Resulting fiber coupling losses ranged from 3 to 6 dB. Possible alternatives to address the aberrations from large count fiber switches include the use of a reduced cladding fiber, for minimizing the fiber bundle lateral extent that is dominated by the fiber's outer diameter, or the placement of a fiber collimator for each fiber. The advantage of placing collimators is that the resulting mode size on the MEMS mirror decreases, resulting in the fiber coupling being less mirror angle dependent.

p0340 An alternative approach to the construction of a $1 \times N$ switch is to cascade several 1×2 switches in a binary tree arrangement. The cascade can be from individual 1×2 switches, whereas in the case of moving waveguides the entire switch can be monolithically integrated onto a single wafer device (b0410 Ollier 2002).

s0120 ### 3.07.4.4.3 Optical cross-connects ($N \times N$)

p0345 Large $N \times N$ fiber switches or OXCs were believed to be the best method of managing the exponentially growing traffic in optical networks at the height of the telecom bubble. The established core network vision foresaw these large switch fabrics routing WDM channels at network switching nodes, offering new wavelength services and providing shared protection services (b0015 Al-Salameh *et al.* 2002). However, sales of these large switches did not meet the high expectations. The large switches required an upfront investment for handling future traffic demand. Two main OXC designs were pursued by many companies. The first is a beam scanning switch using analog multistate mirrors, starting from sizes of 64×64 and growing to fiber port counts of 1296×1296. The second is a crossbar switch implementation with digital bistate mirrors, most of these switches were 8×8 in size, with some as large as 32×32. The smaller switch modules could be used in a Clos architecture to construct large switch equivalents. Yet even the smaller switch versions saw their viability wither with the downturn in service providers' infrastructure investment and as interest shifted to switching WDM channels using WSSs.

p0350 Small optical fiber switches of the crossbar design are planar in structure, with the input linear fiber array arranged at one facet of the switch and the output linear fiber array arranged at a second facet of the switch, at 90° to the first facet (**Figure 20**). The fiber arrays are mated to matching collimating lens arrays, such that the beams from the input and output fibers generate a regular grid. Each beam from an input fiber intersects every beam of the output fiber. For an input/output array of N fibers, there are thus N^2 such beam intersections. Switching from any input fiber to any output fiber in the crossbar design is accomplished by placing a mirror at the respective beam intersection position. Each of these mirrors is bistable; in one state it is not in the beam path, whereas in the second state it is at 45° and completes the connection. Several factors impact the design and performance of crossbar switch. There is no way to fine-tune the mirror position to maximize the coupling efficiency. Because each mirror will have an independent misalignment from an ideal setting, these switches have considerable loss variation for each possible input/output connection. Additionally, even with an ideal mirror position, an additional source of loss variation in the switch is the optical path length

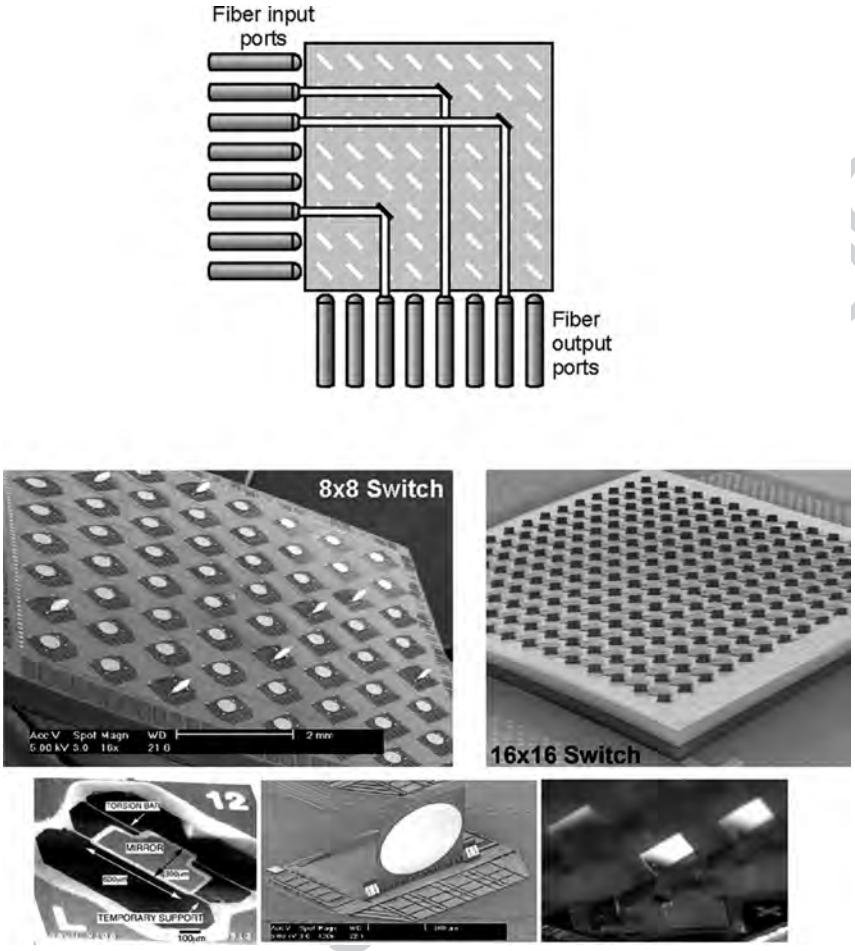

f0100 **Figure 20** Planar crossbar $N \times N$ fiber switch. *Top*: Schematic representation. *Middle*: Image of 2D matrix of digital microelectromechanical systems (MEMS) mirrors. *Bottom*: Details of exemplary MEMS digital mirrors. Left mirror rotates 90° out of plane with electrostatic actuation, middle mirror rotates with scratch drive, and right mirror lifts with a seesaw actuator. (Source: Lin L Y, Goldstein E L, Tkach R W 1999 Free-space micromachined optical switches for optical networking. *IEEE J. Select. Top. Quant. Electron*. **5**, 4–9, © [1999] IEEE; Toshiyoshi H, Fujita H 1996 Electrostatic micro torsion mirrors for an optical switch matrix. *J. Microelectromech. Syst.* **5**, 231–7, © [1996] IEEE; Lin L Y, Goldstein E L, Tkach R W 1998 Free-space micromachined optical switches with submillisecond switching time for large-scale optical crossconnects. *IEEE Photon. Technol. Lett.* **10**, 525–7, © [1998] IEEE; De Dobbelaere P *et al.* 2002 Digital MEMS for optical switching. *IEEE Commun. Mag.* **40**, 88–95, © [2002] IEEE.)

differences for each possible connection, with the difference between the shortest beam path to the longest being twice the length of the fiber array. Finally, as the beam strikes the metalized surface of the mirror at 45°, the reflection adds some polarization-dependent loss (~0.4 dB). The optical path length of the crossbar switch scales with the product of the fiber count, N, and the fiber pitch, P. Placing a requirement on the beam size, w_0, to accommodate for the propagation distance, L, one finds that $L \propto \left(w_0^2/\lambda\right) \propto N \times P$. Because the fiber pitch is also linearly proportional to the beam size, we can conclude that $N \propto (w_0/\lambda)$, or that the collimated beam size also scales linearly with N, to accommodate for the longer propagation distance. The major implication of having the fiber array length as well as the fiber pitch scale linearly with N, is that the physical extent of the crossbar switch will scale with N^2, making the crossbar switch impractical for large fiber port counts due to wafer size limitations. An exemplary design of a 16×16 crossbar switch leads to a mirror diameter of 320 µm and a lateral length of 8 mm (b0445 Ryf *et al.* 2006). Doubling the fiber port count to a 32×32 switch size doubles the mirror size to 640 µm and quadruples the lateral length to 32 mm. One unique feature of the crossbar switch is the ability to utilize both sides of the micromirror for establishing a second

simultaneous connection (Lin *et al.* 1999). Such architecture has been proposed for implementing add-drop functionality with no additional hardware requirements (**Figure 21**).

p0355 The digital MEMS micromirrors of the crossbar switch are required to have large motion comparable to the beam size. Such a large motion is best achieved with long lever arms used to amplify the actuator's motion. The originally demonstrated crossbar switch used polysilicon torsion mirrors supported by long slender rods that enabled the mirrors to rotate 90° out of plane using electrostatic actuation and a mechanical stopper (Toshiyoshi and Fujita 1996). Later pop-up mirrors achieved 90° rotation from the substrate using a translation distance of 22 μm from a scratch drive actuator with submillisecond switching time (Lin *et al.* 1998). The insertion losses of these early research prototypes were 10 dB or higher. Subsequent commercialization of crossbar switches reduced the losses to 2–3 dB by using MEMS micromirrors with better pointing accuracy (Dobbelaere *et al.* 2002). The improvement is provided by decoupling the mirror angle, critical for efficient fiber coupling, from the mirror motion. This was achieved by utilizing mirror translation as opposed to rotation, using a seesaw structure.

p0360 Large optical fiber switches of the beam scanning design utilize the free-space volume of the switch, with an input 2D fiber array at one facet of the switch and an output 2D fiber array at the opposing facet (**Figure 22**). The fiber arrays are mated to matching collimating lens arrays, forming light beams from the input fibers onto the output fibers. To establish a connection from any input fiber to any output fiber, the beam from the input is directed to the desired output and then realigned to efficiently couple into the output fiber. Thus, every connection is required to have two beam scanning elements. Because there are N input and output fibers in an $N \times N$ switch, the number of actuators in the switch is $2N$, in comparison to N^2 of the crossbar switch. However, each actuator has to assume one of N possible positions for each switching state. Mirrors can be introduced to fold the propagation length between the input and output fiber arrays, resulting in a more compact switch form factor. When MEMS micromirrors perform the beam scanning, they can be part of the folding mechanism. The path length variation in the beam steering switch is relatively small, as the distance between the input and output fiber arrays, L, is much larger than the arrays' lateral extent. The fiber arrays' lateral extent scales as the product of the pitch, P, and the square root of port count, $\sqrt{N}$, due to the 2D array layout. The beam scanning range $\Delta\theta$ is proportional to the ratio of the lateral extent to the distance between the arrays, or $\Delta\theta \propto \left(P\sqrt{N}/L\right)$. Placing a requirement on the beam size, w_0, to accommodate for the propagation distance, L, one finds that $L \propto \left(w_0^2/\lambda\right)$. Because the pitch, P, is also proportional to w_0, by substitution we find the scaling of the beam scan range $\Delta\theta \propto \left(\sqrt{N}\lambda/P\right)$, of the

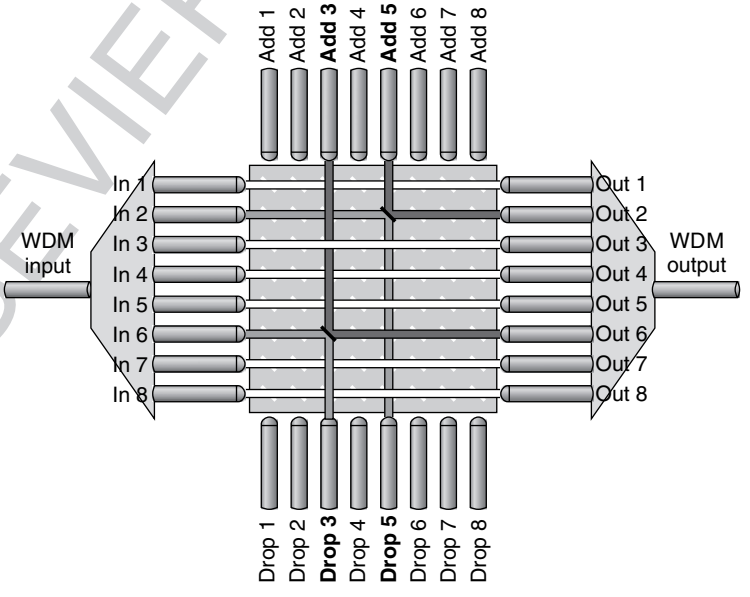

f0105 **Figure 21** Use of planar crossbar switch for wavelength add-drop functionality.

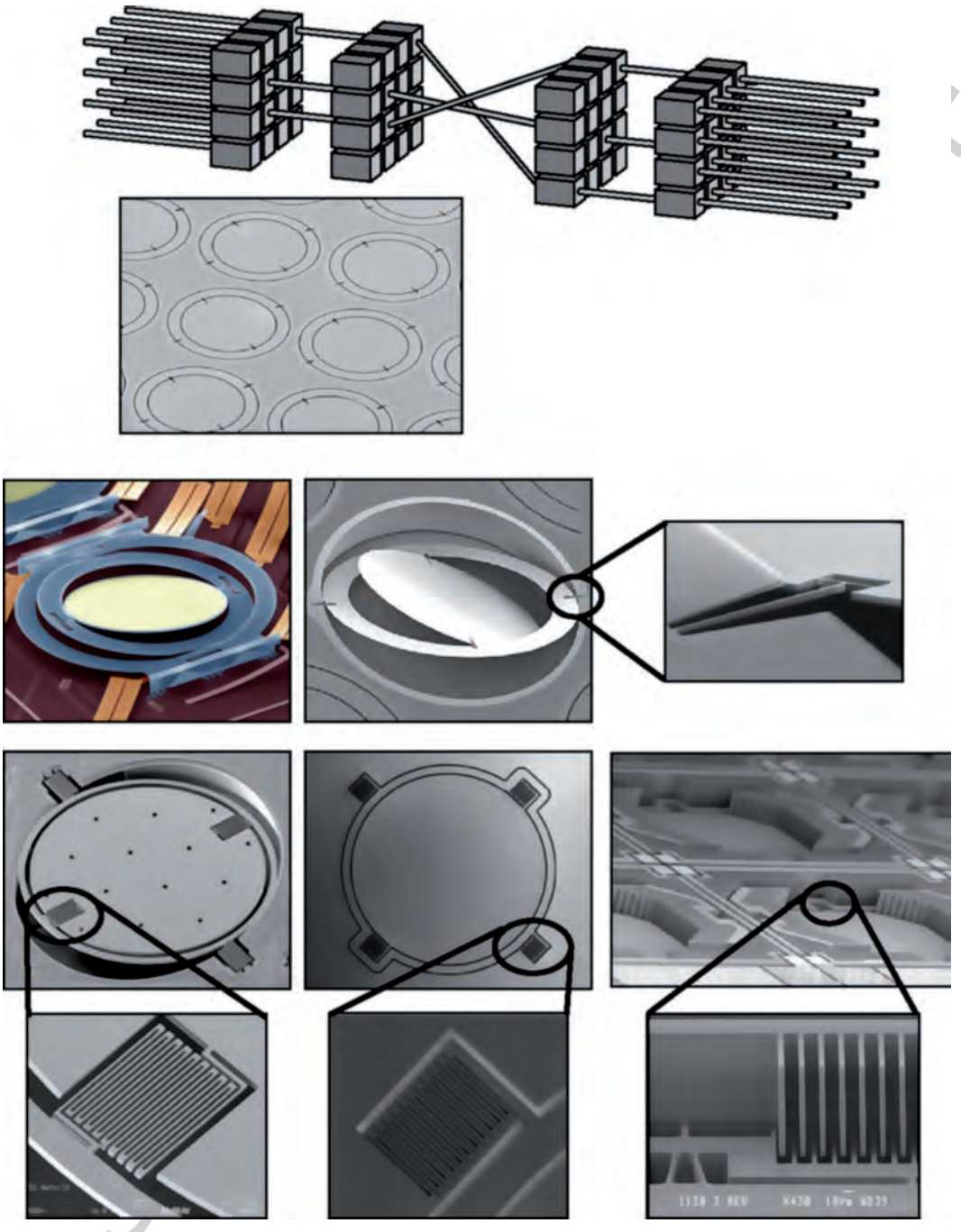

f0110 **Figure 22** Three-dimensional $N \times N$ fiber switch *Top*: Schematic representation. *Middle*: Image of high fill factor 2D array of scanning microelectromechanical systems (MEMS) mirrors. *Bottom*: Details of exemplary MEMS scanning mirrors and their spring design detail. Top left mirror fabricated in surface micromachining process, other mirrors using silicon bulk processing. Spring design details show torsion rod, serpentine springs, and V-shaped mirror support, designed to provide the motion range, resonance frequencies, and in-plane stiffness. (Source: Aksyuk V A *et al.* 2003 Beam-steering micromirrors for large optical cross-connects. *IEEE J. Lightwave Technol.* **21**, 634–42, © [2003] IEEE; Chu P B *et al.* 2005 Design and nonlinear servo control of MEMS mirrors and their performance in a large port-count optical switch. *IEEE J. Microelectromech. Syst.* **14**, 261–73, © [2005] IEEE; Zheng X *et al.* 2003 Three-dimensional MEMS photonic cross-connect switch design and performance. *IEEE J. Select. Top. Quant. Electron.* **9**, 571–8, © [2003] IEEE; Yano M *et al.* 2003 Optical MEMS for photonic switching – compact and stable optical crossconnect switches for simple, fast, and flexible wavelength applications in recent photonic networks. *IEEE J. Select. Top. Quant. Electron.* **11**, 383–94, © [2003] IEEE.)

propagation distance $L \propto \left(N\lambda/(\Delta\theta)^2\right)$, and of the lateral dimension $P\sqrt{N}$. The physical extent of the switch scale more gracefully with the fiber count N; linearly in propagation distance and as the square root in the lateral dimension. An exemplary design of a 256×256 OXC with a 1 mm pitch requires a propagation distance of 86 mm, a lateral dimension of 16 mm × 16 mm, and a mirror tilt range of ~10° (Ryf *et al.* 2006). Additional optical elements, such as lenses or microprisms, can be introduced in the beam scanning switch to eliminate the tilt angle dependence on the spatial locations of the input and output fibers.

p0365 Several methods can perform the beam scanning operation. The most common is the use of two MEMS micromirrors in the beam path, in a folded Z-shaped configuration (Kim *et al.* 2003b, Neilson *et al.* 2004a, Ryf *et al.* 2006). Because the micromirrors are required to rotate about two axes, they are typically supported by a gimbal structure. The gimbal is not a working port of the mirror, hence, the mirror fill factor is reduced. The fill factor impacts the design as the fiber pitch has to increase beyond the limit imposed by the beam size. Moreover, the beam has to be well contained within the mirror's aperture to eliminate beam clipping losses. The MEMS micromirrors can be fabricated using surface micromachining processes of polysilicon or bulk processing of single-crystalline silicon. Typical mirror parameters are 500–800 μm diameter, ~100–200 V electrostatic actuation using three or four electrodes placed underneath the mirror, and 5–10 ms switching times (Aksyuk *et al.* 2003, Chu *et al.* 2005, Zheng *et al.* 2003). When properly designed, the losses of a 238×238 MEMS micromirror beam scanning OXC are in the 1–2 dB range. Loss contributors are the collimators' aberrations and antireflection coatings, and the micromirrors's reflectivity, curvature, and clipping. Other beam scanning methods are based on lateral displacement of the fiber or collimator with respect to each other (**Figure 23**). The collimator lens can be placed on an electrostatically actuated x–y stage

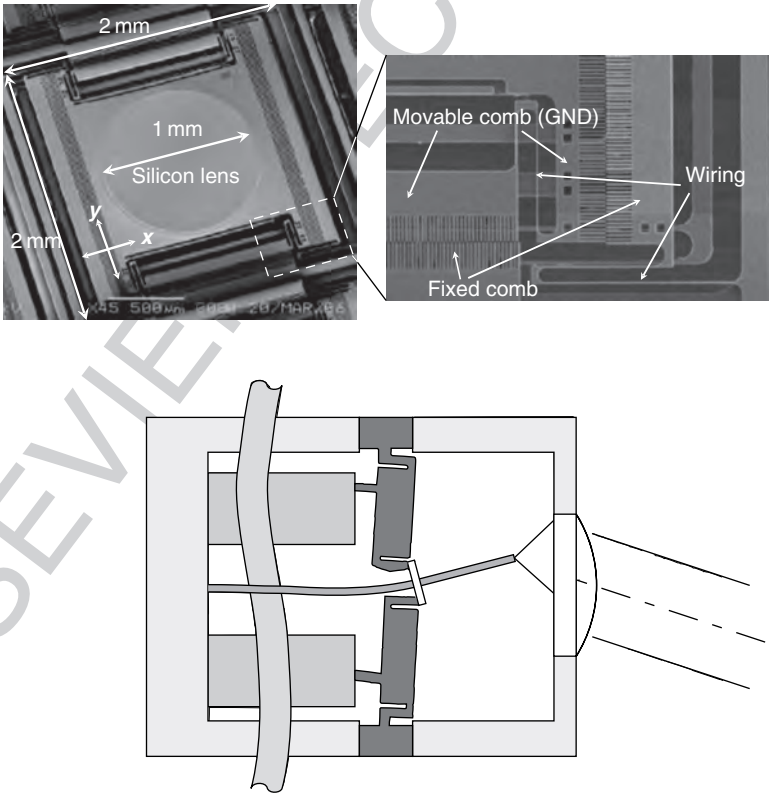

f0115 **Figure 23** Alternative beam-scanning techniques for $N \times N$ fiber switch. *Top*: Lateral movement of the collimator lens. (Source: Takahashi K *et al.* 2006A 3D optical crossconnect using microlens scanner with topologically layer switching architecture. *IEEE Optical MEMS Conference*, Piscataway, NJ, USA, © [2006] IEEE.) *Bottom*: Lateral movement of the fiber tip. (Source: Hagood N W *et al.* 2004 Beam-steering optical switching apparatus. *US Pat.* 6 738 539, May 18.)

to achieve scanning (Takahashi *et al.* 2006, Toshiyoshi[b0530] *et al.* 2003). However, the fill factor of the lens aperture to the fiber pitch is poor due to comb-drive actuation mechanism surrounding the lens, and the amount of lens displacement is limited. As an alternative, the fiber tip can be translated with respect to the lens (Hagood[b0215] *et al.* 2004, Truex[b0535] *et al.* 2003). A large displacement of the fiber tip is achieved by tilting the fiber from a pivot point farther away from the lens. Due to the relatively large forces required to bend an optical fiber, piezoelectric actuators are used. The optical path in this arrangement is extremely clear, comprised only of the two collimators. Measured optical losses of the connections average an impressive 1 dB.

s0125 ### 3.07.4.5 MEMS Wavelength-Selective Switches

p0370 DWDM transmission has provided greatly enhanced data transport capacity on a single fiber, with today's state-of-the-art systems capable of carrying multiple terabits per second. The economic basis behind DWDM is the sharing of the fiber resources, components, and optical amplifiers across many wavelength channels. To maximize the efficiency of the transport layer, the data traffic should remain in the optical regime and undergo optical to electronic to optical (OEO) conversion only when necessary, which is either when the data in a particular channel has to be extracted for consumption or regenerated due to OSNR limitations. The system capability that is required for maximizing the efficiency is the ability to aggregate and disaggregate wavelength channel in the optical domain, allowing the remaining data paths to continue in the optical domain. This function, referred to as OADM, was initially implemented with an optical demultiplexer and multiplexer with a fiber patch panel disposed between them. The requirement to support remote provisioning and fast restoration functions in the OADM were addressed by the more flexible ROADM, which replaced the fiber patch panel with an optical fiber switch fabric. However, the architecture composed of a demultiplexer, switch, and multiplexer suffers from accumulated losses and channel passband filtering, which limit the potential reach of the transmission. A complete ROADM solution should provide wide, flat passband as well as dynamic power equalization across the channels for meeting the physical layer requirements.

p0375 WSSs are transparent optical switching subsystems, which can route and attenuate wavelength channel in meeting with ROADM requirements. A WSS contains some means of separating or demultiplexing the wavelength channels at the ingress ports, followed by an optical switch fabric and means of recombining or multiplexing back the wavelengths into one or more egress ports, following the switch function. There is no wavelength conversion or OEO inside a WSS; the switch is optically transparent for the photons carrying the data. The simplest WSS is a channel blocker, with a single input and output fiber, having the capability to power equalize or completely attenuate the WDM channels. The more capable $1 \times K$ WSS has a single input and K output fibers, adding the capability to independently route the individual WDM channels among the K fibers. Finally, the $K \times K$ wavelength-selective cross-connect (WSXC) handles K input and K output fibers with the ability to switch any wavelength from any input fiber to any output fiber, provided there is no wavelength contention. The drawback of the WSXC is its sensitivity to failures; if the switch malfunctions or needs to be replaced, then all the WDM traffic flowing on the K fibers is halted. The $1 \times K$ WSS module, which can be used to construct an equivalent $K \times K$ WSXC, is a more robust solution as the traffic is partitioned according to originating fiber port, and only a subset of the traffic will be affected by a single failure.

3.07.4.5.1 Channel blocker s0130

p0380 The channel blocker is based on a free-space optical system that spectrally resolves the optical communication bandwidth, originally conceived for an amplifier gain flattening application (Ford[b0185] and Walker 1998). However, for independent DWDM channel access, the optical system is designed to provide higher resolution (Neilson[b0390] *et al.* 2004b). The light from an input/output fiber is collimated by a long focal length lens onto a diffraction grating, such that a large region of the grating is illuminated (**Figure 24**). The diffraction grating generates angular dispersion on account of the wavelength dependence of the diffraction angle. The diffracted light is refocused by the long focal length lens onto the same plane of the fiber tip, but displaced from it, and is incident onto a reflective pixelated modulator. The optical layout is identical to that of a spectrometer, which results in a spatially dispersed optical signal. The dispersive imaging arrangement demultiplexes the input DWDM channels in space, such that the information bandwidth of each wavelength channel is well contained within an active pixel

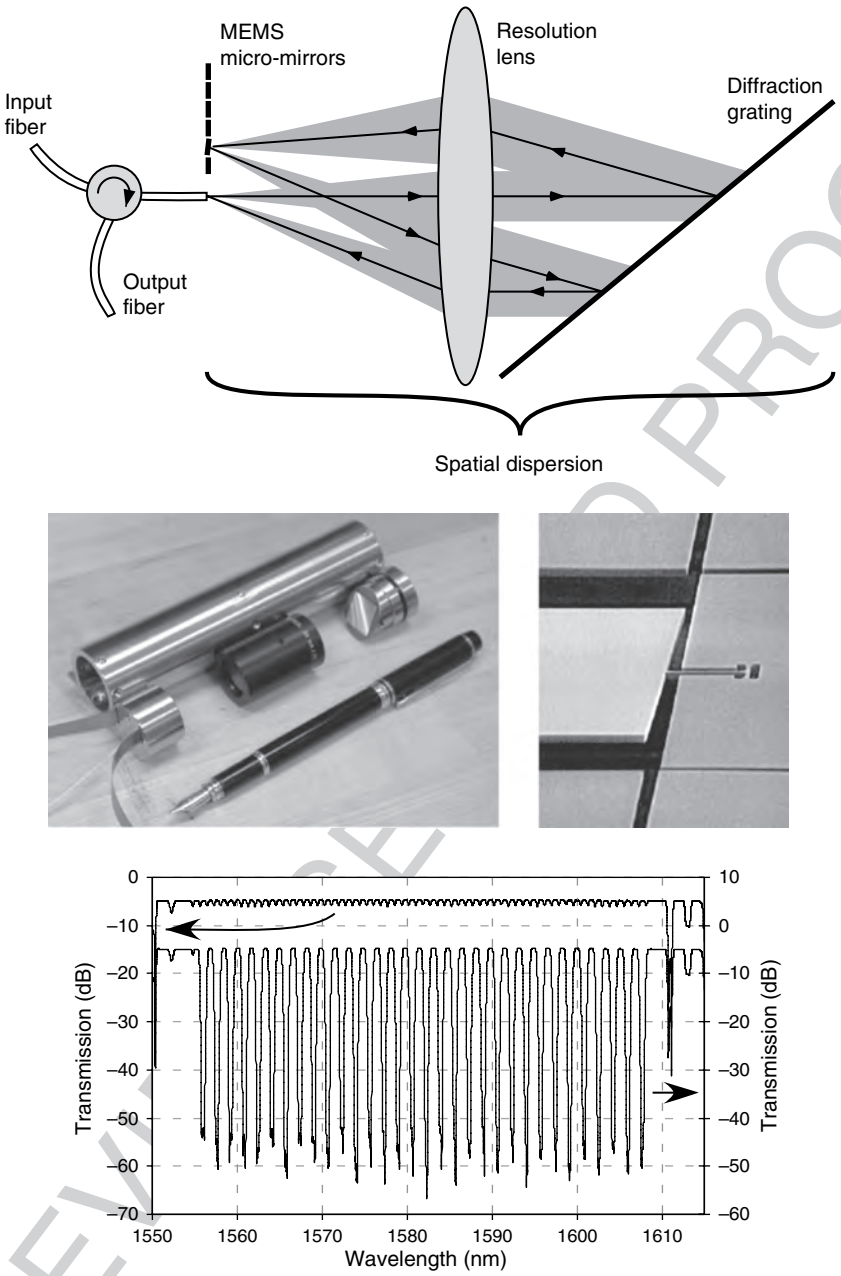

f0120 **Figure 24** Wavelength blocker. *Top*: Schematic layout. *Middle*: Images of blocker package and microelectromechanical systems (MEMS) torsion mirror array. *Bottom*: Optical power spectrum of all wavelength division multiplexing (WDM) channels in through and alternating blocking patterns. (Source: Neilson D T *et al.* 2004b Channel equalization and blocking filter utilizing microelectromechanical mirrors. *IEEE Select. Top. Quant. Electron.* **10**, 563–9, © [2004] IEEE.)

element. The light is collected back from the active modulating elements and coupled into an output fiber after back propagating through the dispersive arrangement (reversing the original spatial dispersion). Ensuring that the mode size on the device array plane is less than the active pixel width yields the desired wide passband characteristics. This can be achieved by a judicious choice of the diffraction grating frequency and effective focal length of the imaging setup. Furthermore, a wide spatial margin between the incident beam and the pixel edges results in guard bands, which allow for drift in laser

source, optical system misalignment, and provides a more abrupt interchannel transition. The active pixel ated device can be chosen from multiple available technologies, although LC modulators (Bouevitch[b0090] *et al.* 2002, Rhee[b0430] *et al.* 2001), MEMS tilting mirror arrays (Neison *et al.* 2004), and DMEMS (Ramani[b0425] 2006) are often the technology of choice. The loss mechanism of each of these technologies is different; MEMS tilting mirrors change the propagation direction of the reflected beams, which introduces a loss when coupling back to the output single-mode fiber, LC attenuates the intensity of the light transmitted through the pixels by polarization rotation and extinction via a crossed polarization (reflective designs are also possible, without loss of generality), and DMEMS control the reflected intensity by adjusting the phase difference between reflective ribbons (with the remaining light diffracting outside the numerical aperture of the optical system).

p0385 A 100 GHz channel-spacing blocker based on an array of MEMS tilting micromirrors demonstrates the attractiveness of channel blockers for handling 64 DWDM channels (Neilson[b0390] *et al.* 2004b). The channel passbands provided by the switch are very wide and flat, and the insertion loss of the switch is less than 5 dB. Channel blocking with greater than 40 dB attenuation was measured. More importantly, the 0.5 dB passband is 58 GHz wide, and the 3 dB bandwidth is 87 GHz. The measured chromatic dispersion within the passband was less than 2 ps nm^{-1}. Polarization-dependent losses were less than 0.35 dB. Such optical channel performance can handle signals with 10 and 40 Gb s^{-1} data rates with minimal impairment, even when the signal traverses several channel blockers in cascade. The MEMS micromirrors of the channel blocker were based on a single-crystal silicon fabrication process, patterned with a 248-nm deep ultraviolet (DUV) stepper to define submicrometer-wide springs and very small lateral gaps between the mirrors (0.4 μm). Torsion rods are used as springs and the 1-μm-thick mirrors have a tilt range of 8° at 150 V. The mirrors are actuated using electrostatic force from electrodes on an electrode chip placed below the mirrors chip. The mirror surfaces are aluminum coated to give high reflectively at 1.55 μm, and exhibit mirror resonant frequencies exceeding 20 KHz. MEMS-based channel blockers have not fared well in the marketplace, as LC-based modulators obtain similar performances with the LC modulating element and drive electronics costing a fraction of the MEMS solution.

3.07.4.5.2 Wavelength-selective 1 × K switches s0135

The 1 × *K* WSS expands the free-space optical system of the channel blocker to allow for the introduction of *K* + 1 fiber ports. The WSS design is based on two major subassemblies; the first used to spatially overlap the beams from the individual input and output fibers, to allow for switching between multiple ports, and the second to spectrally resolve the channels and introduce the wavelength selectivity (**Figure 25**). The role of the first subassembly is to image the input and *K* output optical fibers end faces onto an angular multiplexed common magnified spot. This subassembly converts the distinct spatial locations of the fibers to unique angular propagation directions. The second subassembly introduces the desired wavelength-selectivity property with the use of a diffraction grating. It spatially disperses the input magnified common spot, consisting of the *N* WDM channels, onto the MEMS micromirror array, such that each channel is imaged upon a separate mirror in the array for independent addressing. Each micromirror in the array can be tilted to a desired angle, which subsequently determines the selected output fiber array, on a WDM channel basis. The first subassembly determines the optical beam magnification ratio, the fiber array layout, and the required mirror tilts to reach each output fiber. The second subassembly determines the amount of spatial dispersion for separating the WDM channels and obtaining the necessary passband characteristic. p0390

The optical subassembly responsible for imaging the optical fiber end faces onto a common magnified spot is comprised of a fiber array, a matching microlens array, and a condenser lens whose aperture subtends all the beam apertures from the fibers. The fiber array consists of *K* + 1 fibers, where one fiber is assigned to carry the input signal and the remaining *K* fibers are the output fibers. The microlens array and fibers are coaxially aligned and result in collimated beams arranged in a 1D array to accommodate mirrors with a single tilt axis. Gaps are introduced between some of the lens apertures to allow for a variable attenuation feature by the beam scanning method without giving rise to crosstalk. The condenser lens focuses the *K* + 1 collimated beams at its back focal plane, where the beams are superimposed and differentiated only in propagation direction. The optical arrangement of the first subassembly implements a telescopic imaging system of the fiber modes via the lenses from the microlens array and the condenser lens. The imaging operation magnifies the p0395

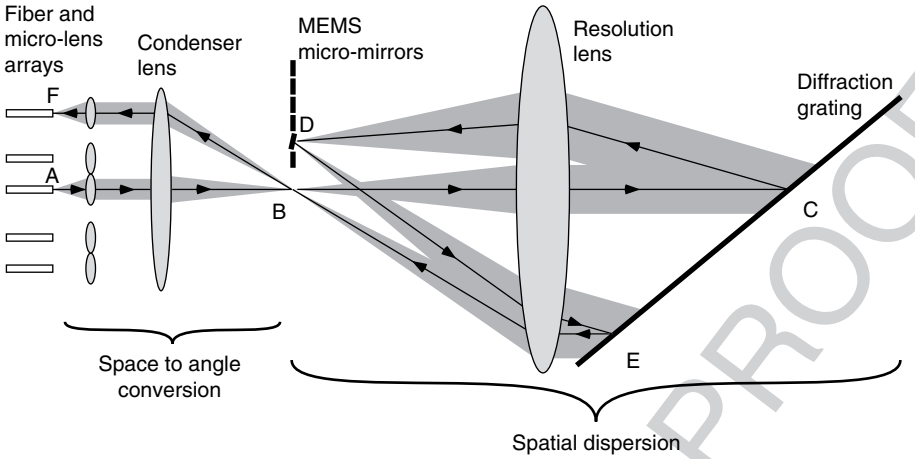

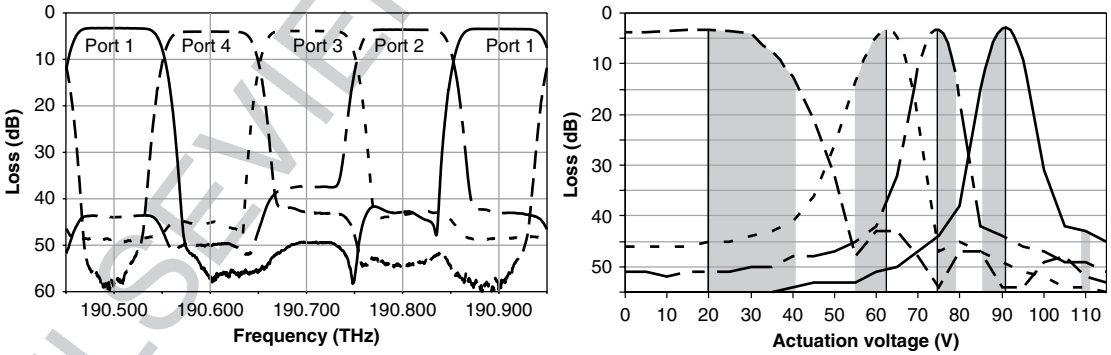

f012.5 **Figure 25** Wavelength-selective 1 × *K* switch. *Top*: Schematic layout. *Middle*: Image of wavelength-selective switches (WSSs) package. *Bottom – Left*: Optical power spectrum detail of dense wavelength division multiplexing (DWDM) channels demonstrating switching to four output ports with wide passbands. *Bottom – Right*: Voltage versus coupling curve for one channel (mirror), scanning the four output ports with support for 10 dB dynamic range of attenuation (gray zones) and blocking. (Source: Marom D M *et al.* 2005a Wavelength-selective 1 × *K* switches using free-space optics and MEMS micromirrors: Theory, design, and implementation. *IEEE J. Lightwave Technol.* **23**, 1620–30, © [2005] IEEE.)

optical beam emerging from the single-mode fiber by the ratio of the condenser lens to the microlens focal lengths. Anamorphic optics can be introduced into the optical subassembly to increase the number of fiber ports without increasing the magnified spot size in the dispersion direction, which sets the resolution requirements. Additionally, polarization diversity elements are integrated into the optics for use with high-efficiency diffraction gratings that only support one polarization.

p0400 The second optical subassembly disperses the magnified mode that was generated by the first subassembly and images it on the micromirror array. Its design is similar to a spectrometer with a Littrow mounted diffraction grating. A single lens collimates the light that is then incident on the grating. The diffracted light, which is propagating back toward the lens and is angularly dispersed, is imaged by the same lens onto the micromirror array. As is well known from classical spectrography, the spectral resolution of the instrument increases with increasing focal length and grating frequency, and with decreasing input slit size. In the WSS, the magnified mode size is equivalent to a spectrograph slit size. The spectral performance of the free-space WSS is directly related to the dimensionless ratio ξ, which is defined as the ratio of MEMS micromirror size to the magnified spot mode size (Marom *et al.* 2005). All the optical system parameters of the WSS contribute to this dimensionless ratio; the focal lengths of the lenses, the grating frequency, and the fiber mode. The ratio measures how well the Gaussian mode is confined within the micromirror. The channel passband performance of the WSS is derived by solving the frequency-dependent, power-coupling efficiency integral. Using a simplifying assumption that the MEMS array has a 100% fill factor, the frequency-dependent coupling efficiency is defined by

$$|\eta(\nu)|^2 = \frac{1}{4}\left\{\mathrm{erf}\left[\sqrt{2}\xi\left(1-\frac{2\nu}{\nu_{\mathrm{ch}}}\right)\right] + \mathrm{erf}\left[\sqrt{2}\xi\left(1+\frac{2\nu}{\nu_{\mathrm{ch}}}\right)\right]\right\}^2$$

where ν is the temporal frequency variable, ν_{ch} is the DWDM channel separation, and erf is the error function. Thus, passband requirements can be accommodated in the design of the WSS by varying the ratio of the mirror size to the magnified Gaussian mode size, which sets ξ, in fulfillment of the optical transport requirements.

p0405 The first reported WSS was configured as a 1×4 switch with support for 128 channels on a 50-GHz grid (Marom *et al.* 2002). The switch had a worst-case insertion loss of 5 dB, with 1 dB passband width of 37 GHz, and 3 dB width of 44.5 GHz. The broad flat-top filter shape enables the switch to be cascaded in transparent systems carrying $10\,\mathrm{Gb\,s^{-1}}$ data rates. Further WSS development was focused on 1×4 configuration, based on a 100-GHz grid, with support for 64 channels and $40\,\mathrm{Gb\,s^{-1}}$ data rates, along with 10 dB spectral equalization dynamic range (Marom *et al.* 2003a). These later WSSs were compact and fully packaged, had a 4 dB insertion loss, 77 GHz wide passbands at the -1 dB level, polarization-dependent losses below 0.3 dB, and chromatic dispersion within the passband below $10\,\mathrm{ps\,nm^{-1}}$. Two different MEMS micromirror arrays were designed for the switch; one based on surface micromachining of polysilicon and the other on bulk processing of a SOI wafer (Greywall *et al.* 2003, López *et al.* 2002). In the polysilicon approach, a double-hinge activation mechanism is defined. An actuation plate, anchored at one edge, is tilted to small angles via an underlying parallel plate electrode and a 4 μm gap. The mirror is attached to the free edge of the actuation plate and to the substrate with unequal arm lengths, allowing large mirror tilt angles out of plane via angle amplification. The mirror, actuator plate, and springs are etched in 1.5-μm-thick polysilicon. Spring features are typically 0.5 μm wide, and the gap between adjacent mirrors is 0.7 (~99% fill ratio). In the SOI approach, a 10-μm-thick layer of polysilicon is deposited over the patterned 1-μm-thick single-crystalline silicon and is used to define the actuator electrodes and ground shields. The electrode attracts the short actuator arm via an electrostatic fringe field, resulting in mirror rotation out of plane about the torsion springs. The monolithic structure has a further advantage that it does not exhibit rotational snap-down. Both the polysilicon and SOI micromirrors achieved 6.5° mechanical rotation at a driving voltage of 100 V, and had approximately millisecond scale switching times. Several other free-space WSS and 1D MEMS mirror array efforts have been reported, with similar functionality to that described above (Bernstein *et al.* 2004, Ducellier *et al.* 2002, Marom *et al.* 2006, Tsuboi *et al.* 2004, Wu *et al.* 2002). When using a mirror array with a single rotation axis, transient effects might occur on intermediate fiber ports as the beam is scanned along it (**Figure 26**). To achieve hitless switching, mirrors with two rotation axes have been developed, so that the beam can be first moved off the array, then to the position closest to the desired fiber, and finally moved back to couple only to the desired port. This poses a design

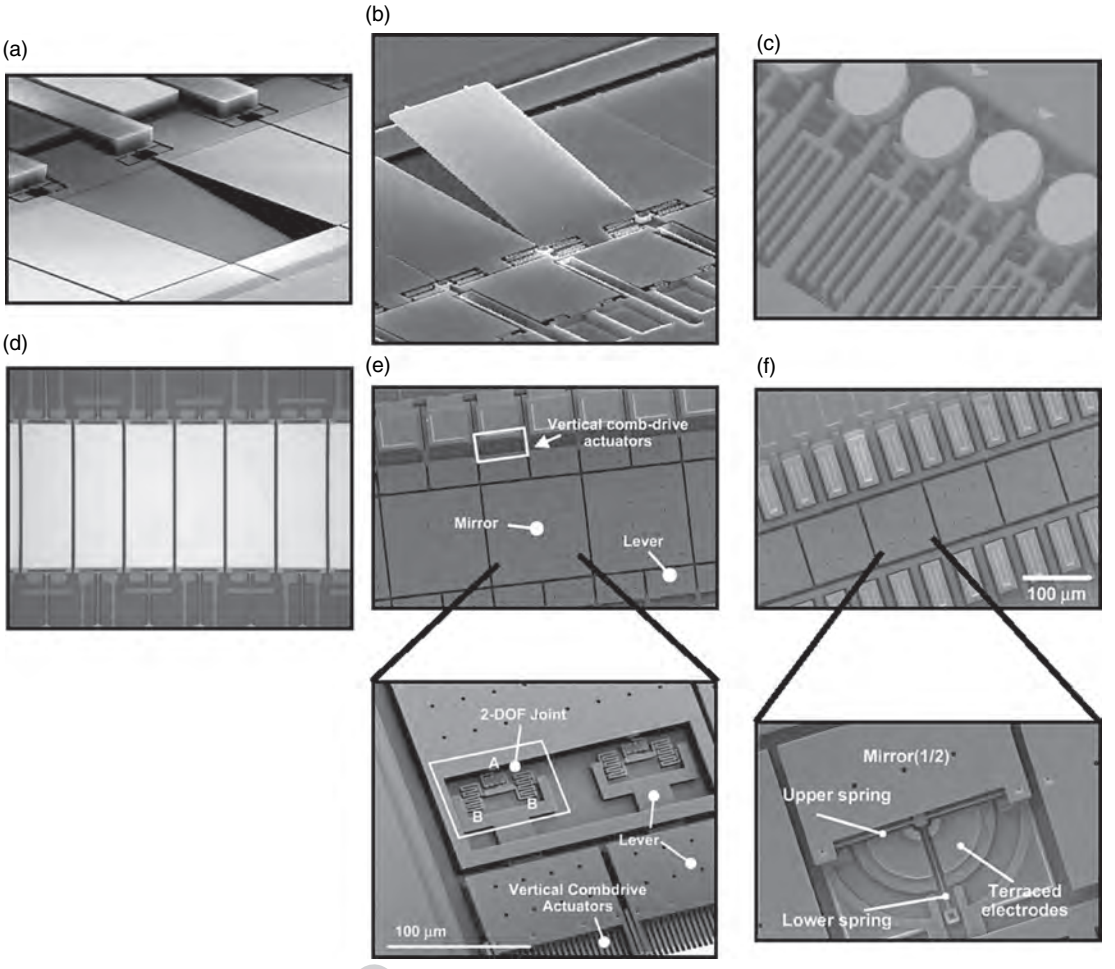

f0130 **Figure 26** One-dimensional, high fill factor, microelectromechanical systems (MEMS) micromirror arrays for wavelength-selective switching applications. Mirrors can tilt preferentially with rotation axis parallel to dispersion (a–c), or normal to dispersion (d), or in both axis with underlying actuators (e, f) for hitless operation. (Source: López D *et al.* 2002 Monolithic MEMS optical switch with amplified out-of-plane angular motion. IEEE Optical MEMS conference, Lugano, Switzerland, © [2002] IEEE; Greywall D S *et al.* 2003 Monolithic, fringe-field-activated crystalline silicon tilting mirror devices. *IEEE J. Microelectromech. Syst.* **12**, 702–7, © [2003] IEEE; Tsuboi O *et al.* 2004 A high-speed comb-driven micromirror array for 1 × *N* 80-channel wavelength selective switches. *IEEE Int. Conference on Optical MEMS*, Takamatsu, Japan, © [2004] IEEE; Bernstein J J *et al.* 2004 MEMS tilt-mirror spatial light modulator for a dynamic spectral equalizer. *IEEE J. Microelectromech. Syst.* **13**, 272–8, © [2004] IEEE; Tsai J-c, Wu M C 2005 Gimbal-less MEMS two-axis optical scanner array with high fill-factor. *IEEE J. Microelectromech. Syst.* **14**, 1323– 8, © [2005] IEEE; Tsai J-c, Wu M C 2006a A high post-count wavelength-selective switch using a large scan-angle, high fill-factor, two-axis MEMS scanner array. *IEEE Photon. Technol. Lett.* **18**, 1439–41, © [2006] IEEE.)

challenge as the mirror array is still required to fulfill the high fill ratio requirement. Several such two-axis micromirror implementations have been reported (Kouma *et al.* 2005, Tsai and Wu 2005, 2006a). Furthermore, with two-axis mirror technology, the number of fiber ports *K* served by the WSS can be increased by arranging the fibers in a 2D array (Tsai and Wu 2006b, Tsi *et al.* 2006).

p0410 While the free-space WSS arrangement performs very well, its size and packaging of discrete optical elements is challenging from an optomechanical point of view. Many of the optical elements can be eliminated by utilizing a hybrid planar lightwave circuit (PLC) and free-space optics arrangement (Marom *et al.* 2004, 2005b, Ducellier *et al.* 2004). The input and output fibers of the WSS are attached to the PLC, which distributes the light into an array of waveguides with constantly increasing path lengths. The light radiating out of the waveguide array is angularly dispersed, and with a single lens is converted to spatial

dispersion that is incident onto the MEMS micromirror array. Reflected light is incident into a desired waveguide array on the PLC for coherently recombining the light into the output fiber. Introducing the PLC platform into the WSS enables to customize each waveguide array, and in one example introduce a demultiplexer directly into the WSS. Other approaches attempt to combine the entire WSS functionality – consisting of the demultiplexing, switching with MEMS micromirrors, and remultiplexing – onto a single PLC (Fuchs 2004, Chi *et al.* 2005).

s0140 ***3.07.4.5.3 Wavelength-selective $K \times K$ switches***

p0415 The optical switching requirement at network nodes originates from K fibers, carrying N DWDM channels. The number of individually switched channels is therefore $K \times N$, which can quickly scale to many hundreds of channels. For precisely that reason, large port count OXCs were developed. However, the switching functionality can also be provided by using $2K$ modules of $1 \times K$ WSS (or even K modules as in **Figure 27**) (Marom *et al.* 2003b). This elegant solution provides all the switching functionality carried by $K(K-1)$ interconnecting fibers between the WSS modules. If we assume that four fibers are introduced, $K = 4$, and each fiber carries 80 channels, $N = 80$, then all the traffic is routed on 12 fibers using four WSS modules. The OXC alternative requires $K \times N = 320$ fibers in both input and output sides, a fiber management nightmare! The entire architecture can even be implemented in planar optics with specially integrated free-space tilting micromirrors on a single silicon wafer (Chi *et al.* 2006). Another alternative is the wavelength-selective $K \times K$ switch, or WSXC. The WSXC internally handles the demultiplexing, switching, and

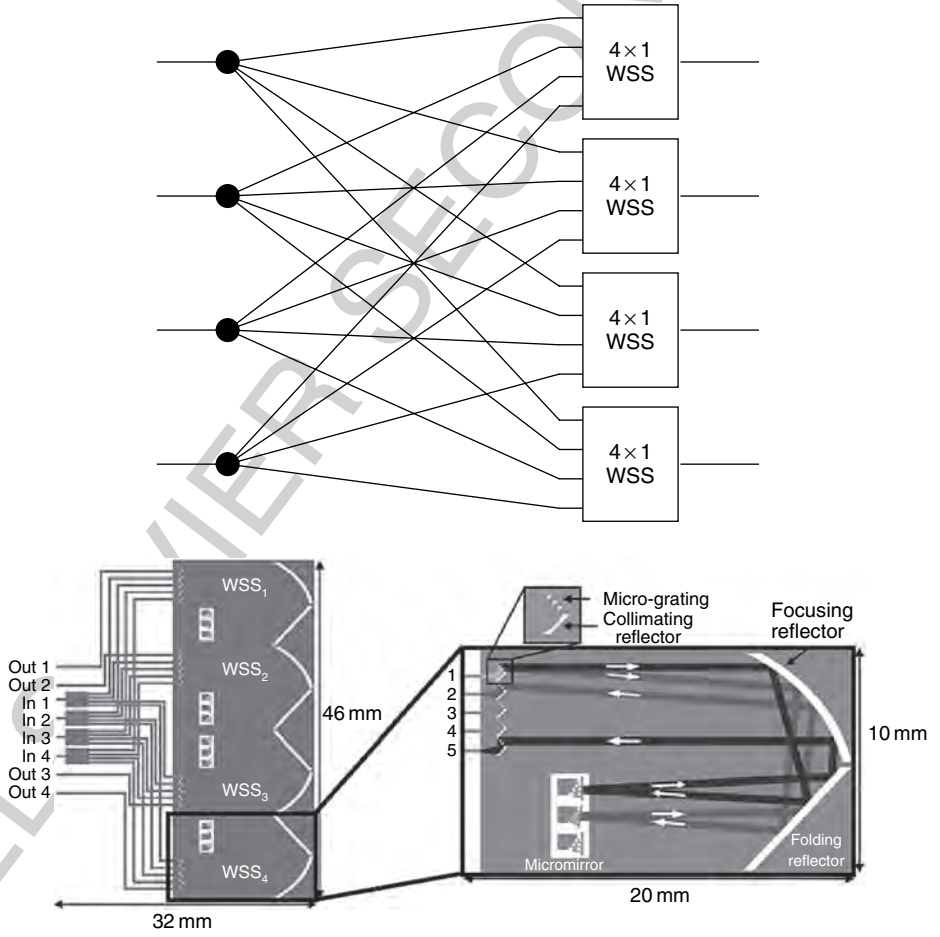

f0135 **Figure 27** *Top*: Wavelength-selective $K \times K$ cross-connect architecture comprising individual $1 \times K$ wavelength-selective switches (WSSs) in a broadcast and select architecture. *Bottom*: Planar implementation of 4×4 wavelength-selective cross-connect architecture on a single silicon wafer. (Source: Chi C H *et al.* Silicon-based, monolithic, 4×4 wavelength-selective switch with on-chip micromirrors. *Optical Fiber Conference (OFC 2006)*, Anaheim, CA, March 2006, © [2006] IEEE.)

remultiplexing of all K input/output fibers, further reducing the fiber management complexity, at the expense of complex switch architecture.

p0420 A demonstrated WSXC introduced PLCs with demultiplexer and multiplexer functionality into a transparent OXC fabric (b0440 Ryf *et al.* 2001). The custom PLC placed the demultiplexed waveguides on a pitch $P = 1.25$ mm matched to a microlens array and the micromirror array. The collimated beams were incident onto the micromirrors for switching, much the same way as the collimated beams a from a fiber array are generated. The passband performance of the WSXC is dictated by the demultiplexer/multiplexer implementation, which are typically not as wide and flat as those achieved by regular WSS. Thus, cascadability using this solution is questionable. A reported alternative performs the demultiplexing with a free-space grating, and selects the bandwidth for switching by the MEMS micromirror array (b0465 Solgaard *et al.* 2002). With this solution, the bandwidth is defined by the micromirror array fill factor and shape, much the same as for the WSS. However, there is little information on any implementation attempts of this WSXC.

s0145 3.07.5 Conclusions

p0425 Optical microsystems with MEMS actuators can offer the functionality, flexibility, low power consumption, low insertion loss, and compactness required for optical communication networks. Reported optical microsystems have demonstrated most of the passive and slow active enabling elements for optical networking, such as ROADM, fiber cross-connect switching, channel selection filters for monitoring, and tunable dispersion compensating elements. The maturation of MEMS technology fortuitously coincided with, or even helped to enable, the transition to optical networking, by demonstrating the feasibility of performing the required tasks for reconfigurable networks. This has led to intensive research and development efforts in the last 10 years, by established corporate research centers, academia, and start-up companies. Unfortunately, many of these efforts have since ceased, as the forecasted market demand never materialized and consolidation and investor pull-out resulted in company shut downs. This downturn came as a predictable counter response to the hype and overselling by the investment community, leading to the infamous telecom bubble of 1999–2001.

p0430 While most of the private and institutional capital poured into telecom microsystem development may have been written off, the industry effort helped to further advance microoptics, microfabrication, packaging, and related fields. This has benefited the related microsystem scientific and industrial communities, with innovation sprouting out in sensing, bioengineering, and nanotechanology applications. Moreover, telecom industry spending is now experiencing steady growth once again on a more rational base spending level, due to a recovery of the industry (**Figure 28**), with the strongest growth in the metropolitan and fiber access spaces. Companies that have survived the downturn are growing once again, and there are signs of a resurgence of start-up activity. The renewed interest and more stable and sustainable marketplace ensure that optical communication networks will continue to serve as a driving force for innovations in optical microsystems.

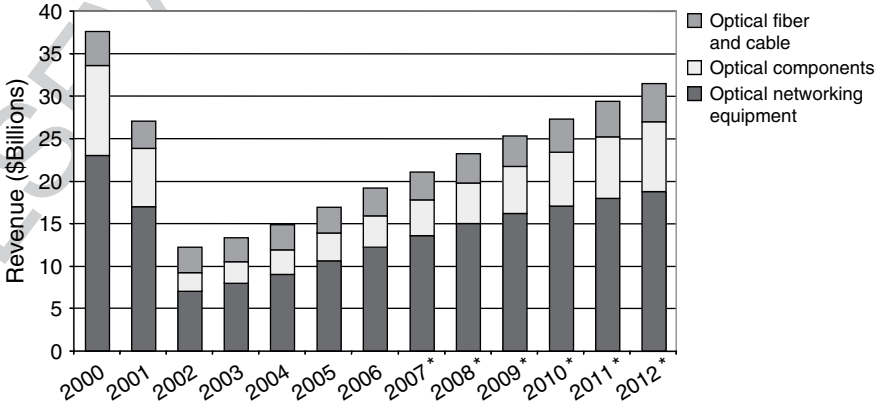

f0140 **Figure 28** Global communications revenue and forecast by segment, 2000–2012. (Source: OIDA Optoelectronics Industry Development Association.)

References

b0005 Aksyuk V A, Giles C R, Dentai A, Burrus E C, Burrus C A, Stulz L, Bishop D 1999 Optically-powered optical power limiter for use in lightwave networks. *Micro Electro Mechanical Systems (MEMS)*, Orlando, FL, USA

b0010 Aksyuk V A, Pardo F, Carr D, Greywall D, Chan H B, Simon M E, Gasparyan A, Shea H, Lifton V, Bolle C, Arney S, Frahm R, Paczkowski M, Haueis M, Ryf R, Neilson D T, Kim J, Giles C R, Bishop D 2003 Beam-steering micromirrors for large optical cross-connects. *IEEE J. Lightwave Technol.* **21**, 634–642

b0015 Al-Salameh D Y, Korotky S K, Levy D S, Murphy T O, Patel S H, Richards G W, Tentarelli E S 2002 Optical switching in transport networks: Applications, requirements, architecture, technologies, and solutions. In: Kaminow I and Li T (eds.) *Optical Fiber Telecommunications IV A. Chap. 7*. Academic Press, San Diego, CA

b0020 Amano T, Koyama F, Hino T, Arai M, Mastutani A 2000 Multiple wavelength micromachined GaAlAs/GaAs vertical cavity filter array. *IEEE Optical MEMS Conference*, Kauai, HI, USA

b0025 Angulo Barrios C, Almeida V R, Panepucci R R, Schmidt B S, Lipson M 2004 Compact silicon tunable Fabry-Pérot resonator with low power consumption. *IEEE Photon. Technol. Lett.* **16**, 506–508

b0030 Anthon D, Berger J D, Tselikov A 2004a C + L band MEMS tunable external cavity semiconductor laser. *Optical Fiber Conference (OFC)*, Los Angeles, CA, USA,paper WL2

b0035 Anthon D, King D, Berger J D, Dutta S, Tselikov A 2004b Mode-hop free sweep tuning of a MEMS tuned external cavity semiconductor laser. *Conference on Lasers and Electro-Optics (CLEO)*, San Francisco, CA, USA

b0040 Bakke T, Tigges C P, Lean J J, Sullivan C T, Spahn O B 2002 Planar microoptomechanical waveguide switches. *IEEE J. Select. Top. Quant. Electron.* **8**, 64–72

b0045 Barber B, Giles C R, Askyuk V, Ruel R, Stulz L, Bishop D 1998 A fiber connectorized MEMS variable optical attenuator. *IEEE Photon. Technol. Lett.* **10**, 1262–1264

b0050 Bashir A, Katila P, Ogier N, Saadany B, Khalil D A 2004A MEMS-based VOA with very low PDL. *IEEE Photon. Technol. Lett.* **16**, 1047–1049

b0055 Belikov R, Solgaard O 2003 Optical wavelength filtering by diffraction from a surface relief. *Opt. Lett.* **28**, 447–449

b0060 Berger J D, Zhang Y, Grade J D, Lee H, Hrinya S, Jerman H 2001 Widely tunable external cavity diode laser using a MEMS electrostatic rotary actuator. *Optical Fiber Conference (OFC)*, Anaheim, CA, USA,paper TuJ2

b0065 Berger J D, Ilkov F, King D, Anthon D 2003 Widely tunable, narrow optical bandpass Gaussian filter using a silicon microactuator. *Optical Fiber Conference (OFC)*, Atlanta, GA, USA ,paper TuN2

b0070 Berger J, Anthon D, Drake J, Ilkov F, Shreeram J, Verdonck C 2004 MEMS-tunable 10 Gb/s APD receiver for broadcast and select CATV networks. *Optical Fiber Conference (OFC)*, Los Angeles, CA, USA ,paper ThQ3

b0075 Bernstein J J, Dokmeci M R, Kirkos G, Osenar A B, Peanasky J, Pareek A 2004 MEMS tilt-mirror spatial light modulator for a dynamic spectral equalizer. *IEEE J. Microelectromech. Syst.* **13**, 272–8

b0080 Blake M 2003 C-MEMS filter aims at monitoring. *EE Times*, March 24

b0085 Bonenfant P A, Jones M L 2004 OFC 2003 workshop on wavelength selective switching based optical networks. *IEEE J.* **22**, 305–9

b0090 Bouevitch O, Touahri D, Morgan J P, Panteleev S, Reimer C 2002 Channel-power equalizer and dynamic gain equalizer based on the optical bench platform. *2002 Dig. IEEE/LEOS Summer Topical Meetings*, Mont Tremblant, QC, Canada, pp. MD1-4–5

b0095 Chang-Hasnain C J 2000 Tunable VCSEL. *IEEE J. Select. Top. Quant. Electron.* **6**, 978–87

b0100 Cheng C, Lee C, Yeh J A 2004 Retro-reflection type MOEMS VOA. *IEEE Photon. Technol. Lett.* **16**, 2290–2

b0105 Chi C-H, Tsai J-C, Lee M C M, Hah D, Wu M C 2005 Integrated 1×4 wavelength-selective switch with on-chip MEMS micromirrors. *Conference Quantum Electronics and Laser Science (QELS)*, Baltimore, MD, USA

b0110 Chi C-H, Tsai J-C, Hah D, Mathai S, Lee M C M, Wu M C 2006 Silicon-based, monolithic, 4×4 wavelength-selective switch with on-chip micromirrors. *Optical Fiber Conference (OFC 2006)*, Anaheim, CA, March 2006

b0115 Chu P B, Brener I, Chuan P, Lee S-S, Dadap J I, Park S, Bergman K, Bonadeo N H, Chau T, Chou M, Doran R A, Gibson R, Harel R, Johnson J J, Lee C D, Peale D R, Tang B, Tong D T K, Tsai M J, Wu Q, Zhong W, Goldstein E L, Lin L Y, Walker J A 2005 Design and nonlinear servo control of MEMS mirrors and their performance in a large port-count optical switch. *IEEE J. Microelectromech. Syst.* **14**, 261–73

b0120 Coldren L A, Fish G A, Akulova Y, Barton J S, Johansson L, Coldren C W 2004 Tunable semiconductor lasers: A tutorial. *IEEE J. Lightwave Technol.* **22**, 193–202

b0125 Daleiden J, Irmer S, Rangelov V, Romer F, Tarraf A, Prott C, Strassner M, Hillmer H 2002 Record wavelength tuning of 127 nm for vertical cavity Fabry–Perot filter. *IEEE Optical MEMS Conference*, Lugano, Switzerland

b0130 Darcie T E, Driessen P F, Osusky M, Lin W 2005 Optical network control overlay using silicon VOA arrays. *IEEE Photon. Technol. Lett.* **17**, 513–15

b0135 De Dobbelaere P, Falta K, Gloeckner S, Patra S 2002 Digital MEMS for optical switching. *IEEE Commun. Mag.* **40**, 88–95

b0140 Diemeer M B J, Dekker R 2002 MEMS VOA with polymeric thermal microactuators. *Eur. Conf. Optical Communication (ECOC)*, Copenhagen, Denmark

b0145 Dono N R, Green P E Jr., Liu K, Ramaswami R, Tong F F-K 1990 A wavelength division multiple access network for computer communication. *IEEE J. Select. Areas Commun.* **8**, 983–94

b0150 Ducellier T, Bismuth J, Roux S F, Gillet A, Merchant C, Miller M, Mala M, Ma Y, Tay L, Sibille J, Alavanja M, Deren A, Cugalj M, Ivancevic D, Dhuler V, Hill E, Cowen A, Shen B, Wood R 2002 The MWS 1×4: A high performance wavelength switching building block. *Eur. Conf. Optical Communications (ECOC)*, Copenhagen, Denmark

b0155 Ducellier T, Hnatiw A, Mala M, Shaw S, Mank A, Touahri D, McMullin D, Zami T, Lavigne B, Peloso P, Leclerc O 2004 Novel, high-performance, hybrid waveguide-MEMS, 1×9 wavelength-selective switch in a 32 cascade loop experiment. *Eur. Conf. Optical Communication (ECOC)*, Stockholm, Sweden

b0160 Feldman R D, Harstead E E, Jiang S, Wood T H, Zirngibl M 1998 An evaluation of architectures incorporating wavelength division multiplexing for broad-band fiber access. *IEEE J. Lightwave Technol.* **16**, 1546–59

b0165 Field L A, Burriesci D L, Robrish P R, Ruby R C 1995 Micromachined 1×2 optical fiber switch. *Proc. Tech. Dig. 8th Int. Conf. Solid-State Sensors Actuators (Transducers '95).* Stockholm, Sweden, Vol. 1, pp. 344–7

b0170 Finot M, McDonald M, Daiber A, Chapman W B, Li D, Epitaux M, Zbinden E, Bennet J, Kozlovsky W J, Verdiell J-M 2004 Automated optical packaging technology for 10 Gb/s transceivers and its application to a low-cost full C-band tunable transmitter. *Intel Technol. J.* **8**, 101–14

b0175 Fishman D A, Correa D L, Goode E H, Downs T L, Ho A Y, Hale A, Hofmann P, Basch B, Gringeri S 2006 The rollout of optical networking: LambdaXtreme national network deployment. *Bell Labs Tech. J.* **11**, 55–63

b0180 Ford J E, DiGiovanni D J 1998 $1 \times N$ fiber bundle scanning switch. *IEEE Photon. Technol. Lett.* **10**, 967–9

b0185 Ford J E, Walker J A 1998 Dynamic spectral power equalization using micro-opto-mechanics. *IEEE Photon. Technol. Lett.* **10**, 1440–2

b0190 Ford J E, Walker J A, Greywall D S, Goossen K W 1998 Micromechanical fiber-optic attenuator with 3 μs response. *IEEE J. Lightwave Technol.* **16**, 1663–70

b0195 Fuchs D T, Doerr C R, Aksyuk V A, Simon M E, Stulz L W, Chandrasekhar S, Buhl L L, Cappuzzo M, Gomez L, Wong-Foy A, Laskowski E, Chen E, Pafchek R 2004 A hybrid MEMS-waveguide wavelength selective cross connect. *IEEE Photon. Technol. Lett.* **16**, 99–101

b0200 Giles C R, Aksyuk V, Barber B, Ruel R, Stulz L, Bishop D 1999 A silicon MEMS optical switch attenuator and its use in lightwave subsystems. *IEEE J. Select. Top. Quant. Electron.* **5**, 18–25

b0205 Godil A 2002 Diffractive MEMS technology offers a new platform for optical networks. *Laser Focus World* **38**, 181–5

b0210 Greywall D S, Pai C-S, Oh S-H, Chang C-P, Marom D M, Busch P A, Cirelli R A, Taylor J A, Klemens F P, Sorsch T W, Bower J E, Lai W Y-C, Soh H T 2003 Monolithic, fringe-field-activated crystalline silicon tilting mirror devices. *IEEE J. Microelectromech. Syst.* **12**, 702–707

b0215 Hagood N W, Ghandi K, Cloutier B, Borgen M 2004 Beam-steering optical switching apparatus. US Pat. 6 738 539, May 18

b0220 Herding M, Richardt F, Woias P 2003 A novel approach to low-cost optical fiber switches. *IEEE Optical MEMS Conference*, Waikoloa, HI, USA

b0225 Hirata T, Mitama I, Abe M, Makita K, Shiba K, Hane K, Sasaki M 2005 Development of MEMS-based optical surge suppressor. *Optical Fiber Communication Conference (OFC)*, Anaheim, CA, USA

b0230 Hoffmann M, Kopka P, Voges E 1999 All-silicon bistable micromachincal fiber switch based on advanced bulk micromachining. *IEEE J. Select. Top. Quant. Electron.* **5**, 46–51

b0235 Hohlfeld D, Zappe H 2005 Thermally tunable optical thin-film filters with sub-nanometer resolution, 41.7 nm continuous tuning range. *IEEE MEMS*, Miami, FL, USA

b0240 Isamoto K, Kato K, Morosawa A, Chong C, Fujita H, Toshiyoshi H 2004 A 5-V operated MEMS variable optical attenuator by SOI bulk micromachining. *IEEE J. Select. Top. Quant. Electron.* **10**, 570–8

b0250 Kaminow I P, Doerr C R, Dragone C, Koch T, Koren U, Saleh A A M, Kirby A J, Ozveren C M, Schofield B, Thomas R E, Barry R A, Castagnozzi D M, Chan V W S, Hemenway B R Jr., Marquis D, Parikh S A, Stevens M L, Swanson E A, Finn S G, Gallager R G 1996 A wideband all-optical WDM network. *IEEE J. Select. Areas Commun.* **14**, 780–799

b0255 Kanamori Y, Aoki Y, Sasaki M, Hosoya H, Wada A, Hane K 2003 Driving of optical fiber by surface-micromachined cam-micromotor for the applications to variable optical attenuator. *IEEE Optical MEMS Conference*, Waikoloa, HI, USA

b0260 Kanamori Y, Kitani T, Hane K 2006 Movable guided-mode resonant grating filters by four bimorph actuators for wavelength selective dynamic reflection control. *IEEE Optical MEMS Conference*, Piscataway, NJ, USA

b0265 Kim C-K, Lee M-L, Jun C-H, kim Y T 2003a 47 nm tuning of thermally actuated Fabry–Perot tunable filter with very low power consumption. *IEEE Optical MEMS Conference*, Waikoloa, HI, USA

b0270 Kim J, Nuzman C J, Kumar B, Lieuwen D F, Kraus J S, Weiss A, Lichtenwalner C P, Papazian A R, Frahm R E, Basavanhally N R, Ramsey D A, Aksyuk V A, Pardo F, Simon M E, Lifton V, Chan H B, Haueis M, Gasparyan A, Shea H R, Arney S, Bolle C A, Kolodner P R, Ryf R, Neilson D T, Gates J V 2003b 1100/spl times/ 1100 port MEMS-based optical crossconnect with 4-dB maximum loss. *IEEE Photon. Technol. Lett.* **15**, 1537–9

b0275 Kimura T, Fujimura N, Kanbara N 2004 Wide range tunable filter module based on MEMS tilt mirror. *IEEE Optical MEMS Conference*, Takamatsu, Japan

b0280 Kner P, Kageyama T, Boucart J, Stone R, Sun D, Nabiev R F, Pathak R, Yuen W 2003 A long-wavelength MEMS tunable VCSEL incorporating a tunnel junction. *IEEE Photon. Technol. Lett.* **15**, 1183–5

b0285 Kouma N, Tsuboi O, Soneda H, Ueda S, Sawaki I 2005 Fishbone-shaped vertical comb actuator for dual axis 1-D analog micromirror array. *Solid State Sensors, Actuators, and Microsystems (Transducers '05)*. Seoul, Korea

b0290 Lee M-C M, Wu M.C. 2005 MEMS-actuated microdisk resonators with variable power coupling ratios. *IEEE Photon. Technol. Lett.* **17**, 1034–6

b0295 Li M Y, Yuen W, Li G S, Chang-Hasnain C J 1998 Top-emitting micromechanical VCSEL with a 31.6-nm tuning range. *IEEE Photon. Technol. Lett.* **10**, 18–20

b0300 Li X, Antoine C, Daesung L, Jen-Shiang W, Solgaard O 2006 Tunable blazed gratings. *IEEE J. Microelectromech. Sys.* **15**, 597–604

b0305 Lin L Y, Goldstein E L, Tkach R W 1998 Free-space micromachined optical switches with submillisecond switching time for large-scale optical crossconnects. *IEEE Photon. Technol. Lett.* **10**, 525–7

b0310 Lin L Y, Goldstein E L, Tkach R W 1999 Free-space micromachined optical switches for optical networking. *IEEE J. Select. Top. Quant. Electron.* **5**, 4–9

b0315 Lipson A, Yeatman E M 2005 Free-space MEMS tunable optical filter on (110) silicon. *IEEE Optical MEMS Conference*, Oulu, Finland

b0320 Littman M G, Metcalf H J 1978 Spectrally narrow pulsed dye laser without beam expander. *Appl. Opt.* **17**, 2224–7

b0325 Liu K, Littman M G 1981 Novel geometry for single-mode scanning of tunable lasers. *Opt. Lett.* **6**, 117–18

b0330 López D, Simon M E, Pardo F, Aksyuk V, Klemens F, Cirelli R, Neilson D T, Shea H, Sorsch T, Ferry E, Nalamasu O, Gammel P L 2002 Monolithic MEMS optical switch with amplified out-of-plane angular motion. *IEEE Optical MEMS conference*, Lugano, Switzerland

b0335 Marom D M, Neilson D T, Greywall D S, Basavanhally N R, Kolodner P R, Low Y L, Pardo F, Bolle C A, Chandrasekhar S, Buhl L, Giles C R, Oh S-H, Pai C S, Werder K, Soh H T, Bogart G R, Ferry E, Klemens F P, Teffeau K, Miner J F, Rogers S, Bower J E, Keller R C, Mansfield W 2002 Wavelength selective 1 × 4 switch for 128 WDM channels at 50 GHz spacing. *Optical Fiber Communication Conference (OFC)*, Anaheim, CA, USA pp. 857–9

b0340 Marom D M, Neilson D T, Greywall D S, Aksyuk V A, Simon M E, Basavanhally N R, Kolodner P R, Low Y L, Pardo F, Bolle C A, Pai C S, López D, Taylor J A, Bower J E, Leuthold J, Gibbons M A, Giles C R 2003a Wavelength selective 4 × 1 switch with high spectral efficiency, 10 dB dynamic equalization range and internal blocking capability. ECOC 2003, Rimini, Italy, September 21–25, 2003, Paper Mo3.5.3

b0345 Marom D M, Neilson D T, Leuthold J, Gibbons M A, Giles C R 2003b 64 Channel 4 × 4 wavelength-selective cross-connect for 40 Gb/s channel rates with 10 Tb/s throughput capacity. *Eur. Conf. Optical Communications (ECOC)*, Rimini, Italy

b0350 Marom D M, Doerr C R, Basavanhally N R, Cappuzzo M, Gomez L, Chen E, Wong-Foy A, Laskowski E 2004 Wavelength-selective 1 × 2 switch utilizing a planar lightwave circuit stack and a MEMS micromirror array. *Optical MEMS 2004*, Takamatsu, Japan,August 2004

b0355 Marom D M, Neilson D T, Greywall D S, Pai C-S, Basavanhally N R, Aksyuk V A, López D O, Pardo F, Simon M E, Low Y, Kolodner P, Bolle C A 2005a Wavelength-selective 1 × K switches using free-space optics and MEMS micromirrors: Theory, design, and implementation. *IEEE J. Lightwave Technol.* **23**, 1620–1630

b0360 Marom D M, Doerr C R, Cappuzzo M, Chen E, Wong-Foy A, Gomez L 2005b Hybrid free-space and planar lightwave circuit wavelength-selective 1 × 3 switch with integrated

drop-side demultiplexer. *Eur. Conf. Optical Communication (ECOC)* 993–4

b0365 Marom D M, Möller L, Su L, López D, Pardo F, Klemens F, Bower E, Ferry E 2006 Compatibility of flat-passband, 200GHz-wide wavelength-selective switch for 160 Gb/s transmission rates. *Optical Fiber Conference (OFC)*, Anaheim, CA, USA,paper OTuF6

b0370 Marxer C, de Rooij N F 1999 Micro-opto-mechanical 2×2 switch for single-mode fibers based on plasma-etched silicon mirror, electrostatic actuation. *IEEE J. Lightwave Technol.* **17**, 2–6

b0375 Marxer C, Griss P, de Rooij N F 1999 A variable optical attenuator based on silicon micromechanics. *IEEE Photon. Technol. Lett.* **11**, 233–235

b0380 McDonald M, Daiber A, Finot M, Su X. 2006 Wavelength filter with integrated thermal control used as an intracavity DWDM laser tuning element. *IEEE Optical MEMS Conference*, Piscataway, NJ, USA

b0385 Neilson D T, Frahm R, Kolodner P, Bolle C A, Ryf R, Kim J, Papazian A R, Nuzman C J, Gasparyan A, Basavanhally N R, Aksyuk V A, Gates J V 2004a 256×256 Port optical cross-connect subsystem. *IEEE J. Lightwave Technol.* **22**, 1499–1509

b0390 Neilson D T, Tang H, Greywall D S, Basavanhally N R, Ko L, Ramsey D A, Weld J D, Low Y L, Pardo F, López D O, Busch P, Prybyla J, Haueis M, Pai C S, Scotti R, Ryf R 2004b Channel equalization and blocking filter utilizing microelectromechanical mirrors. *IEEE Select. Top. Quant. Electron.* **10**, 563–569

b0395 Niederer G, Herzig H P, Shamir J, Thiele H, Schnieper M, Zschokke C 2004 Tunable, oblique incidence resonant grating filter for telecommunications. *Appl. Opt.* **43**, 1683–1684

b0400 Nielson G N, Seneviratne D, Lopez-Royo F, Rakich P T, Avrahami Y, Watts M R, Haus H A, Tuller H L, Barbastathis G 2005 Integrated wavelength-selective optical MEMS switching using ring resonator filters. *IEEE Photon. Technol. Lett.* **17**, 1190–1192

b0405 Niemi T, Uusimaa M, Tammela S, Heimala P, Kajava T, Kaivola M, Ludvigsen H 2001 Tunable silicon etalon for simultaneous spectral filtering and wavelength monitoring of a DWDM transmitter. *IEEE Photon. Technol. Lett.* **13**, 58–60

b0410 Ollier E 2002 Optical MEMS devices based on moving waveguides. *IEEE J. Select. Top. Quant. Electron.* **8**, 155–162

b0415 Peter Y-A, Gonte F, Herzig H P, Dandliker R 2002 Micro-optical fiber switch for a large number of interonnects using a deformable mirror. *IEEE Photon. Technol. Lett.* **14**, 301–303

b0420 Pezeshki B, Vail E, Kubicky J, Yoffe G, Zou S, Heanue J, Epp P, Rishton S, Ton D, Faraji B, Emanuel M, Hong X, Sherback M, Agrawal V, Chipman C, Razazan T 2002 20-mW widely tunable laser module using DFB array and MEMS selection. *IEEE Photon. Technol. Lett.* **14**, 1457–1459

b0425 Ramani C M 2006 Optical MEMS: Boom, bust and beyond. *National Fiber Optics Engineers Conference (NFOEC)*, Anaheim, CA, USA

b0430 Rhee J-K, Garcia F, Ellis A, Hallock B, Kennedy T, Lackey T, Lindquist R G, Kondis J P, Scott B A, Harris J M, Wolf D, Dugan M 2001 Variable passband optical add-drop multiplexer using wavelength selective switch. In: *27th Eur. Conf. Optical Communication (ECOC'01).Amsterdam, The Netherlands, Vol. 4*

b0435 Rosenblatt D, Sharon A, Friesem A A 1997 Resonant grating waveguide structures. *IEEE J. Quant. Electron.* **33**, 2038–2059

b0440 Ryf R, Bernasconi P, Kolodner P, Kim J, Hickey J P, Carr D, Pardo F, Bolle C, Frahm R, Basavanhally N, Yoh C, Ramsey D, George R, Kraus J, Lichtenwalner C, Papazian R, Gates J, Shea H R, Gasparyan A, Muratov V, Griffith J E, Prybyla J A, Goyal S, White C D, Lin M T, Ruel R, Nijander C, Amey S, Neilson D T, Bishop D J, Pau S, Nuzman C, Weis A, Kumar B, Lieuwen D, Aksyuk V, Greywall D S, Lee T C, Soh H T, Mansfield W M, Jin S, Lai W Y, Huggins H A, Barr D L, Cirelli R A, Bogart G R, Teffeau K, Vella R, Mavoori H, Ramirez A, Ciampa N A, Klemens F P, Morris M D, Boone T, Liu J Q, Rosamilia J M, Giles C R 2001 Scalable wavelength-selective crossconnect switch based on MEMS and planar waveguides. *Eur. Conf. Optical Communication (ECOC)*. Amsterdam, The Netherlands

Ryf R, Neilson D T, Aksyuk V A 2006 MEMS based optical switching. In: El-Bawab T S (ed.) *Optical Switching*. Springer, New York b0445

Saadany B, Malak M, Marty F, Mita Y, Khalil D, Bourouina T 2006 Electrostatically-tuned optical filter based on silicon Bragg reflectors. *IEEE Optical MEMS Conference*, Piscataway, NJ, USA b0450

Sagberg H, Lacolle M, Johansen I-R, Lovhaugen O, Solgaard O, Sudbo A S 2003 Configurable spectral filter with an array of diffraction gratings. *IEEE Optical MEMS Conference*, Waikoloa, HI, USA b0455

Saleh B E A, Teich M C 1991 *Fundamentals of Photonics*. Wiley, New YorkM b0460

Solgaard O, Heritage J P, Bhattarai A R 2002 Multi-wavelength cross-connect optical switch. US Pat.6 374 008, April 16 b0465

Stuart H R, Baumann F H, Wong-Foy A 2003 Monolithic integration of optical waveguides, MEMS-based switching in silicon-on-insulator. *Proc. SPIE 5347* 137–144 b0470

Sugihwo F, Larson M C, Harris J S 1998 Micromachined widely tunable vertical cavity laser diodes. *IEEE J. Microelectromech. Syst.* **7**, 48–55 b0475

Syms R R A, Zou H, Stagg J 2004a MEMS iris mechanism. *IEEE Optical MEMS Conference*, Takamatsu, Japan b0480

Syms R R A, Zou H, Stagg J, Moore D F 2004b Multistate latching MEMS variable optical attenuator. *IEEE Photon. Technol. Lett.* **16**, 191–193 b0485

Taesombut N, Uyeda F, Chien A A, Smarr L, DeFanti T A, Papadopoulos P, Leigh J, Ellisman M, Orcutt J 2006 The OptIPuter: High-performance, QoS-guaranteed network service for emerging E-science applications. *IEEE Commun. Mag.* **44**, 38–45 b0490

Takahashi K, Kwon H N, Mita M, Saruta K, Lee J H, Fujita H, Toshiyoshi H 2006A 3D optical crossconnect using microlens scanner with topologically layer switching architecture. *IEEE Optical MEMS Conference*, Piscataway, NJ, USA b0495

Tarraf A, Riemenschneider F, Strassner M, Daleiden J, Irmer S, Halbritter H, Hillmer H, Meissner P 2004 Continuously tunable 1.55-mm VCSEL implemented by precisely curved dielectric top DBR involving tailored stress. *IEEE Photon. Technol. Lett.* **16**, 720–722 b0500

Tayebati P, Wang P, Vakhshoori D, Lu C-C, Azimi M, Sacks R N 1998 Half-symmetric cavity tunable microelectromechanical VCSEL with single spatial mode. *IEEE Photon. Technol. Lett.* **10**, 1679–1681 b0505

Tilleman M M, Kozhekin A, Cohen R, Haronian D, Nusinsky I 2005 Coupling losses in multimode waveguides due to misalignment. *IEE Proc. Optoelectron.* **152**, 145–150 b0510

Ton D, Yoffe G W, Heanue J F, Emanuel M A, Zou S Y, Kubicky J, Pezeshki B, Vail E C 2004 2.5-Gb/s Modulated widely tunable laser using an electroabsorption modulated DFB array and MEMS selection. *IEEE Photon. Technol. Lett.* **16**, 1573–1575 b0515

Torman M, Peter Y-A, Niederman P, Hoogerwerf A, Stanley R 2006 Deformable MEMS grating for wide tunability and high operating speed. *J. Opt. A Pure Appl. Opt.* **8**, S337–S340 b0520

Toshiyoshi H, Fujita H 1996 Electrostatic micro torsion mirrors for an optical switch matrix. *J. Microelectromech. Syst.* **5**, 231–237 b0525

Toshiyoshi H, Su G-D J, LaCosse J, Wu M C 2003 A surface micromachined optical scanner array using photoresist b0530

lenses fabricated by a thermal reflow process. *IEEE J. Lightwave Technol.* **21**, 1700–1708

b0535 Truex T A, Bent A A, Hagood N W 2003 Beam-steering optical switch fabric utilizing piezoelectric actuation technology. *National Fiber Optics Engineers Conference (NFOEC)*, Orlando, FL, USA

b0540 Tsai J-c, Wu M C 2005 Gimbal-less MEMS two-axis optical scanner array with high fill-factor. *IEEE J. Microelectromech. Syst.* **14**, 1323–1328

b0545 Tsai J-c, Wu M C 2006a A high port-count wavelength-selective switch using a large scan-angle, high fill-factor, two-axis MEMSscanner array. *IEEE Photon. Technol. Lett.* **18**, 1439–1441

b0550 Tsai J-c, Wu M C 2006b Design, fabrication, characterization of a high fill-factor, large scan-angle, two-axis scanner array driven by a leverage mechanism. *IEEE J. Microelectromech. Syst.* **15**, 1209–1213

b0555 Tsai J-c, Huang S T-Y, Hah D, Wu M C 2006 $1 \times N^2$ wavelength-selective switch with two cross-scanning one-axis analog micromirror arrays in a 4-f optical system. *IEEE J. Lightwave Technol.* **24**, 897–903

b0560 Tsuboi O, Kouma N, Soneda H, Okuda H, Mi X, Ueda S, Sawaki I 2004 A high-speed comb-driven micromirror array for $1 \times N$ 80-channel wavelength selective switches. *IEEE Int. Conf. Optical MEMS*, Takamatsu, Japan

b0565 Unamuno A, Uttamchandani D 2005 Hybrid MOEMS tunable filter for interrogation of fiber Bragg grating sensors. *IEEE Photon. Technol. Lett.* **17**, 202–204

b0570 Unamuno A, Uttamchandani D 2006 MEMS variable optical attenuator with Vernier latching mechanism. *IEEE Photon. Technol. Lett.* **18**, 88–90

b0575 Wilson G, Chen C J, Gooding P, Ford J E 2006 Spectral passband filter with independently variable center wavelength, bandwidth. *IEEE Photon. Technol. Lett.* **18**, 1660–1662

b0580 Wong C W, Jeon Y, Barbastathis G, Kim S-G 2004 Analog piezoelectric-driven tunable gratings with nanometer resolution. *IEEE J. Microelectromech. Syst.* **13**, 998–1005

b0585 Wu M C, Tsai J-c , Huang S, Hah D 2002 MEMS WDM routers using analog micromirror arrays. *Lasers and Electro-Optics Society, 2002 (LEOS 2002)*, The 15th Annual Meeting of the IEEE, Glasgow, Scotland, November 10–14, 2002, Vol. 2, pp. 582–3, www.telcordia.com. See website for documentation availability details

b0590 Yano M, Yamagishi F, Tsuda T 2003 Optical MEMS for photonic switching – compact and stable optical crossconnect switches for simple, fast, and flexible wavelength applications in recent photonic networks. *IEEE J. Select. Top. Quant. Electron.* **11**, 383–394

b0595 Yao J, Lee M-C M, Leuenberger D, Wu M C 2005 Wavelength- and bandwidth-tunable filters based on MEMS-actuated microdisk resonators. *Optical Fiber Conference (OFC)*, Anaheim, CA, USA,paper OTuM1

b0600 Ye Y, Dixit S, Ali M 2000 On joint protection/restoration in IP-centric DWDM-based optical transport networks. *IEEE Commun. Mag.* **38**, 174–183

b0605 Yeh J A, Jiang S-S, Lee C 2006 MOEMS variable optical attenuators using rotary comb drive actuators. *IEEE Photon. Technol. Lett.* **18**, 1170–1172

b0610 Yu K, Solgaard O 2004 Tunable optical transversal filters based on a Gires–Tournois interferometer with MEMS phase shifters. *IEEE J. Select. Top. Quant. Electron.* **10**, 588–597

b0615 Yun S-S, Lee J-H 2003 A micromachined in-plane tunable optical filter using the thermo-optic effect of crystalline silicon. *J. Micromech. Microeng.* **13**, 721–725

b0620 Yun S-S, Jo K W, Lee J H 2003 Crystalline Si-based in-plane tunable Fabry-Perot Filter with wide tunable range. *IEEE Optical MEMS Conference*, Waikoloa, HI, USA

b0625 Zhang X M, Liu A Q 2000 A MEMS pitch-tunable grating add/drop multiplexers. *IEEE Optical MEMS Conference*, Kauai, HI, USA

b0630 Zheng X, Kaman V, Yuan S, Xu Y, Jerphagnon O, Keating A, Anderson R C, Poulsen H N, Liu B, Sechrist J R, Pusarla C, Helkey R, Blumenthal D J, Bowers J E 2003 Three-dimensional MEMS photonic cross-connect switch design and performance. *IEEE J. Select. Top. Quant. Electron.* **9**, 571–578

b0635 Zou S Y, Olson R W, Pezeshki B, Vail E C, Yoffe G W, Rishton S A, Emanuel M A, Sherback M A 2004 Narrowly spaced DFB array with integrated heaters for rapid tuning applications. *IEEE Photon. Technol. Lett.* **16**, 1239–1241

Biographies

Dan Marom earned the B.Sc. degree in Mechanical Engineering (1989) and the M.Sc. degree in Electrical Engineering (1995), both from Tel-Aviv University. He was awarded the Ph.D. degree in Electrical Engineering by the University of California, San Diego, in 2000. In his doctoral research, under the guidance of Prof. Yeshaiahu (Shaya) Fainman, Dan explored nonlinear wave mixing for optical signal processing of ultrafast waveforms.

From 2000 until 2005, Dr. Marom was employed as a Member of the Technical Staff at Bell Laboratories, then part of Lucent Technologies, where he pioneered the work on Wavelength-Selective Switches (WSS), a critical element for the realization of reconfigurable optical networks using MEMS (Micro-Electro-Mechanical-System) technology.

Dr. Marom joined the faculty of the Applied Physics Department in the fall of 2005, where he is pursuing his research interests in creating photonic devices for switching and manipulating optical signals.

Dr. Dan Marom is active in the scientific community, serving or has served on program committees of leading conferences such as OFC, CLEO, IEEE LEOS, and IEEE Optical MEMS. Dan is the first recipient of the Peter Brojde Excellence in Engineering Award (2006), received the Golda Meir Fellowship (2006), was a Fannie and John Hertz Foundation Fellow during his doctoral studies (1996–2000), and received a Powell Foundation Fellowship (1995).